AER/AGS Special Report 104

Alberta Energy Regulator

Initial Seismic Hazard Assessment for the Induced Earthquakes Near Fox Creek, Alberta (between January 2013 and January 2016)

AGS
ALBERTA GEOLOGICAL SURVEY

AER/AGS Special Report 104

Initial Seismic Hazard Assessment for the Induced Earthquakes Near Fox Creek, Alberta (between January 2013 and January 2016)

R. Schultz[1] and Nanometrics Inc.[2]

[1] Alberta Energy Regulator
Alberta Geological Survey
[2] Nanometrics Inc.

November 2019

ISBN 978-1-4601-0163-6

Author addresses:
Nanometrics Inc.
250 Herzberg Road
Kanata, ON K2K 2A1
Canada
613.592.6776
Email: contact-us@nanometrics.ca

Published November 2019 by:
Alberta Energy Regulator
Alberta Geological Survey
4th Floor, Twin Atria Building
4999 – 98th Avenue
Edmonton, AB T6B 2X3
Canada

Tel: 780.638.4491
Fax: 780.422.1459
E-mail: AGS-Info@aer.ca
Website: ags.aer.ca

Contents

Acknowledgements

Funding for this report was provided by the Alberta Energy Regulator in support of a broader study to understand the induced earthquakes near Fox Creek. Ground motion waveform data was provided by public seismic networks including the Regional Alberta Observatory for Earthquake Studies Network (RAVEN), the TransAlta Dam Monitoring Network, the Canadian Rockies and Alberta Network (CRANE), the Alberta Telemetered Seismograph Network, the Canadian National Seismograph Network, and privately owned operator seismic networks. Earthquake catalogues were composed of publicly available data—including data from Natural Resources Canada, the AGS, and the Canadian Induced Seismicity Collaboration (http://www.inducedseismicity.ca/)—supplemented by privately owned operator catalogues. Thank you to Kristine Haug (AGS) for her contributions to making this work possible and her diligent work in managing this project.

Abstract

This report assesses the seismic hazard near the town of Fox Creek, Alberta. It is a combined release of two reports produced by Nanometrics Inc., with input from Western University, using public and private ground motion data. These reports include probabilistic seismic hazard assessments for the years 2013 through 2015 and ShakeMaps of the largest magnitude events induced between January 2013 and January 2016. The hazard forecasts assume earthquake rate and location models based on annually binned catalogued events, regionally calibrated ground motion prediction equations, and tectonic considerations of maximum magnitude.

The results of this analysis suggest significant change (1–2 orders of magnitude) to the prior background hazard estimates for various spectral periods (0.1–5 s). Specifically, hazard maps at 0.04% chance of exceedance in 1 year reach 10–20% of standard gravity in expected peak ground acceleration at the town of Fox Creek. Deaggregation of the seismic hazard maps suggests much of the hazard in forecast scenarios is the result of the potential occurrence of earthquakes of M_w >5. In addition to probabilistic forecasts, ShakeMaps were developed for events larger than 3.5 M_w. Instrumental intensities from these events range between III and IV in Fox Creek, which is consistent with reports of felt ground motion.

This is preliminary work and is superseded by Short-Term Hindcasts of Seismic Hazard in the Western Canada Sedimentary Basin Caused by Induced and Natural Earthquakes (https://doi.org/10.1785/0220180285).

1 Introduction

Recently, the Western Canada Sedimentary Basin (WCSB) has seen a marked increase in the rate of earthquakes associated with hydraulic fracturing operations (Atkinson et al., 2016). Induced earthquakes have the potential for significant shaking, increasing seismic hazard, and may pose a risk to critical infrastructure. In recent years, earthquakes of ~4 M_w have been observed in the Montney play near Pink Mountain (Babaie Mahani et al., 2016) and Duvernay play near Fox Creek (Schultz et al., 2015a), producing ground motions felt at nearby towns. Despite the propensity for induced earthquakes to change seismic hazard (Peterson et al., 2016b), these events are often excluded from consideration in building codes due to their transient nature, and may be excluded from probabilistic seismic hazard analysis (PHSA; Cornell, 1968) due to uncertainties in accurately incorporating their effects (Halchuk et al., 2014).

This report characterizes the change to seismic hazard in the region near Fox Creek due to hydraulic fracturing operations (Appendix 1). Presently, there is a lack of consensus in suggested approaches to incorporate induced seismicity in PSHA (Peterson et al., 2015; Atkinson et al., 2015a). Thus, the following paragraphs discuss the current scientific issues, justifications for our choices in addressing these issues, and shortcomings of the initial Fox Creek hazard model.

2 Probabilistic Seismic Hazard Analysis Approach

2.1 Ground Motion Prediction Equations

It has been suggested that ground motions from induced and natural earthquakes may be discernible at higher frequencies because induced events tend to have lower stress drop values that offset the effect of their shallow depth (Hough, 2014). Whether this stress drop effect is truly characteristic of induced earthquakes or simply a consequence of shallow focal depths remains to be addressed (Atkinson et al., 2015b).

To address this point as completely as possible, the ground motion prediction equations (GMPEs) in this study were calibrated to ground motions from the most complete waveform and catalogue datasets obtainable. Our ground motion database was composed of data from the regional, public seismic networks (Gu et al., 2011; Stern et al., 2013; AGS, 2013; Eaton, 2014; Schultz et al., 2015b; Earthquakes Canada, 2016) and supplemented by private, operator-owned seismic networks. GMPEs in this study are only calibrated up to earthquakes of magnitude 4, the largest magnitude events observed in the Fox Creek region (Wang et al., 2016). The GMPEs used in the study were modified from pre-existing models (Atkinson, 2015; Yenier and Atkinson, 2015) and likely represent a best guess at the ground shaking intensity attenuation from larger magnitude events. Despite this, earthquakes beyond 4 M_w would be required to more accurately model shaking attenuation in the region.

Further to these points, site effects were considered using surficial geology maps of the region (Fenton et al., 2013). Surficial soil conditions provide an approximate understanding of site amplification in the region. However, we note that more direct measurements of near-surface effects (e.g., Castellaro et al., 2008) could better quantify seismic energy amplification in the Fox Creek region.

2.2 Transient Temporal and Spatial Clustering

Rate and location models of seismicity are important components of PSHA, significantly affecting the expected ground motions (Atkinson et al., 2015a). In general, induced earthquakes are temporally transient and dependent on the specifics of the anthropogenic cause. Contrary to this, PSHA assume a stationary Poisson process for the earthquakes involved. Thus, a proper incorporation of time- and

space-dependent elements to the rate and location models of induced seismicity remains a considerable challenge.

Within the Fox Creek region, earthquakes related to hydraulic fracturing have been observed as clusters transient in both time and space, often occurring and becoming nearly quiescent again during a period of months (Schultz et al., 2016b). To date, no models that sufficiently reflect the tectonic, hydrological, geological, operational, and economic controls driving the clustering of these earthquakes have been described in the Fox Creek region. Instead, the rate and location models used in this study focus on simplicity and transparency of assumptions (e.g., naively assuming a Poisson process on an annual basis). Similar to other studies (Peterson et al., 2016a, 2016b), yearly seismic hazard snapshots are analyzed based on empirical observations and assumed applicability to future seismic hazard. Following this approach, our rate/location model was chosen to reflect the actualized clustering of earthquakes observed in the region (as catalogue resolution would allow) plus the averaged background tectonic rate. Work concerning statistical or physical approaches to geological controls on seismogenic activation potential (e.g., Schultz et al., 2016a; Ghofrani and Atkinson, 2016) coupled with operational and economic considerations would yield significant improvements to forecasts of seismic hazard in the Fox Creek region.

2.3 Maximum Magnitude

In general, the maximum magnitude for natural earthquakes in a PSHA is a difficult parameter to assess (e.g., Zöller et al., 2013; Holschneider et al., 2014), often requiring adequate understanding of the tectonic setting and connectivity of the fault network or access to historical records (Bakun et al., 2011). In the case of induced seismicity, this difficulty is further confounded by additional operational considerations. For example, previous studies have suggested that the largest magnitude of induced earthquakes may be limited by the amount of fluid injected (McGarr, 2014), reservoir geometry (Shapiro et al., 2011), or a weighted compromise between uncontrolled tectonic slip and rupture propagation behaviour (Gischig, 2015). Still, other studies have cast doubt on these conjectures, instead suggesting that the largest magnitude events may still be statistically indiscernible from tectonic considerations in most cases (Elst et al., 2016).

For the purpose of this report, we have opted to assume tectonic control on the earthquakes near Fox Creek. This choice was made for both the simplicity in assuming the worst-case scenario of seismic hazard change and evidence that at least some earthquakes in the WCSB may deviate from injection-based expected maximums (Atkinson et al., 2016). If future studies definitely associate operational controls to the maximum inducible magnitude in this region, then the PSHA could be updated to reflect these contributions.

2.4 Supplementary ShakeMaps

The previous sections outline some of the choices made in the composition of the PSHA for Fox Creek. We acknowledge that the adjustment of these parameters can have a significant effect on the output ground motion exceedance probabilities (e.g., Atkinson et al., 2015a; Peterson et al., 2015). Due to these inherent uncertainties and subjectivity, this report has been supplemented with standard ShakeMaps (Wald et al., 2005) for the four largest-magnitude events (Appendix 2). This additional analysis allows readers who are skeptical of our parameter choices to contrast PSHA determinations against estimated ground shaking intensities observed in the Fox Creek area.

3 References

Alberta Geological Survey (2013): Regional Alberta Observatory for Earthquake Studies Network, International Federation of Digital Seismograph Networks, Other/Seismic Network, doi:10.7914/SN/RV.

Atkinson, G.M. (2015): Ground-motion prediction equation for small-to-moderate events at short hypocentral distances, with application to induced-seismicity hazards; Bulletin of the Seismological Society of America, v. 105, no. 2A, p. 981–992, doi:10.1785/0120140142.

Atkinson, G.M., Ghofrani, H. and Assatourians, K. (2015a): Impact of induced seismicity on the evaluation of seismic hazard: Some preliminary considerations; Seismological Research Letters, v. 86, no. 3, p. 1009–1021, doi:10.1785/0220140204.

Atkinson, G., Assatourians, K., Cheadle, B. and Greig, W. (2015b): Ground motions from three recent earthquakes in western Alberta and northeastern British Columbia and their implications for induced-seismicity hazard in eastern regions; Seismological Research Letters, v. 86, no. 3, p. 1022–1031, doi:10.1785/0220140195.

Atkinson, G.M., Eaton, D.W., Ghofrani, H., Walker, D., Cheadle, B., Schultz, R., Shcherbakov, R., Tiampo, K., Gu, J., Harrington, R.M., Liu, Y., van de Baan, M. and Kao, H. (2016): Hydraulic fracturing and seismicity in the Western Canada Sedimentary Basin; Seismological Research Letters, v. 87, no. 3, p. 631–647, doi:10.1785/0220150263.

Babaie Mahani, A., Schultz, R., Kao, H., Walker, D., Johnson, J. and Salas, C. (in press): Fluid injection and seismic activity in the northern Montney Play, British Columbia, Canada, with special reference to the 17 August 2015 Mw 4.6 induced earthquake; Bulletin of the Seismological Society of America, v. 107, no. 2.

Bakun, W.H., Stickney, M.C. and Rogers, G.C. (2011): The 16 May 1909 Northern Great Plains earthquake; Bulletin of the Seismological Society of America, v. 101, no. 6, p. 3065–3071, doi:10.1785/0120110054.

Castellaro, S., Mulargia, F. and Rossi, P.L. (2008): VS30: Proxy for seismic amplification?; Seismological Research Letters, v. 79, no. 4, p. 540–543, doi:10.1785/gssrl.79.4.540.

Cornell, C.A. (1968): Engineering seismic risk analysis; Bulletin of the Seismological Society of America, v. 58, no. 5, p. 1583–1606.

Earthquakes Canada (2016): National earthquake database; Natural Resources Canada, URL <http://www.earthquakescanada.nrcan.gc.ca/stndon/NEDB-BNDS/index-en.php> [January 2017].

Eaton, D. (2014): Alberta Telemetered Seismograph Network (ATSN): Real-time monitoring of seismicity in northern Alberta; Canadian Society of Exploration Geophysicists Recorder, v. 39, no. 3, p. 30–33.

Elst, N.J., Page, M.T., Weiser, D.A., Goebel, T.H. and Hosseini, S.M. (2016): Induced earthquake magnitudes are as large as (statistically) expected; Journal of Geophysical Research: Solid Earth, v. 121, no. 6, p. 4575–4590, doi:10.1002/2016JB012818.

Fenton, M.M., Waters, E.J., Pawley, S.M., Atkinson, N., Utting, D.J. and Mckay, K. (2013): Surficial geology of Alberta; Alberta Energy Regulator, AER/AGS Map 601, scale 1:1 000 000, URL <http://ags.aer.ca/publications/MAP_601.html> [January 2017].

Gischig, V.S. (2015): Rupture propagation behavior and the largest possible earthquake induced by fluid injection into deep reservoirs; Geophysical Research Letters, v. 42, no. 18, p. 7420–7428, doi:10.1002/2015GL065072.

Ghofrani, H. and Atkinson, G. (2016): A preliminary statistical model for hydraulic fracture-induced seismicity in the Western Canada Sedimentary Basin (WCSB); Geophysical Research Letters, doi:10.1002/2016GL070042.

Gu, Y.J., Okeler, A., Shen, L. and Contenti, S. (2011): The Canadian Rockies and Alberta Network (CRANE): New constraints on the Rockies and Western Canada Sedimentary Basin; Seismological Research Letters, v. 82, no. 4, p. 575–588, doi:10.1785/gssrl.82.4.575.

Halchuk, S., Allen, T.I., Adams, J. and Rogers, G.C. (2014): Fifth generation seismic hazard model input files as proposed to produce values for the 2015 National Building Code of Canada; Geological Survey of Canada, Open File 7576, 18 p., doi:10.4095/293907.

Holschneider, M., Zöller, G., Clements, R. and Schorlemmer, D. (2014): Can we test for the maximum possible earthquake magnitude?; Journal of Geophysical Research: Solid Earth, v. 119, no. 3, p. 2019–2028, doi:10.1002/2013JB010319.

Hough, S.E. (2014): Shaking from injection-induced earthquakes in the central and eastern United States; Bulletin of the Seismological Society of America, v. 104, no. 5, p. 2619–2626, doi:10.1785/0120140099.

McGarr, A. (2014): Maximum magnitude earthquakes induced by fluid injection; Journal of Geophysical Research: Solid Earth, v. 119, no. 2, p. 1008–1019, doi:10.1002/2013JB010597.

Petersen, M.D., Mueller, C.S., Moschetti, M.P., Hoover, S.M., Rubinstein, J.L., Llenos, A.L., Michael, A.J., Ellsworth, W.L., McGarr, A.F., Holland, A.A. and Anderson, J.G. (2015): Incorporating induced seismicity in the 2014 United States National Seismic Hazard Model—Results of 2014 workshop and sensitivity studies; US Geological Survey, Open-File Report 2015-1070, 69 p., doi:10.3133/ofr20151070.

Petersen, M.D., Mueller, C.S., Moschetti, M.P., Hoover, S.M., Llenos, A.L., Ellsworth, W.L., Michael, A.J., Rubenstein, J.L., McGarr, A.F. and Rukstales, K. S. (2016a): 2016 one-year seismic hazard forecast for the central and eastern United States from induced and natural earthquakes; US Geological Survey, Open-File Report 2016-1035, 52 p., doi:10.3133/ofr20161035.

Petersen, M.D., Mueller, C.S., Moschetti, M.P., Hoover, S.M., Llenos, A.L., Ellsworth, W. L., Michael, A.J., Rubinstein, J.L., McGarr, A.F. and Rukstales, K. S. (2016b): Seismic-hazard forecast for 2016 including induced and natural earthquakes in the central and eastern United States; Seismological Research Letters, v. 87, no. 6, doi:10.1785/0220160072.

Shapiro, S.A., Krüger, O.S., Dinske, C. and Langenbruch, C. (2011): Magnitudes of induced earthquakes and geometric scales of fluid-stimulated rock volumes; Geophysics, v. 76, no. 6, p. WC55–WC63, doi:10.1190/geo2010-0349.1.

Schultz, R., Stern, V., Novakovic, M., Atkinson, G. and Gu, Y.J. (2015a): Hydraulic fracturing and the Crooked Lake Sequences: Insights gleaned from regional seismic networks; Geophysical Research Letters, v. 42, no. 8, p. 2750–2758, doi:10.1002/2015GL063455.

Schultz, R., Stern, V., Gu, Y.J. and Eaton, D. (2015b): Detection threshold and location resolution of the Alberta Geological Survey Earthquake Catalogue; Seismological Research Letters, v. 86, no. 2A, p. 385–397, doi:10.1785/0220140203.

Schultz, R., Corlett, H., Haug, K., Kocon, K., MacCormack, K., Stern, V. and Shipman, T. (2016a): Linking fossil reefs with earthquakes: Geologic insight to where induced seismicity occurs in Alberta; Geophysical Research Letters, v. 43, p. 2534–2542, doi:10.1002/2015GL067514.

Schultz, R., Wang, R., Gu, Y.J., Haug, K. and Atkinson, G. (2016b): A seismological overview of the induced earthquakes in the Duvernay play near Fox Creek, Alberta, Journal of Geophysical Research: Solid Earth, doi:10.1002/2016JB01357.

Stern, V.H., Schultz, R.J., Shen, L., Gu, Y.J., and Eaton, D.W. (2013): Alberta earthquake catalogue, version 1.0: September 2006 through December 2010; Alberta Energy Regulator, AER/AGS Open File Report 2013-15, 29 p., URL <http://ags.aer.ca/publications/OFR_2013_15.html> [January 2017].

Wald, D.J., Worden, B.C., Quitoriano, V. and Pankow, K.L. (2005): ShakeMap manual: technical manual, user's guide, and software guide (No. 12-A1), URL <https://pubs.usgs.gov/tm/2005/12A01/> [January 2017].

Wang, R., Gu, Y.J., Schultz, R., Kim, A. and Atkinson, G. (2016): Source analysis of a potential hydraulic-fracturing-induced earthquake near Fox Creek, Alberta; Geophysical Research Letters, v. 43, p. 564–573, doi:10.1002/2015GL066917.

Yenier, E. and Atkinson, G.M. (2015): An equivalent point-source model for stochastic simulation of earthquake ground motions in California; Bulletin of the Seismological Society of America, v. 105, no. 3, p. 1435–1455, doi:10.1785/0120140254.

Zöller, G., Holschneider, M. and Hainzl, S. (2013): The maximum earthquake magnitude in a time horizon: theory and case studies; Bulletin of the Seismological Society of America, v. 103, no. 2A, p. 860–875, doi:10.1785/0120120013.

Appendix 1 – PSHA Report

Nanometrics

Probabilistic Induced Seismic Hazard Analysis for Fox Creek, Alberta

Revision 1.6

Prepared for: Alberta Energy Regulator

Submitted: June 27, 2016

Alberta Energy Regulator

STRATEGIC INTELLIGENCE
fueled by SCIENCE

ATTENTION: PLEASE READ CAREFULLY.

This document is prepared by Nanometrics Inc. ("**Nanometrics**") for the recipient organization. The information contained in this document is intended to report and provide insights for the use of the recipient organization, who accepts full responsibility for its use. Recipient organization acknowledges that the overall outputs contained in this document must be considered estimates by their nature, as they are dependent upon measurements and mathematical models with varying levels of inherent uncertainty and assumptions that are typical of empirical and statistical analysis. The findings in this document should be assessed as a whole and any attempt to rely on partial analysis or summary descriptions in this document could lead to undue emphasis on particular factors or inaccurate conclusions.

The information in this document is provided with the understanding that this document is intended for use as part of a wider scope of work provided by Nanometrics and Nanometrics is not providing any professional advice or recommending any one course of action based on the contents of this document.

Nanometrics endeavours to provide accurate and reliable information and insights. This document has been provided in good faith based on data collected by Nanometrics which were available at the time the document was generated and which is dependent on various factors including, but not limited to, the number, geographical distribution and performance of commissioned stations which may be affected by factors outside of the control of Nanometrics. All information in this document is provided "as is", without warranty of any kind, express or implied, including, but not limited to any warranties of merchantability, merchantable quality or fitness for a particular purpose. In no event will Nanometrics, or its partners, suppliers, employees or agents, be liable to the recipient organization or anyone else for any loss, damage, cost or expense of any kind, including any consequential, special or similar damages, arising in connection with results obtained from the use of this information, any decision made or action taken in reliance on this document or any information contained in this document.

TABLE OF CONTENTS

1.0 EXECUTIVE SUMMARY

Earthquakes induced by human activities (e.g., mining, reservoir impoundment and hydrocarbon production) are rarely large enough to be either felt locally or detected by regional seismic networks. However, a number of induced seismic events of magnitudes above M3.5 associated with oil and gas operations were recorded in Fox Creek, Alberta, since 2013. In response to the recent seismic activity in the region, Alberta Energy Regulator (AER) has put in place staged protocols to mitigate risks associated with induced seismicity. In order to make scientific decisions related to the induced seismicity risks in the Fox Creek region, associated seismic hazard should be assessed first. With this in mind, AER has started a project to conduct a preliminary study on the probabilistic seismic hazard analysis (PSHA) of induced seismicity in Fox Creek region. This report has been prepared by Nanometrics Inc. for AER. It describes the methodology utilized for the evaluation of induced seismicity hazard in the region.

Estimation of seismic hazard from induced events is conceptually different from that for tectonic earthquakes. Induced seismicity is inherently variable with time because hydrocarbon production is largely dependent on economic forces and public policy decisions. In order to capture the temporal variations in induced seismicity, we perform annual hazard analysis for 2013, 2014 and 2015, separately. In this respect, an induced seismicity earthquake catalog spanning from January 2013 to January 2016 is compiled from local and regional earthquake catalogs. Observed seismic sequences are then examined with time and space to develop models for seismic sources and their recurrence relations. Ground motions obtained from well-recorded induced events are used to drive predictive models for ground motion amplitudes and their uncertainty. Hazard maps are generated by combining uncertainties in earthquake location, magnitude, frequency and ground motions. The study resulted in annual hazard maps for peak ground acceleration and response spectra at periods of engineering interest (0.2s, 0.5s, 1.0s and 2.0s) for alternative annual rates of exceedance (0.2% and 0.04%). The determined induced seismicity hazard for Fox Creek is de-aggregated to different magnitude and distance ranges to investigate the contributions from different seismic sources.

2.0 DELINEATION OF THE SEISMIC HAZARD MAP AND STUDY AREA

We define a geographic area for which probabilistic seismic hazard analysis will be conducted to generate hazard maps. This area is referred to as Seismic Hazard Map (SHM) region. As per AER specification, the SHM region is defined as a 115 km by 104 km area around Fox Creek, Alberta in such a way that it covers the majority of induced seismic activity associated with oil and gas operations in Fox Creek area (Figure 1).

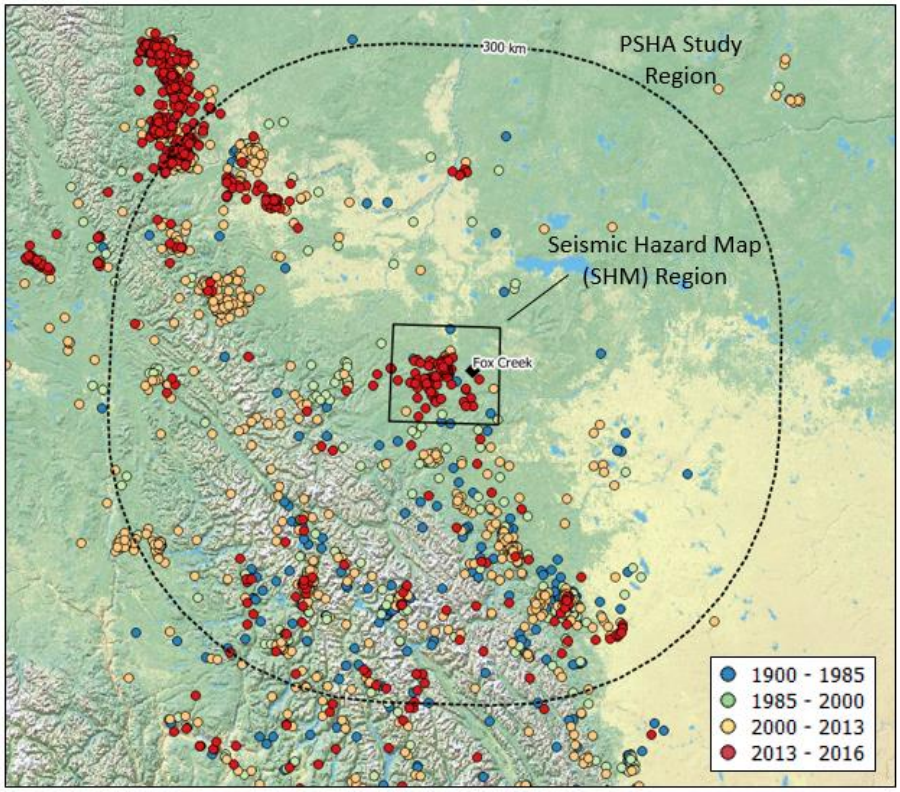

Figure 1 The Seismic Hazard Map (SHM) region and PSHA study region overlaid on the seismicity catalog obtained from NRCan.

Hazard analysis is conducted considering an extended area within which seismic sources may contribute to the overall hazard in the SHM region. This extended area is referred to as PSHA region. In order to delineate the PSHA region, we use ground motion prediction equations (GMPEs) used in the 5th generation Canadian seismic hazard model (Atkinson and Adams, 2013) for the zones in the east and west of Rockies. We deduce that any sources at distances larger than 300 km would not make a significant contribution to the overall hazard in SHM region (Figure 2). Thus, PSHA region is defined as an area that extends 300 km from the SHM region at all azimuths.

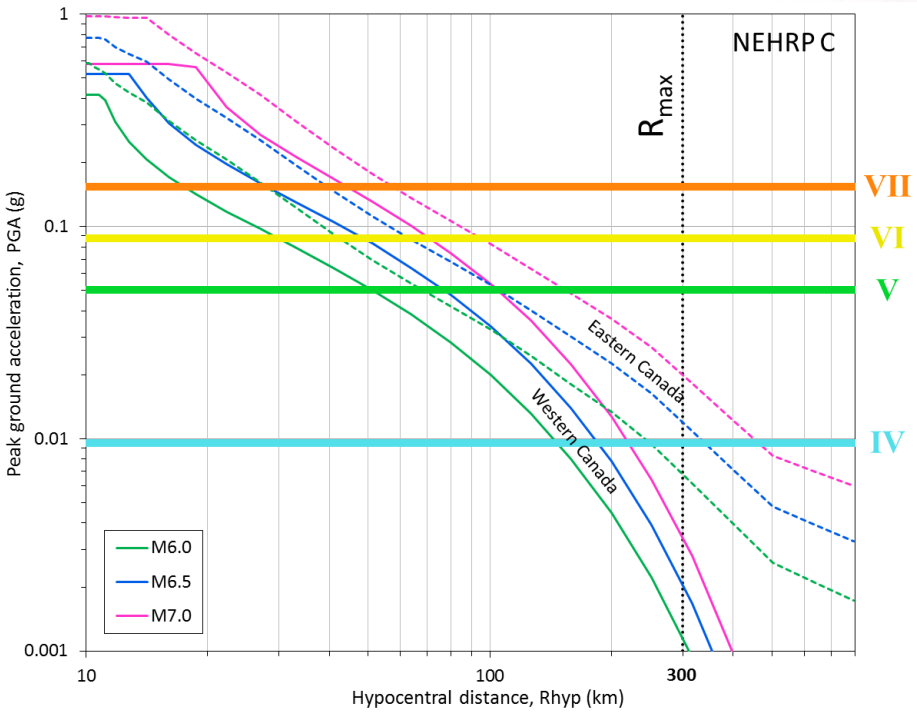

INTENSITY	I	II-III	IV	V	VI	VII	VIII	IX	X+
SHAKING	Not felt	Weak	Light	Moderate	Strong	Very strong	Severe	Violent	Extreme
DAMAGE	none	none	none	Very light	Light	Moderate	Moderate/Heavy	Heavy	V. Heavy

Figure 2 Median PGA estimates obtained from eastern and western North America ground motion models (Atkinson and Adams, 2013), as a function of distance. Horizontal lines indicate estimated PGA levels for different MMI intensities based on Atkinson and Kaka (2007).

3.0 CONSOLIDATION OF RECORDED INDUCED SEISMICITY CATALOG

3.1 INPUT EARTHQUAKE CATALOGS

The earthquake catalog is an essential part of the seismic hazard analysis. We compile an induced seismicity catalog for the Fox Creek region from January 2013 to January 2016, using data from six networks (Figure 3): TransAlta, AER and NRCan networks, and three local networks.

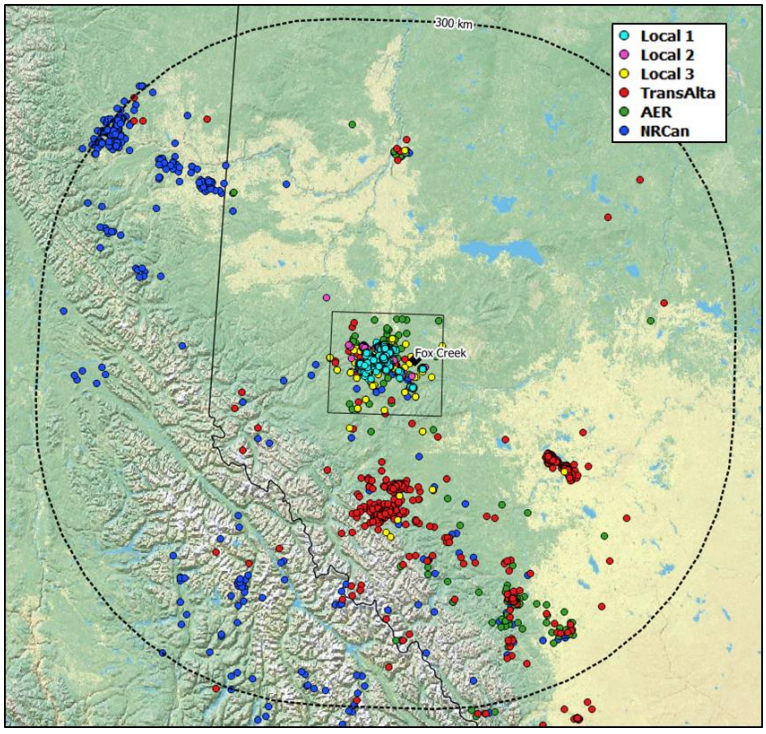

Figure 3 Events compiled from local and regional networks for the time period from January 2013 to January 2016.

We generate the composite earthquake catalog for Fox Creek region in two stages. First, we gather seismic events from local and TransAlta networks, in which accurate event locations were obtained from manually-reviewed phase arrival data and detailed regional velocity models. In order to ensure event uniqueness in the composite catalog, we identify duplicate events. Any events exist in two or more catalogs is classified as the same event if they satisfy all of the following:

- origin times less than 3 seconds apart,
- epicentral locations less than 15 km apart, and
- magnitude difference is smaller than a magnitude unit

For dublicate events, the event information (origin time, epicenter location, depth and magnitude) reported by local networks is given the highest priority, if the event is located within a local network. The event information from TransAlta network is adopted if the event is located outside of the local networks.

In the second stage of catalog compilation, we include the additional events from AER and NRCan catalogs, most of which were occurred before the deployment of local and TransAlta networks. In the composite catalog, the event information reported by AER is given priority over that of NRCan.

3.2 IDENTIFICATION OF BLAST EVENTS

TransAlta catalog include many mining explosions from Keephills, Alberta, confirmed by visual inspection of the recorded waveforms at nearby stations. We also suspect most of events detected in SW Alberta are explosions associated with mining activity. Mining blasts generally occur during local daytime hours, even though many mines operate 24 hours. To identify these events, histograms of origin times (in local time) are examined. As illustrated in Figure 4A, the regional activity is fairly uniform and low from 6 pm to 10 am (for 16 hours) during all days of the week. However, between 10 am and 6 pm (for 8 hours), the activity rate is 3 to 5 times larger than that observed between 6 pm and 10 am, particularly during the weekdays. This increase in activity is particularly evident in the hourly distribution, which indicates a large portion of the events is further constrained to between 1 pm and 2 pm (Figure 4B). Naturally occurring seismicity would be expected to be distributed uniformly throughout the day. This distribution is indicative of human activity.

The epicenters of all seismic events detected by the TransAlta network, between September 2013 and January 2016, are shown in Figure 4C. Triangles represent recording stations of TransAlta network (including other public stations in the region) and pickaxe symbols indicate quarry/mining areas. The dark and light blue dots show epicenters of suspected blast events, occurring between 10 am and 6 pm local time, within 75 km radius of a mine. The majority of these events (94%, light blue dots) are within 30 km of a mine. Based on these observations, we identify such events as suspected blasts and exclude them from the composite catalog.

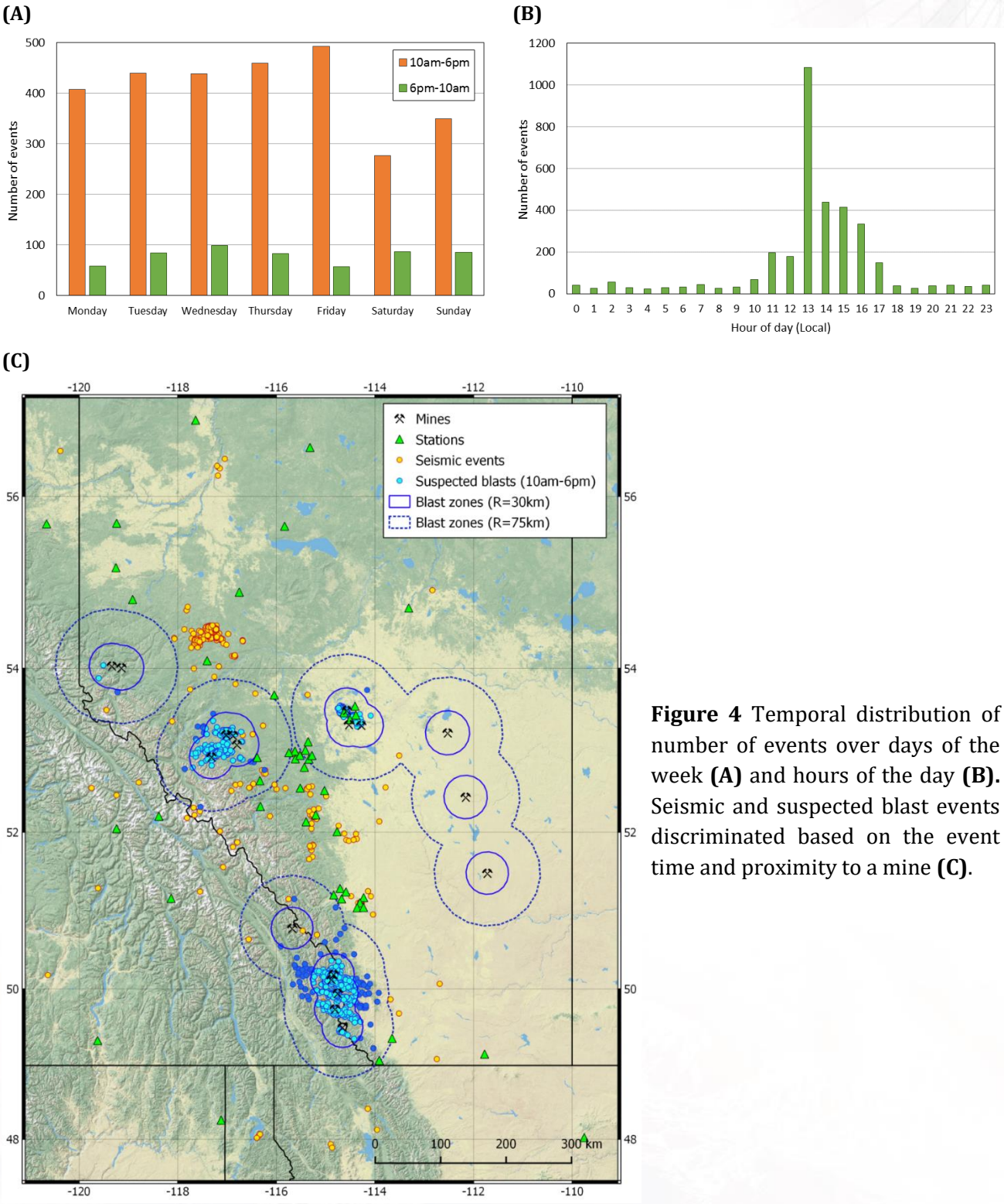

Figure 4 Temporal distribution of number of events over days of the week **(A)** and hours of the day **(B).** Seismic and suspected blast events discriminated based on the event time and proximity to a mine **(C)**.

3.3 LOCAL MAGNITUDE CALCULATION

In the input catalogs, local magnitudes (ML) were determined based on a standard formula that was derived for earthquakes in California. In order to ensure accurate magnitude estimates, we re-calculate ML magnitudes of events for which Wood-Anderson amplitudes from ground motion recordings are available through local and TransAlta networks. We use recently developed western Alberta ML formula (Yenier et al., 2016):

$$\mathrm{M_L} = \log(A) - \log A_0 + S \qquad (1)$$

Where $-\log A_0$ is the regional distance correction derived for western Alberta and S is the site correction term determined for each station. The distance correction term is defined as:

$$-logA_0 = GS' + \gamma(R - 100) + 3 \qquad (2)$$

The γ term is the coefficient of anelastic attenuation, and R is the hypocentral distance (km). The GS' term represents the geometrical spreading normalized at R = 100 km to maintain the original definition of Richter (1935):

$$GS' = GS(R) - GS(R = 100\mathrm{km}) \qquad (3)$$

The decay of WA amplitudes due to geometrical spreading in western Alberta is defined as a trilinear function of hypocentral distance:

$$\mathrm{GS}(R) = \begin{cases} b_1\log(R) & R \le R_1 \\ b_1\log(R_1) + b_2\log(R/R_1) & R_1 < R \le R_2 \\ b_1\log(R_1) + b_2\log(R_2/R_1) + b_3\log(R/R_2) & R > R_2 \end{cases} \qquad (4)$$

where b_1, b_2 and b_3 are rates of geometrical spreading at three distance ranges defined by transition distances R_1 and R_2. Table 1 lists the model coefficients of distance correction derived for western Alberta.

Table 1 Coefficients of distance correction (-logA0) for western Albert local magnitude equation

R_1	R_2	b_1	b_2	b_3	γ
100	220	1.42	-0.78	1.70	0.0011

The regionally-calibrated distance correction model shows a good agreement with the empirical data from western Alberta, as shown in Figure 5 (Yenier et al, 2016). However, the standard Hutton and Boore (1987) and Eaton (1992) models, which are commonly used for magnitude estimation in absence of a regional ML formula, fail to capture the attenuation attributes in western Alberta. Both models over-correct for distance attenuation for R < 30 km and R > 100 km, and do not account for observed Moho-bounce effects. Note that ML estimates from local and regional stations are affected by the biased distance corrections if region-specific attenuation attributes are not considered in magnitude calculations.

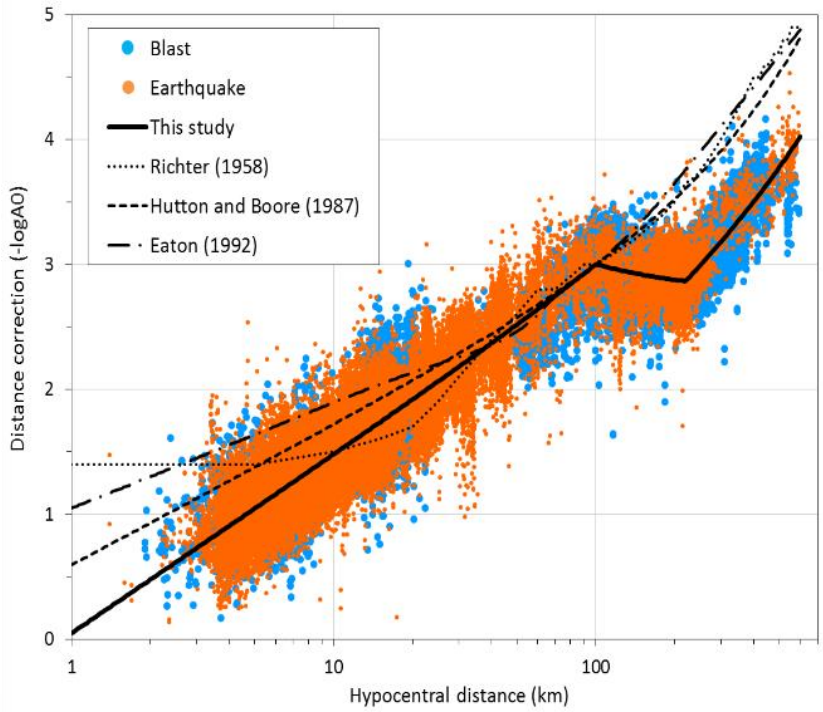

Figure 5 Comparison of the distance correction model (-logA0) developed for western Alberta (solid line) and standard models that are commonly used for magnitude estimation in absence of a regionally-derived ML formula. Circles indicate distance correction obtained from observed amplitudes after correcting for event magnitude and site effects (Yenier et al, 2016).

A total of 62,729 amplitude readings from local and TransAlta networks are used to re-calculate ML magnitudes (Figure 6). The compiled dataset consists mostly of earthquake records from local networks at close distances, and includes records from regional networks at far distances. The updated local magnitudes for the strongest events are listed in Table 2.

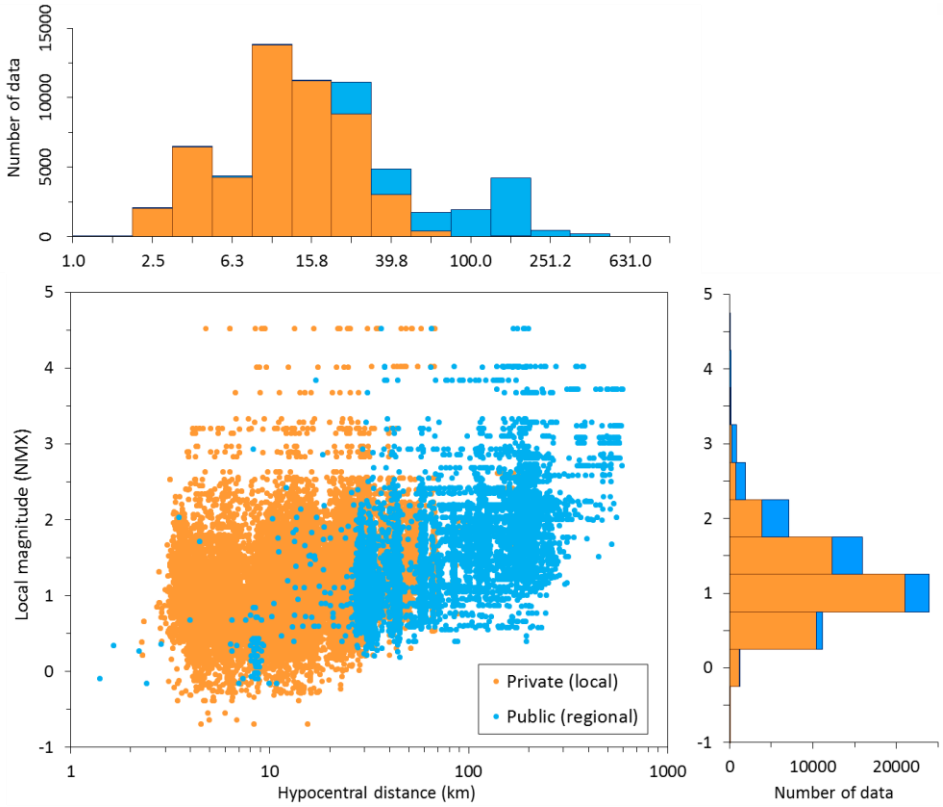

Figure 6 Magnitude and distance distribution of Wood-Anderson amplitude dataset compiled from local and TransAlta networks to determine ML magnitude of events in PSHA region.

Table 2 Local magnitudes for recent large events in Fox Creek area

Event Date & Time	ML (NMX)
2016-01-12 18:27	4.26
2015-06-13 23:57	4.12
2015-01-23 06:49	3.86
2015-01-15 19:18	3.26
2015-01-14 16:06	3.53
2015-01-07 04:50	3.04

3.4 CALIBRATION OF CATALOG ML FOR AER AND NRCAN DATASETS

As outlined in section 3.3, local magnitudes of events obtained from AER and NRCan could not be determined based on the western Alberta ML formula due to the absence of Wood-Anderson amplitudes from recordings of these events. We compared local magnitudes of common events to derive conversion relationships from ML reported in AER and NRCan catalogs to ML determined from western Alberta formula (ML-NMX)

Figure 7A presents the epicenters of the 69 common events in the AER and composite catalogs. All of these events occurred between January 2013 and December 2014. The relationship between AER local magnitudes and those determined from regional formula (ML_{NMX}) is illustrated in Figure 7B. In this figure the individual events are indicated by blue circles and the average values for each magnitude bin is indicated by filled orange circles. The conversion equation from ML_{AER} to ML_{NMX} is as follow:

$$ML_{NMX} = \begin{cases} ML_{AER} - 0.7 & ML_{AER} > 3.0 \\ 0.35 \times ML_{AER} - 0.35 & 1.0 \leq ML_{AER} \leq 3.0 \\ ML_{AER} & ML_{AER} < 1.0 \end{cases} \quad (5)$$

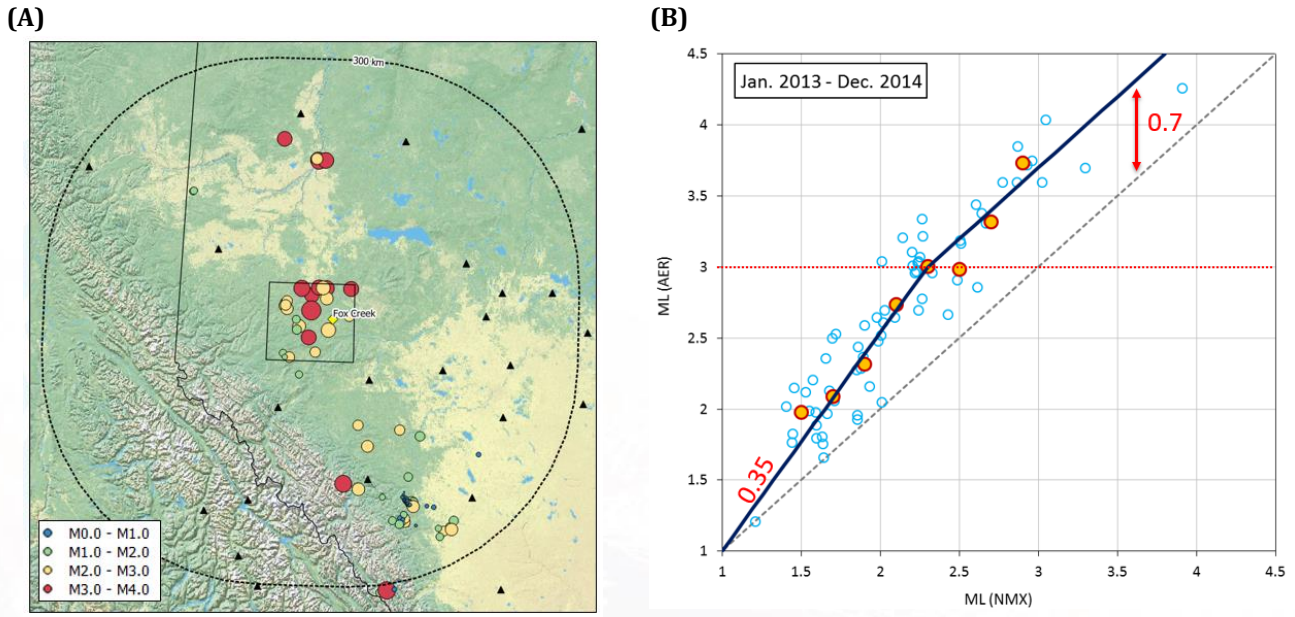

Figure 7 Common events in both AER and composite catalogs **(A);** The conversion relationship between ML_{AER} and ML_{NMX} **(B)**

A similar assessment is performed for 147 events common in the NRCan and composite catalogs (Figure 8A), from January 2013 to January 2016. As illustrated in Figure 8B and C, events were separated into two groups based on origin time:

- January 2013 to December 2014
- January 2015 to January 2016

to assess the influence of changes in network performance on the catalog ML values. No discrepancy was observed between the considered time windows. For both periods, ML_{NRCan} is larger than ML_{NMX} by 0.4 magnitude units, on average. Below is the conversion relationship for both time periods:

$$ML_{NMX} = ML_{NRCan} - 0.4 \quad (6)$$

(A)

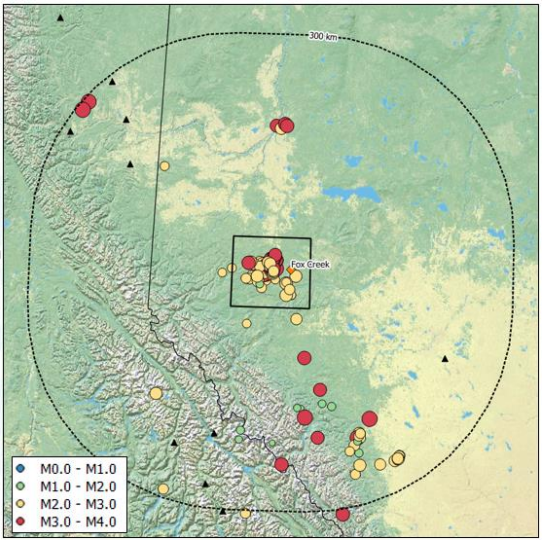

Figure 8 Common events in both NRCan and NMX catalogs **(A);** Difference between ML_{NRCan} and ML_{NMX} for events occurring from Jan. 2013 to Dec. 2014 **(B);** Difference between ML_{NRCan} and ML_{NMX} for events occurring from Jan. 2015 to Jan. 2016 **(C)**.

(B)

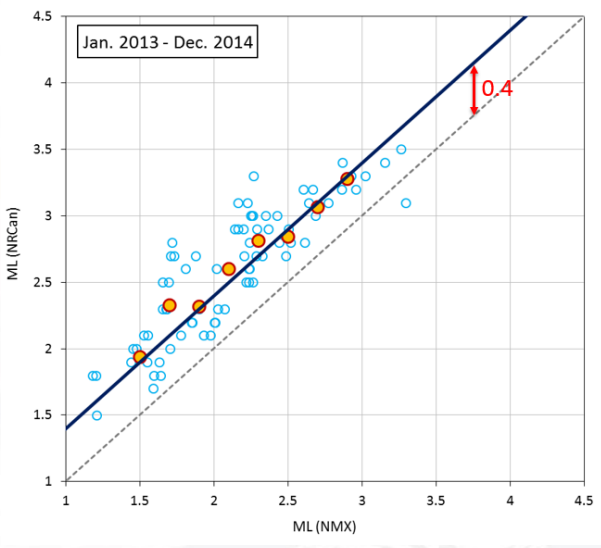

(C)

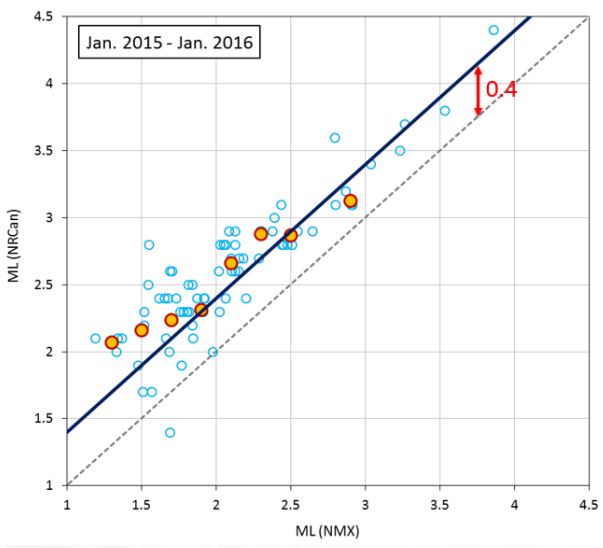

3.5 COMPOSITE CATALOG WITH LOCAL MAGNITUDE

We consolidate six input catalogs, removing the duplicate and blast events and converting of all magnitudes to the uniform local magnitude scale, to create the composited induced seismicity catalog. Figure 9 illustrates the distribution of events in the composite catalog.

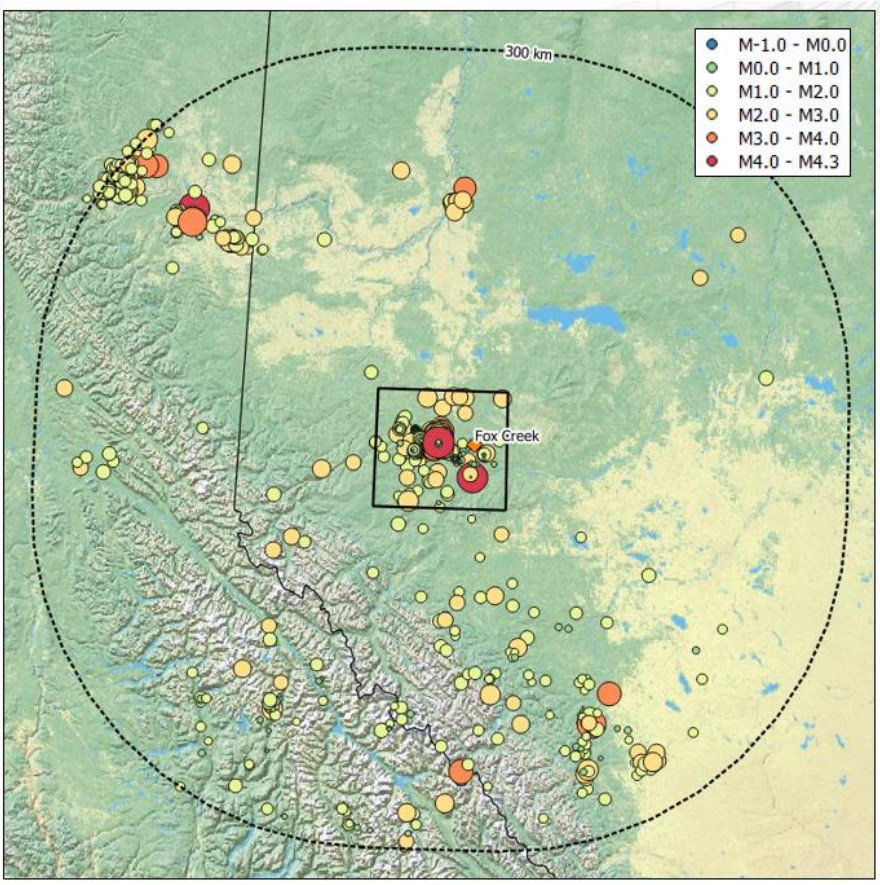

Figure 9 Composite catalog with local magnitude

3.6 CALCULATION OF MW FROM SPECTRAL FITTING

Moment magnitude, Mw, is related to the seismic energy radiated from an earthquake, and is the best single measure of overall size of an earthquake as it is not subject to saturation. We determine Mw of selected well-recorded events to derive a magnitude conversion relationship between ML and Mw. In this respect, we use spectral fitting approach to calculate source parameters of selected events.

The observed ground motion can be considered as product of source, path and site effects in Fourier displacement spectrum (FDS) domain:

$$FDS = Source \times Path \times Site$$

The ground motions are corrected for attenuation and site effect to estimate the apparent source spectra of an event. For attenuation, the eastern North America model of Atkinson and Boore (2014) was used:

- *Geometrical spreading:* $1/R^{1.3}$
- *Anelastic attenuation:* $Q(f) = 525f^{0.45}$

In order to limit any potential errors that may map in to estimated Mw values due to biased estimations in the attenuation model, only recordings within 50 km of an event were used. Vertical motions were used in calculations, assuming that site effects are small enough to be negligible.

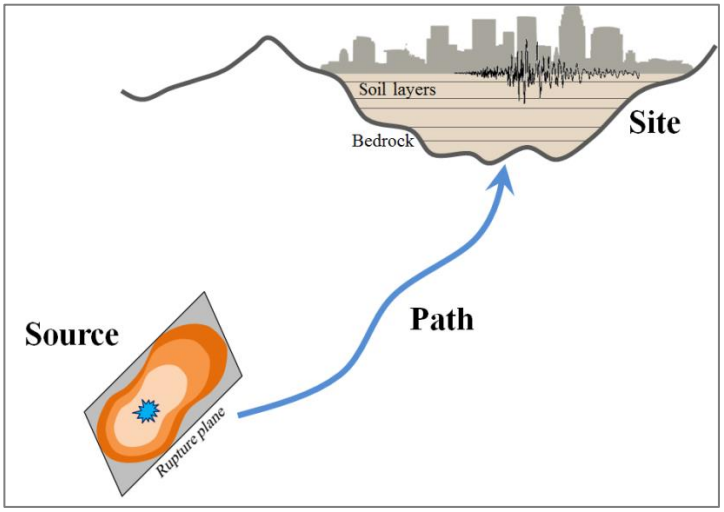

Figure 10 Schematic diagram to illustrate source, path and site effects on recorded waveform

Seismic moment (M_0) and moment magnitude (Mw) are estimated by fitting the theoretical Brune (1970) model to the spectral level ($\Omega 0$) of the average displacement source spectrum calculated from observed ground motions:

$$M_0 = \frac{4\pi\rho\beta^3\Omega_0}{FVR_{\theta\emptyset}} \qquad (7)$$

$$M_w = \frac{2}{3}\log(M_0) - 10.7 \qquad (8)$$

where ρ is density, β is the phase velocity, F is free surface effect, V is the partitioning of seismic energy and $R_{\theta\emptyset}$ accounts for the average radiation pattern (Boore, 2003). In moment magnitude calculations the generic rock model (Boore and Joyner, 1987) was used to estimate crustal properties (ρ and β) at source depths.

Figure 11 illustrates an example of moment magnitude calculation for the large event detected on Jan. 12, 2016 at 18:27:23 near Fox Creek. In order to capture the signal energy, the signal window is defined as the time from P-wave arrival to when 90% of cumulative arias intensity (Figure 11A) is achieved. A signal window starting on S-wave arrival was also evaluated and the results do not show significant differences (Figure 11B green and orange lines).

The Fourier displacement spectrum (FDS) for the raw signal, processed signal and noise is shown in Figure 11B. Bandpass filtering between 0.5 Hz and 40 Hz was applied to the signal. In order to ensure reliable moment magnitude estimation, it is important to consider degree of noise contamination for the frequencies of interest. As such, the usable FDS is defined as being where the signal to noise ratio (SNR) is higher than 3.

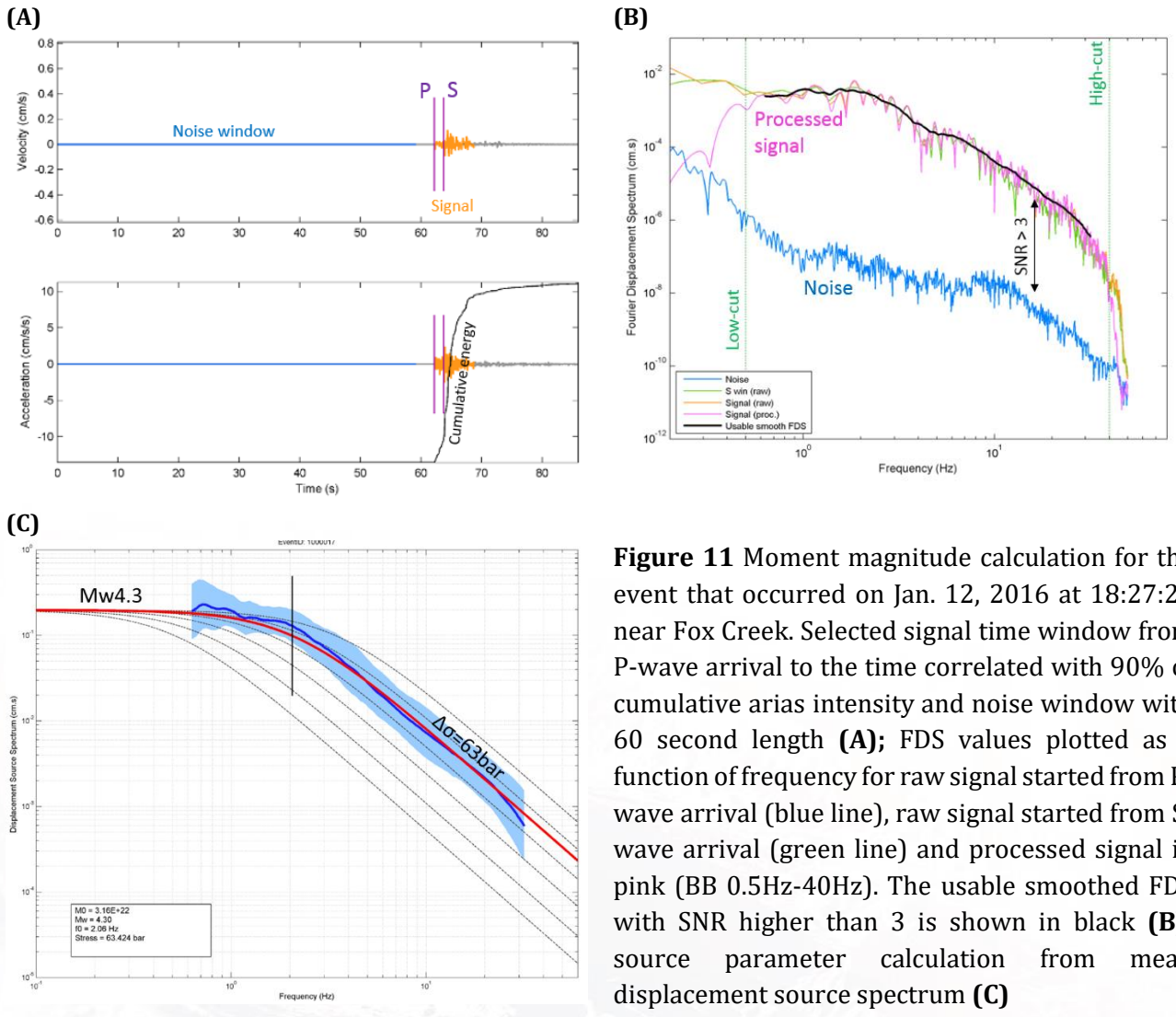

Figure 11 Moment magnitude calculation for the event that occurred on Jan. 12, 2016 at 18:27:23 near Fox Creek. Selected signal time window from P-wave arrival to the time correlated with 90% of cumulative arias intensity and noise window with 60 second length **(A);** FDS values plotted as a function of frequency for raw signal started from P-wave arrival (blue line), raw signal started from S-wave arrival (green line) and processed signal in pink (BB 0.5Hz-40Hz). The usable smoothed FDS with SNR higher than 3 is shown in black **(B);** source parameter calculation from mean displacement source spectrum **(C)**

The above analysis is performed on all the vertical channel ground motions from all stations for this event. The mean displacement source spectrum is determined from observed Fourier spectra after correcting for distance attenuation. Seismic moment and moment magnitude are estimated from low-frequency amplitudes (f<fc) and stress drop is calculated by matching the source spectra at high frequencies (f>fc) (Figure 11C).

Moment magnitudes are calculated using the spectral fitting approach for select well-recorded events, with five or more recordings within 50km, including all events with ML>2 and 50 randomly selected matching events with ML1.0 - ML2.0. To ensure potential noise contamination at low-frequencies is eliminated properly, bandpass filter of 0.5 Hz to 40Hz is applied to events of ML≥2.5, and 1.0 Hz to 40Hz for events of ML<2.5.

In addition to spectral fitting, moment magnitudes are calculated using the pseudo spectral accelerations (PSA), based on an approach proposed by Atkinson et al, 2014 (AGY14) and Novakovic and Atkinson, 2015 (NA15). This simple method takes advantage of the fact that for small events the response spectrum is well-correlated with seismic moment for periods greater than 0.3 second, and can be predicted from a simple stochastic point-source model. The linear equation calculates Mw from the 1 second pseudo-acceleration amplitudes (PSA) for events with Mw≥3 or the 0.3 second PSA for events with Mw<3 at each station. This equation corrects for the effects of attenuation and is defined as:

$$\mathrm{Mw} = \frac{\log PSA_T - C_T + \log Z(R) + \gamma_T R}{1.45} \qquad (9)$$

where γ represents the coefficient of anelastic attenuation and Z(R) is the geometrical attenuation that is given by:

$$\log Z(R) = \begin{cases} 1.3\log R & R \le 50\ km \\ 1.3\log 50 + 0.5\log(R/50) & R > 50\ km \end{cases} \qquad (10)$$

The logarithmic terms are base 10, R is hypocentral distance in km and PSA is in cm/s^2.

The result presented in Figure 12 illustrates that moment magnitudes estimated from spectral fitting agree very well with PSA-based moment magnitudes, as well as Regional Moment Tensor solutions (RMT solutions).

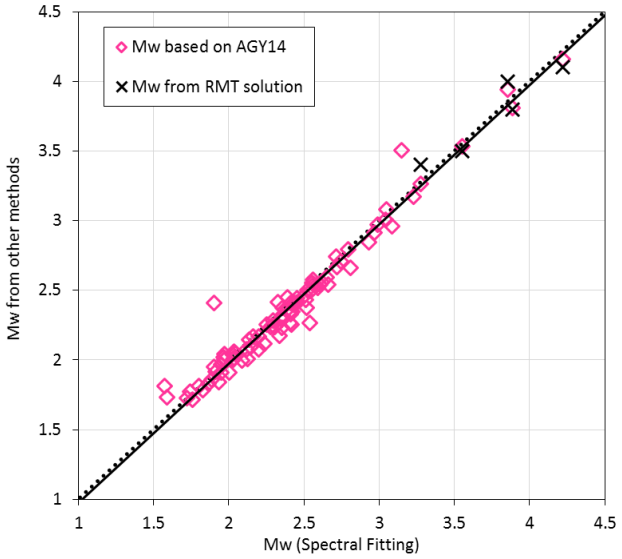

Figure 12 Comparison of moment magnitude estimations from spectral fitting method with PSA-based technique and RMT solutions.

3.7 ML - MW CONVERSION AND FINAL COMPOSITE CATALOG

To generate a uniform catalog with moment magnitudes, the relationship between the newly calculated ML and Mw is evaluated (Figure 13). The resulting ML-Mw conversion equation is defined as:

$$\mathrm{Mw} = \begin{cases} \mathrm{ML} & ML > 3.3 \\ 1.09 + 0.67 \times \mathrm{ML} & ML \leq 3.3 \end{cases} \qquad (11)$$

(A)

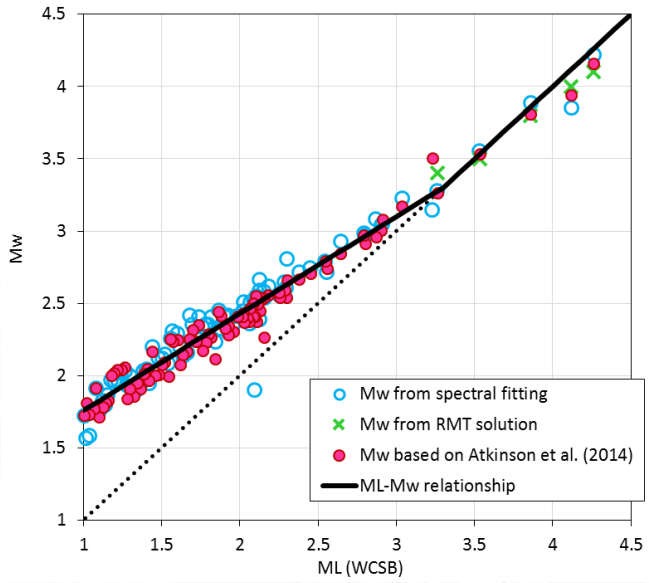

(B)

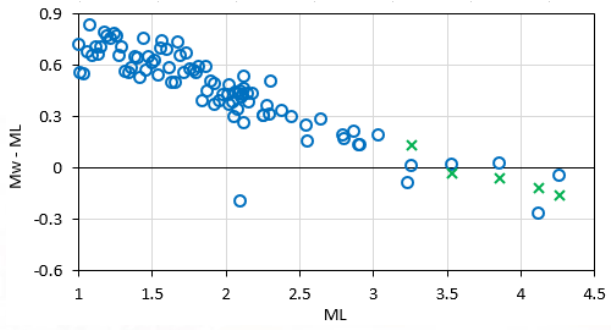

Figure 13 Calculated moment magnitudes from three methods including spectral fitting, PSA-based and RMT solutions are plotted as a function of local magnitude. Both magnitude scales follow 1:1 line for events with ML>3.3. Moment magnitudes are understimated for events with ML≤3.3 **(A);** differences between Mw (from spectral fitting and RMT solution) and ML is plotted as a function of ML **(B)**.

Following conversion of local magnitudes to moment magnitudes, the final composite seismicity catalog with moment magnitude is generated. Note that moment magnitudes from RMT solutions are the preferred magnitude, and were used if available. This catalog includes all induced seismicity recorded by six networks within a 300km radius of the Seismic Hazard Map Region between January 2013 and January 2016 (Figure 14).

(A) **(B)**

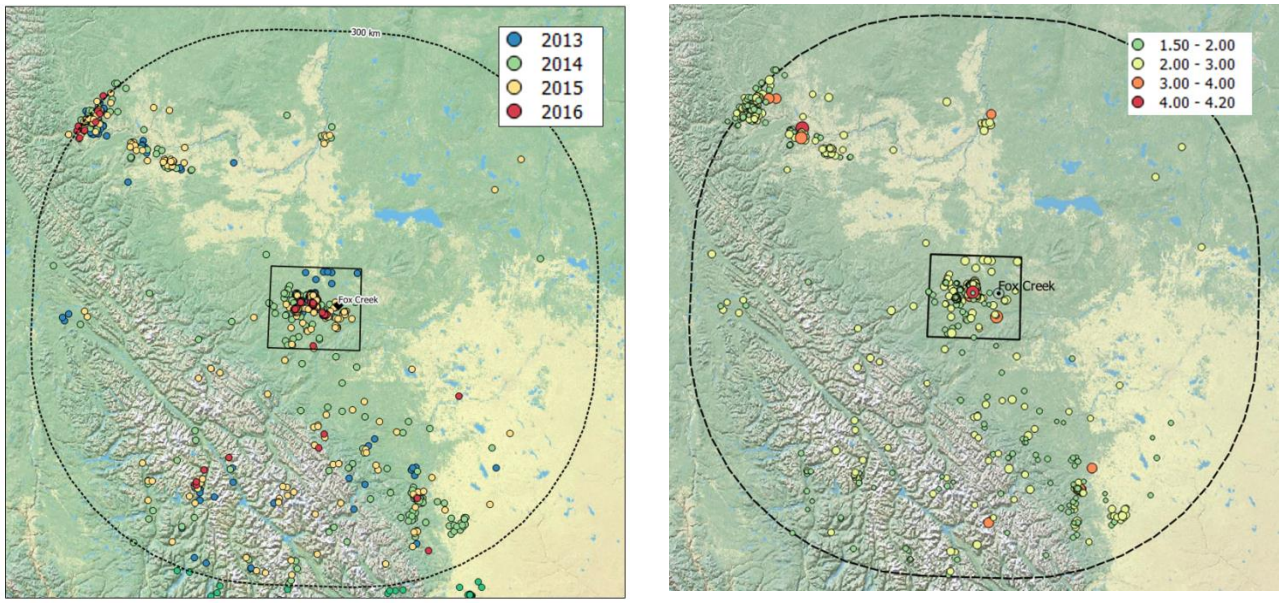

Figure 14 Final composite catalog with moment magnitude Mw>1.5, color coded by time **(A)** and magnitude **(B)**

4.0 IDENTIFICATION OF INDUCED SEISMIC SOURCE ZONES

To capture the spatio-temporal variation of induced seismicity in Fox Creek region, earthquake sequences are examined in time and space domains. We identify 3 years to perform hazard calculations, each of which start on February 1st of the year and end on January 31st of the next year (Figure 15Figure 15).

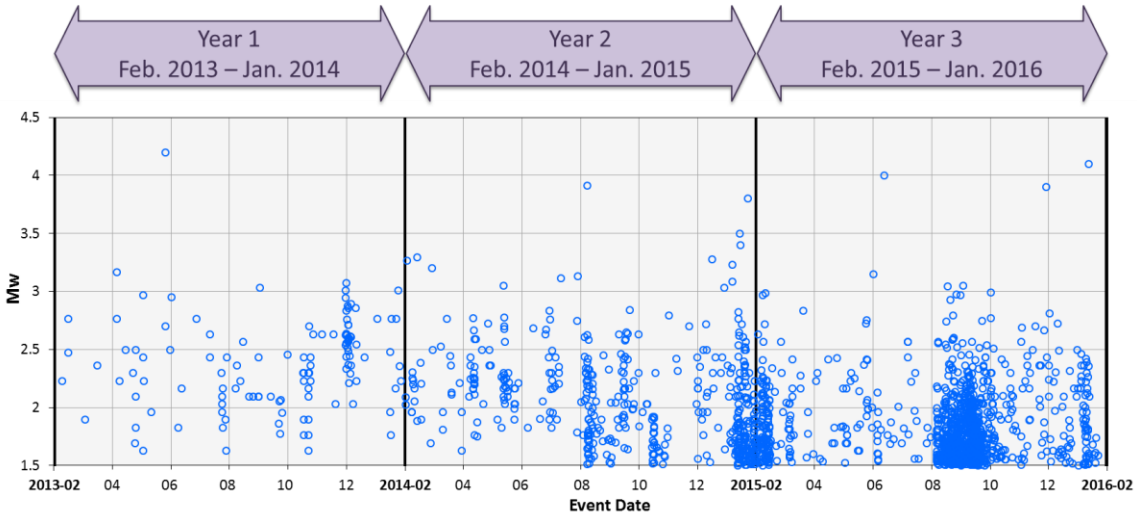

Figure 15 Temporal distribution of event magnitudes for induced events in the composite catalog.

We define source zones for each year based on the visual inspection of clustered activities in the PSHA region. Figure 16 to 18 illustrate the number and locations of the source zones for the three hazard years. Note that the existence of recording stations near an event cluster improves the location accuracy of the events from that cluster. Therefore, the earthquake sequences observed before the deployment of local networks (September 2014) spread over larger areas than those observed during the operation of local networks. This location uncertainty maps into the geometry of those source zones. For this reason, the source zones for 2014 is divided into two time periods as illustrated in Figure 17.

The labels and geometry of source zones are provided in the electronic supplementary shapefiles.

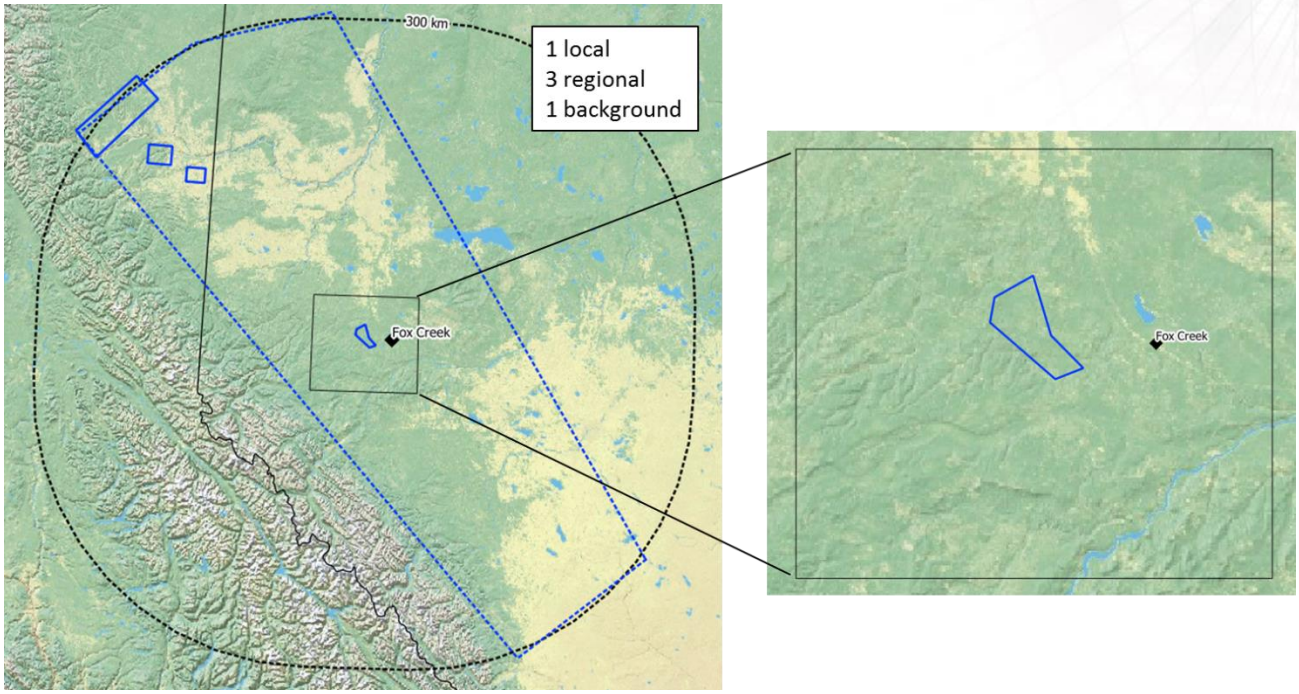

Figure 16 Active zones of induced seismicity in 2013.

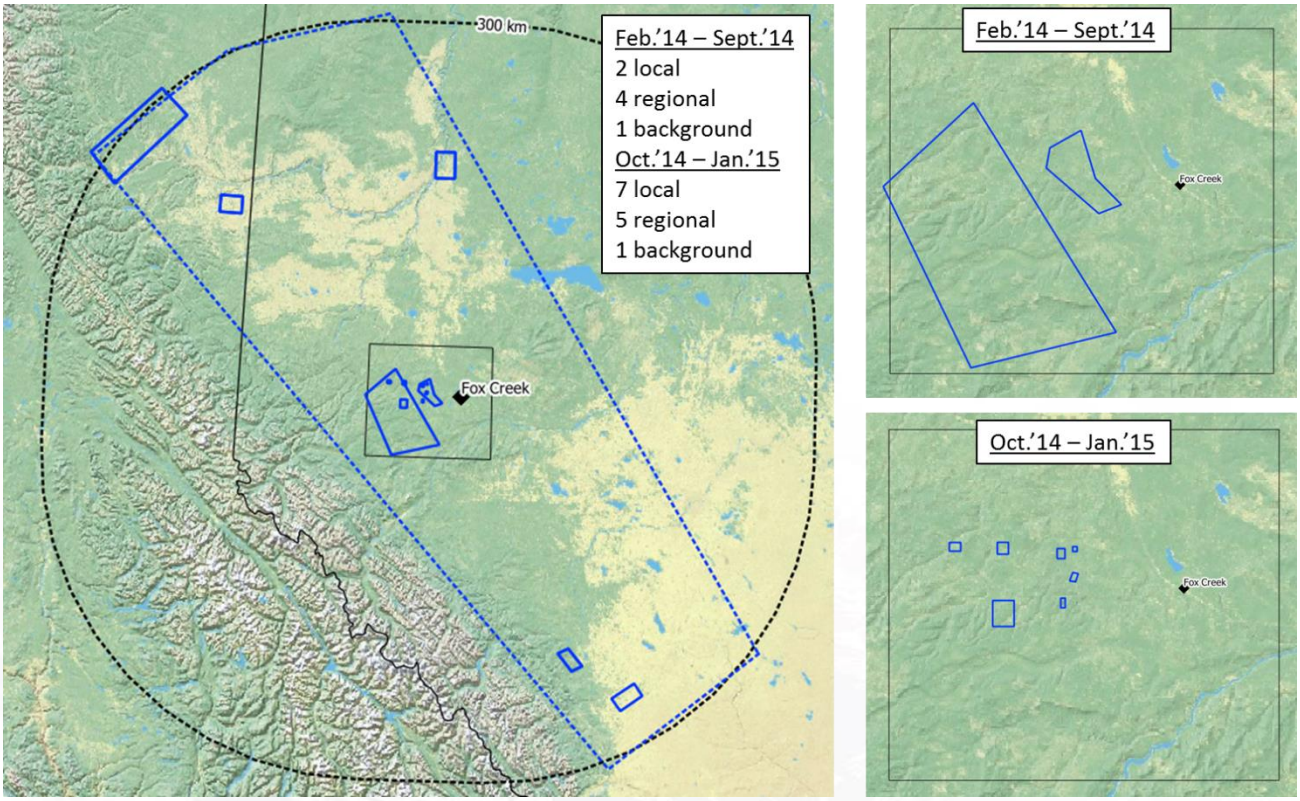

Figure 17 Active zones of induced seismicity in 2014

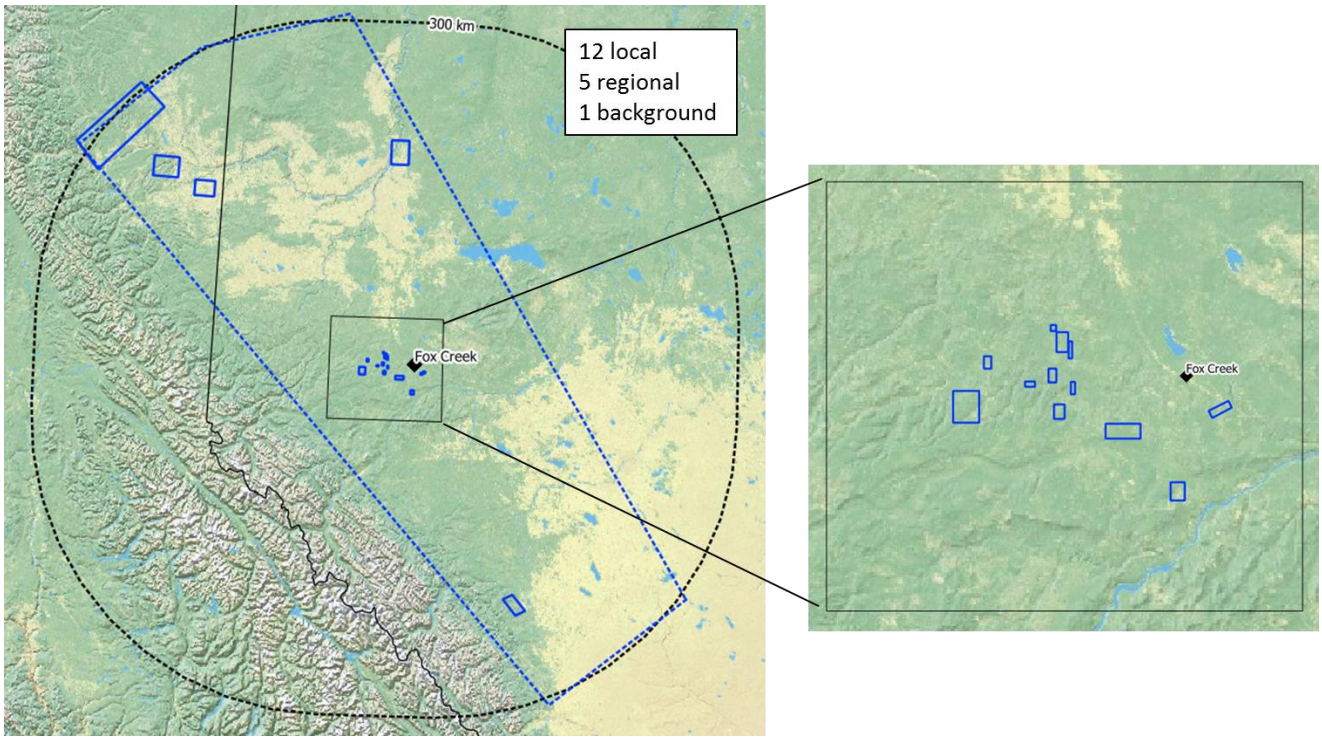

Figure 18 Active zones of induced seismicity in 2015

5.0 MAGNITUDE RECURRENCE RELATIONSHIPS

Once the induced seismicity source zones are defined, we inspect temporal seismic activities in each zone to identify earthquake sequences. Magnitude of completeness (Mc), activity rate for M>Mc and b-values are determined for each sequence, to characterize the magnitude recurrence relationship. The Mc generally attains values between M2.0 and M2.5 for regional and background zones, and does not change much over the three years. However, the magnitude of completeness for local zones in Fox Creek region decreases from Mc=2.6 in 2013 to Mc=1.2-1.5 in 2015, with the deployment of local networks in the region. We observed large variation of b-values (from 0.5 to 2.7) between difference sequences. In order to model probability distribution of magnitudes robustly in hazard analysis, we associated each sequence to a pre-defined b-value based on a hypothesis testing approach.

We identify three classes of b-values to associate with induced seismicity sequences observed in Fox Creek region. The candidate b-values are selected based on the overall spread of magnitude recurrences that are normalized to attain (M≥1.5)=100, for sequences where Mc≤1.5. The standard tectonic value of b=1 is chosen as a default b-value class. The steep and mild b-value classes are selected as 1.6 and 0.6, respectively. Each sequence is associated with a b-value class based on the statistical hypothesis testing of candidate b-values. Additionally, we define a low and high branch for each b-value class in order to account for the epistemic uncertainty in associated b-values.

We give stronger emphasis on the default b-value, unless there is a compelling evidence for steep or mild b-value. We perform a two-tailed hypothesis testing for the default b-value. For each sequence, the expected rate of M≥2.5 events is calculated from observed N(M≥1.5), assuming b=1. Then, the likelihood of observed N(M≥2.5) is calculated, assuming the Poisson distribution. The null hypothesis (H0: b = 1) is rejected in favor of the steep b-value, if the sequence is very active (i.e., observed N(M≥1.5) is larger than 50) and the likelihood of observed N(M≥2.5) is very small ($p < 0.025$).

Figure 19 shows normalized magnitude recurrences for sequences where the default b=1 is selected. We selected b=0.8 (w=0.25) and b=1.2 (w=0.25) as the low and high branches for the default b class. The center-value of default-b class (1.0) is given a weight of w=0.5.

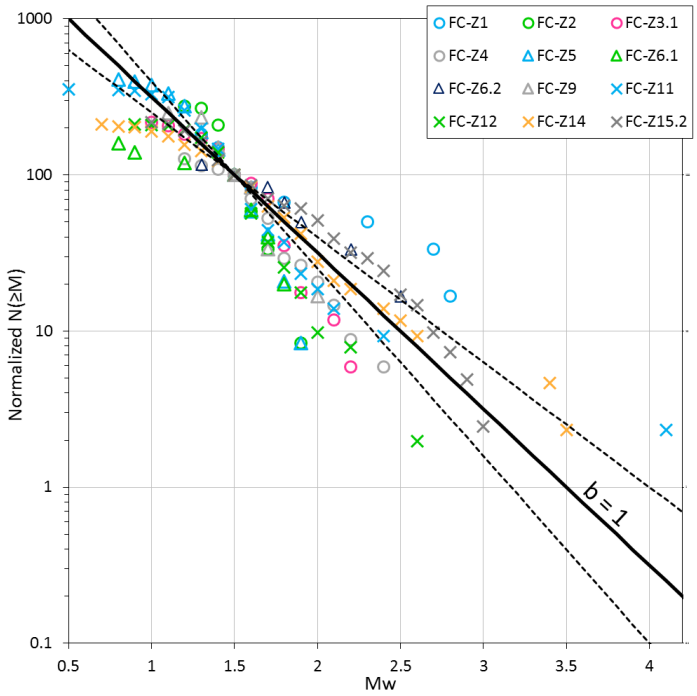

Figure 19 Normalized magnitude recurrences of sequences for which the default b=1 is selected. Dashed lines show normalized magnitude recurrences for low (b=0.8) and high (b=0.8) branches of the default b class.

Figure 20 shows normalized magnitude recurrences for sequences where b=1.6 is selected. For the steep-b class, we consider b=1.4 (w=0.25) and b=1.8 (w=0.25) as the low and high branches. The center-value of steep-b class (1.6) is given a weight of w=0.5.

We define FC-Z8 sequence as a mild-b sequence (0.6) because relatively large numver of M≥3 events were observed compared to the overall activity rate. We selected b=0.5 (w=0.25) and b=0.7 (w=0.25) as the low and high branches for the mild-b class. The center-value of mild-b class (0.6) is given a weight of w=0.5.

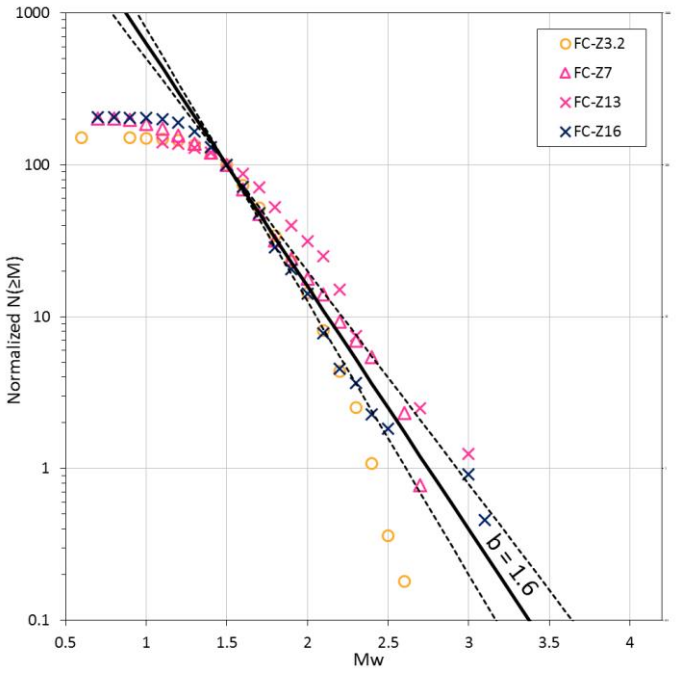

Figure 20 Normalized magnitude recurrences of sequences for which steep b=1.6 is selected. Dashed lines show normalized magnitude recurrences for low (b=1.4) and high (b=1.8) branches of the steep b class.

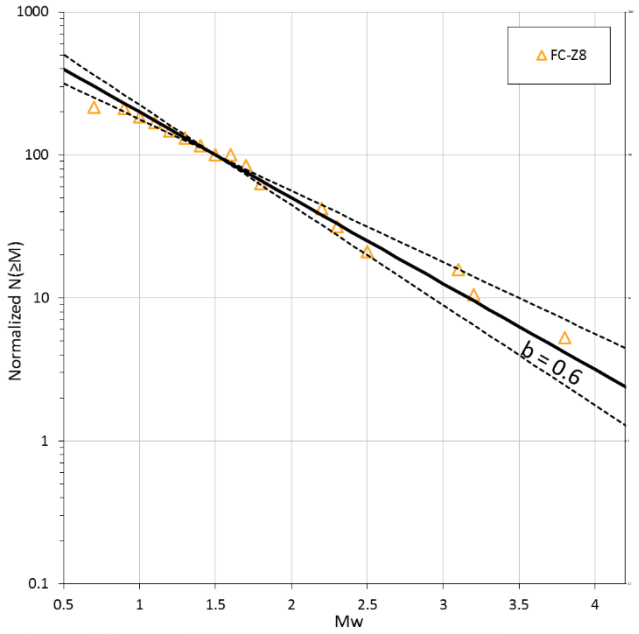

Figure 21 Normalized magnitude recurrence of sequence for which mild b=0.6 is selected. Dashed lines show normalized magnitude recurrences for low (b=0.5) and high (b=0.7) branches of the mild b class.

6.0 GROUND MOTION PREDICTION EQUATION

We adjusted two published ground motion prediction equations (GMPEs) to the observed ground motions in western Alberta to develop a GMPE suite that will be used in induced seismicity hazard calculations for Fox Creek region. A total of 25 events of Mw≥2.8 that were recorded by at least 3 stations within 300 km are selected. 21 of the selected events were obtained in Duvernay.

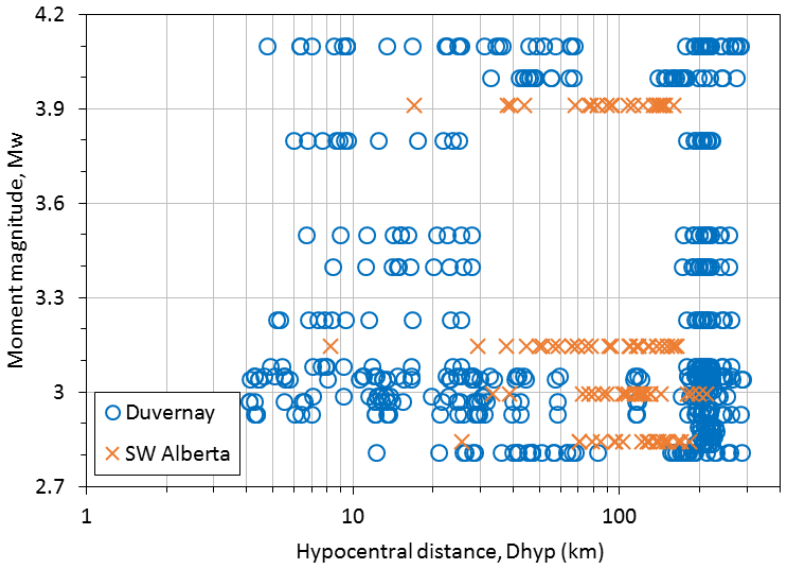

Figure 22 Ground motion dataset used in GMPE adjustment.

The majority of ground motions within 50 km were recorded by stations in Duvernay, whereas far-distance motions were primarily recorded by stations located in SW Alberta. This may cause trade-offs between attenuation and site terms in GMPEs if there is a discrepancy in site effects between the two station groups. We determine H/V ratios of stations in Duvernay and SW Alberta, in order to gain insights into site effect differences between the two station groups.

The average H/V from Duvernay stations are larger than the average H/V from other stations by 0.1 log units, over all periods. Based on this observation, we deduce that stations located in Duvernay and elsewhere show similar site effects, on average. We assume the average of all stations as the reference site condition for the GMPE suite to be developed, ignoring the relative differences between stations. The comparison of average H/V ratios with the site amplifications estimated from Boore et al. (2014) for site class D (V_{S30}=250m/s) show a good agreement over all periods. Therefore, we assume that the average site condition in Duvernay is a class D site.

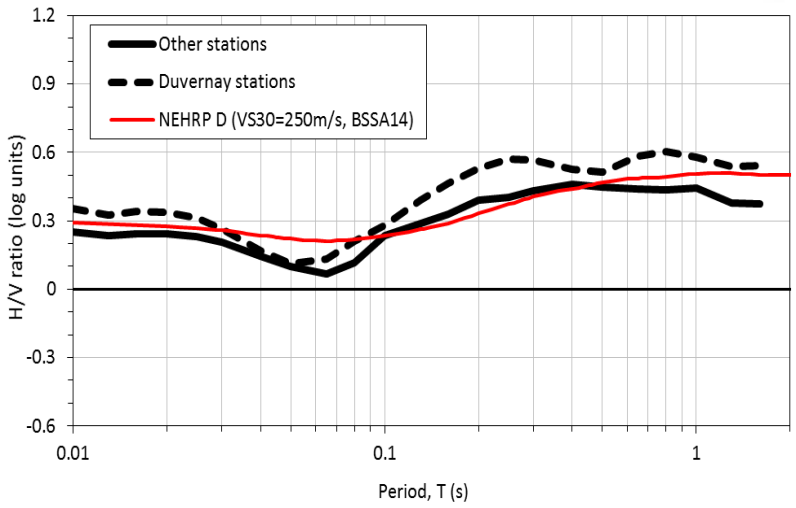

Figure 23 Average H/V ratio for stations located in Duvernay and elsewhere. Red line shows the site amplification for a site class D (VS30=250m/s) estimated based on Boore et al. (2014).

We assess the decay of ground motion amplitudes with distance in order to gain preliminary insight on the regional attenuation attributes. We determine normalized ground motion amplitudes according to the following approach:

1. Identify a reference distance range within which ground motions from different events overlap most.
2. Calculate the geometric mean of amplitudes for each event at the reference distance bin.
3. Normalize observed amplitudes from each event by the mean amplitude calculated at the reference distance bin for the associated event.

This method effectively removes the source effects and reveals the attenuation characteristics in the region. Figure 24 compares the decay of normalized amplitudes with the attenuation models of two alternative GMPEs: Atkinson (2015, referred to as A15) and Yenier and Atkinson (2015, referred to as YA15). It should be noted that the A15 model was for distances less than 50 km and it is extrapolated to larger distances with no modification (i.e., no surface-wave spreading and anelastic attenuation effects are included) in Figure 24. All GMPEs agree well with the ground-motion attenuation observed within 50 km. The A15 model does a relatively better job in capturing the decay of close distance motions (<5 km). Attenuation at far distances (>50km) appears to be between CENA and WNA models for T≥0.2s. For very short periods (T<0.2s), the rate of attenuation at far distances is less than the CENA model.

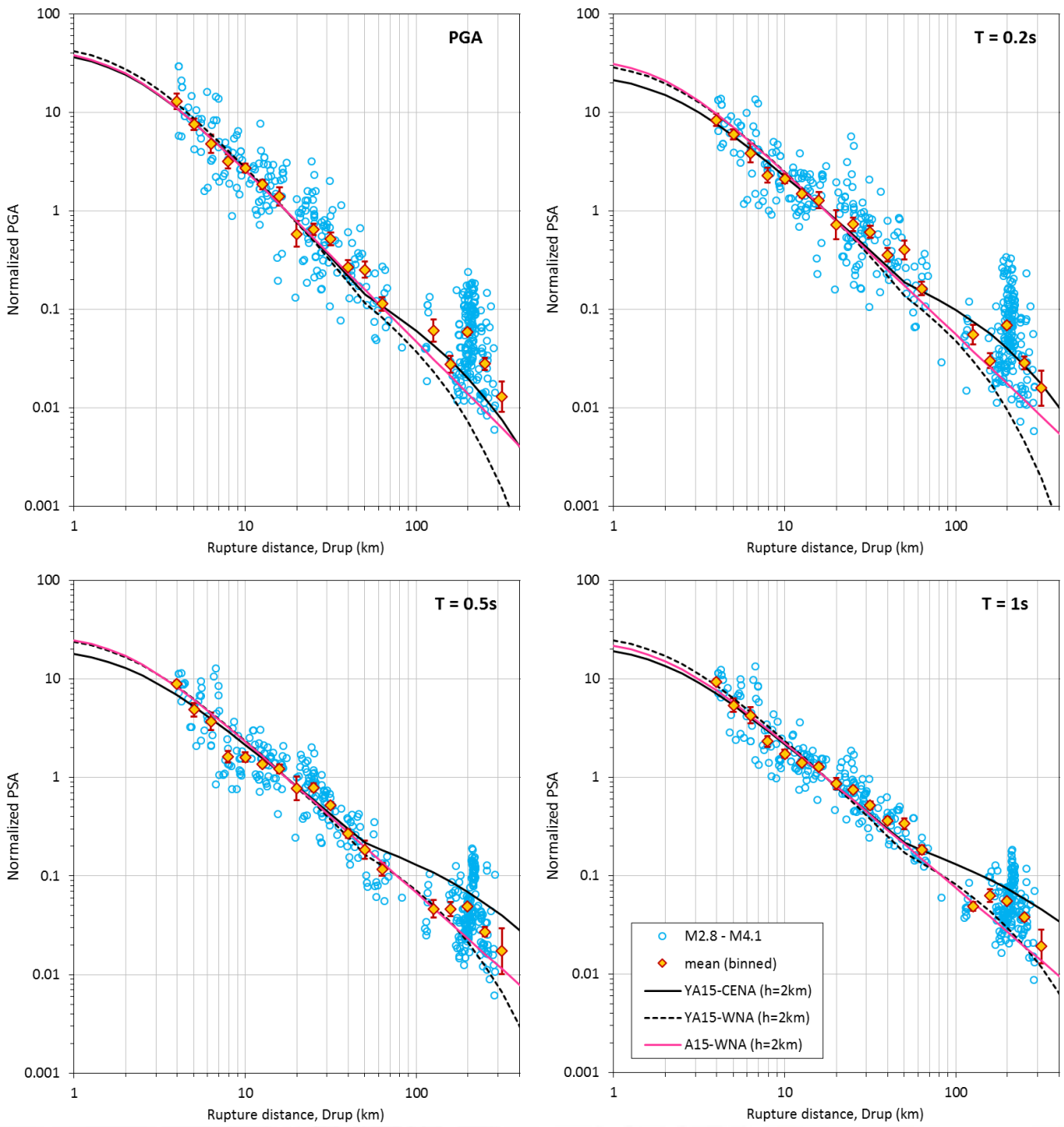

Figure 24 Decay of ground motion amplitudes with distance in western Alberta. Circles indicate normalized amplitudes of individual records obtained from events of M>2.8. Lines represent published GMPEs for CENA (Central and Eastern North America) and WNA (Western North America).

We adjust A15 and YA15-CENA models for the ground motions observed in western Alberta, using the referenced empirical approach (Atkinson, 2008; Atkinson and Boore, 2011; Hassani and

Atkinson 2015), in which a simple adjustment to a well-defined host GMPE is made by examination of residuals in the target region. The models so-developed are referred to here as adjusted models. The method is summarized as follows:

1. Evaluate the host GMPE for the known magnitude and distance and determine model residuals for the observed ground motion data.
2. Calculate average residual for each event using stations within 50km. Event residuals include following effects:
   i. differences in stress between the region for which the host GMPE was developed and western Alberta
   ii. average site effects in western Alberta relative to the reference site condition for the host GMPE (site class B/C; VS30=760m/s)
   iii. all other residual source effects that are missing/different in the host GMPE.
3. Examine the variation of event residuals with magnitude to ensure that the magnitude scaling of the host GMPE is working properly for the recorded events
4. Determine an overall model adjustment by taking the average of event residuals for M>2.8.
5. Determine far-distance (>50km) attenuation adjustment based on inspection of the event-corrected residuals with distance (This is achieved by modeling event-corrected residuals using a trilinear function to accommodate the observed Moho-bounce effects at distances between 70 km and 140 km).
6. Add adjustments determined in steps 4 and 5 to the base GMPE to obtain the regionally adjusted GMPE.

The adjusted A15 model is given as:

$$\log Y_{A15} = (c_0 + \Delta c_0) + c_1\mathbf{M} + c_2\mathbf{M}^2 + c_3 log R + \begin{cases} 0 & R < 70\text{km} \\ \Delta c_3 \log(R/70) & 70 \le R < 140\text{km} \\ \Delta c_3 \log(140/70) & R \ge 140\text{km} \end{cases} \quad (12)$$

where c_0, c_1, c_2 and c_3 terms are model coefficients of the original A15 model. The reader is referred to Atkinson (2015) for details about the original A15 model. The Δc_0 term and the last term in Equation 12 are model adjustments determined in steps 4 and 5 for the A15 model, where:

$$\Delta c_0 = \begin{cases} -0.3 & T < 0.1\text{s} \\ \dfrac{0.5 \log(T/0.1)}{\log(5)} - 0.3 & 0.1s \le T < 0.5\text{s} \\ 0.2 & T \ge 0.5\text{s} \end{cases} \quad (13)$$

$$\Delta c_3 = \begin{cases} 2.2 & T < 0.1\text{s} \\ 2.2 - 1.4\log(T/0.1) & 0.1s \le T < 1\text{s} \\ 0.8 & T \ge 1\text{s} \end{cases} \quad (14)$$

Similarly, the adjusted YA15 model is given as:

$$\log Y_{YA15} = F_M + F_{\Delta\sigma cena} + F_Z + F_{\gamma cena} + \Delta C + \begin{cases} 0 & R < 70\text{km} \\ \Delta b_2 \log(R/70) & 70 \le R < 140\text{km} \\ \Delta b_2 \log(140/70) & R \ge 140\text{km} \end{cases} \quad (15)$$

where F_M, $F_{\Delta\sigma}$, F_Z and F_γ are functions of magnitude scaling, stress adjustment, geometrical spreading and anleastic attenuation for the original YA15 model. Here, $F_{\Delta\sigma}$ and F_γ functions are evaluated for stress and anelastic attenuation models determined for CENA by YA15. The stress model is also constrained at a fixed depth of 3.5 km, consistent with induced events in Fox Creek. The reader is referred to Yenier and Atkinson (2015) for details about the original YA15 model.

The ΔC term and the last term in Equation 15 are model adjustments determined in steps 4 and 5 for the YA15 model, where:

$$\Delta C = \begin{cases} -0.670 & T < 0.08\text{s} \\ \dfrac{0.836\log(T/0.08)}{\log(0.65/0.08)} - 0.670 & 0.08s \le T < 0.65\text{s} \\ 0.166 & T \ge 0.65\text{s} \end{cases} \quad (16)$$

$$\Delta b_2 = \begin{cases} 1.459 & T < 0.13\text{s} \\ -\dfrac{1.459\log(T/0.13)}{\log(0.4/0.13)} + 1.459 & 0.13s \le T < 0.4\text{s} \\ 0 & T \ge 0.4\text{s} \end{cases} \quad (17)$$

Figure 25 and 26 shows the adjusted A15 and YA15 models in comparison to the observed amplitudes, for different magnitude bins. Both models agree well with the empirical observations. Adjusted A15 model, however, performs better for the large magnitude bin. Note that both adjusted GMPEs show a tendency to under predict amplitudes at the close distances for M3.8-M4.1 bin, which are primarily from the M4.1 event occurred on January 12, 2016, in Fox Creek region. It is not known if the elevated ground motions are a feature of this particular event, or is generic

for large events in the region. Also note the lack of ground motions at distances less than 5 km, which puts additional ambiguity on the close-distance saturation attributes of large events (M>4). These features require careful consideration in the modeling of epistemic uncertainty in the GMPEs.

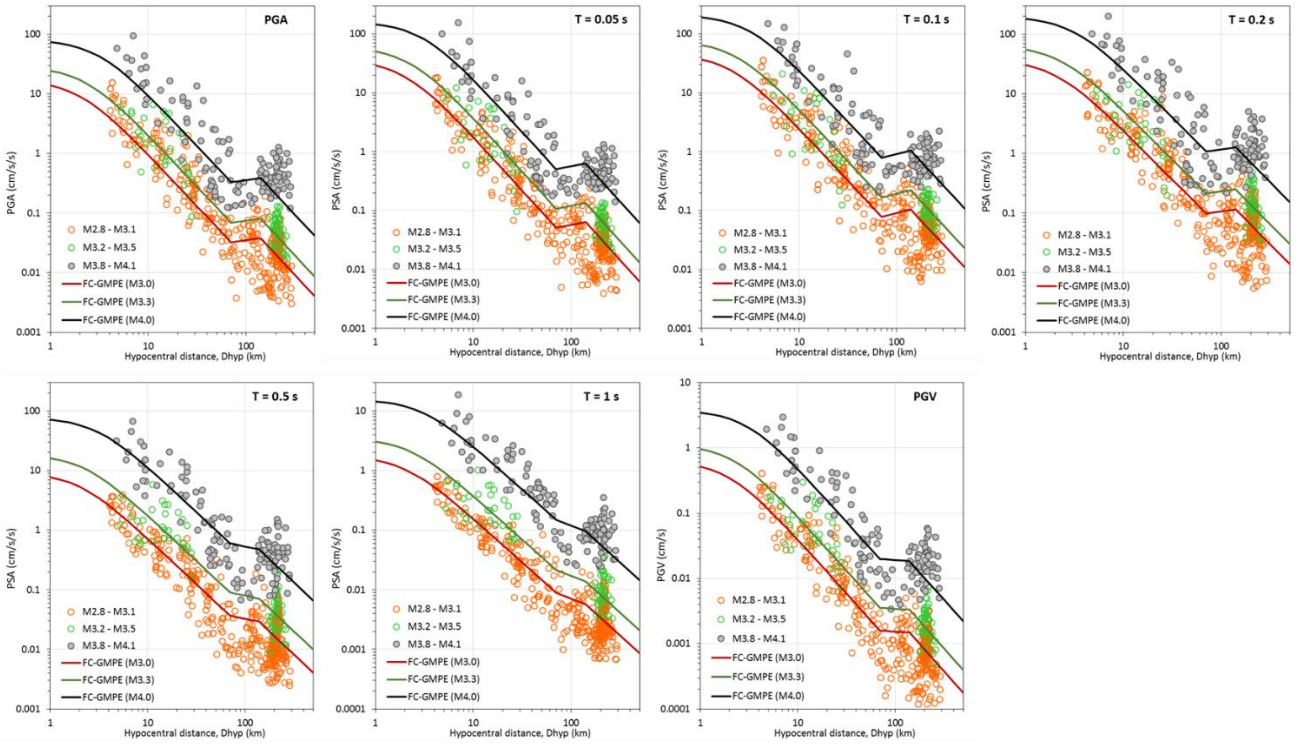

Figure 25 Comparison of observed ground motions with the predictions of adjusted A15 model.

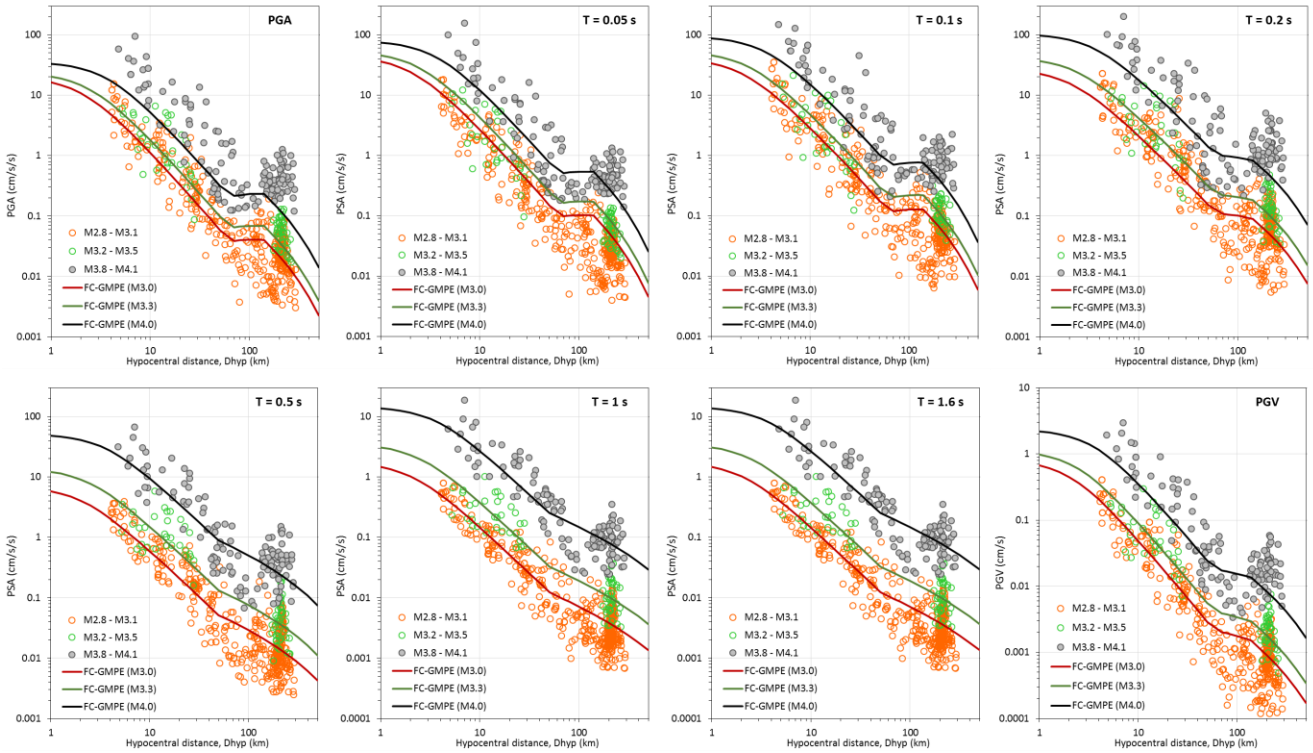

Figure 26 Comparison of observed ground motions with the predictions of adjusted YA15 model.

The adjusted A15 model is chosen as the center branch for GMPE suite to be used in PSHA because it agrees better with the observed amplitudes for M3.8-M4.1 events in Fox Creek. We adopted the aleatory uncertainty (σ) recommended by Atkinson and Adams (2013) for NBCC. The lower and upper branches of the GMPE suite are determined based on following criteria:

1. The epistemic uncertainty (Δ) should not be less than that considered in NBCC for WNA models: Δ=min(0.1+0.0007R,0.3).
2. The lower and upper branches should be wide enough to capture the discrepancy between the median ground motion estimates of adjusted YA15 model and the center branch (A15).
3. The high branch should accommodate the residual trend noted for M3.8-M4.1 events at short distances.

The epistemic uncertainty for Fox Creek GMPE suite is defined as:

$$\Delta = \max(0.5-0.15\log R, 0.3) \qquad (18)$$

Figure 27 shows the logarithm of the ratio of the adjusted YA15 model to the center GMPE (adjusted A15 model) for different magnitudes (M4 to M7), as a function of distance. Black lines shows the -Δ and +Δ values subtracted from and added to the center GMPE. Circles indicate model residuals for M3.8-M4.1 events for the center GMPE. The +Δ values well accommodate the residual

trends observed at close distances. Negative and positive delta factors are wide enough to capture the discrepancy between YA15 model and the center GMPE. Δ is added to and subtracted from center GMPE to obtain upper and lower GMPE branches.

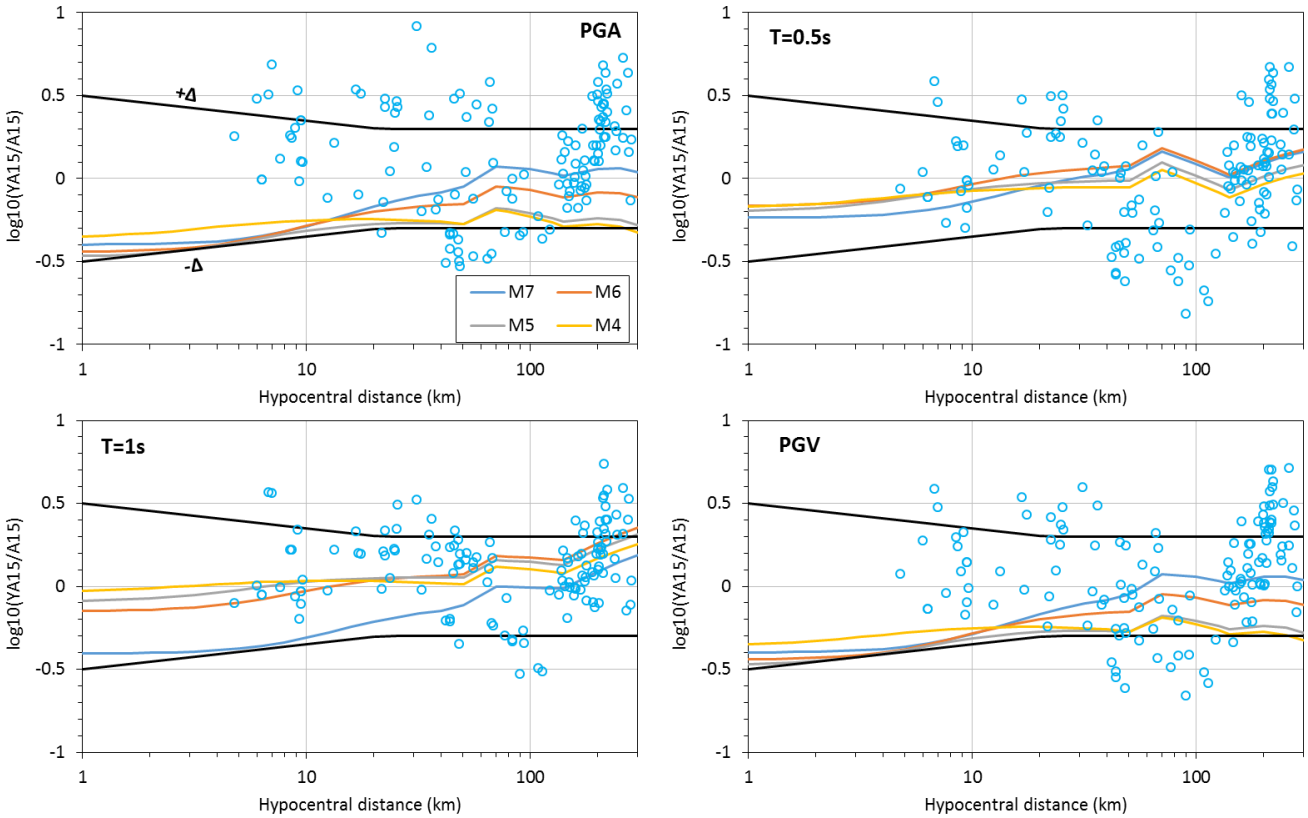

Figure 27 Ratio of the adjusted YA15 model to the center GMPE (adjusted A15 model).

The derived GMPE suite correspond to the average site condition in Fox Creek region, which is assumed to be site class D (stiff soil, VS30=250m/s). It is worth mentioning that site effects are assumed to be the same for all magnitudes, regardless of the intensity of ground shaking. Figure 28 illustrates the GMPE suite for different magnitudes and spectral periods, as a function of distance. The ground motion prediction tables of the derived GMPE suite are provided in the electronic supplementary of this report.

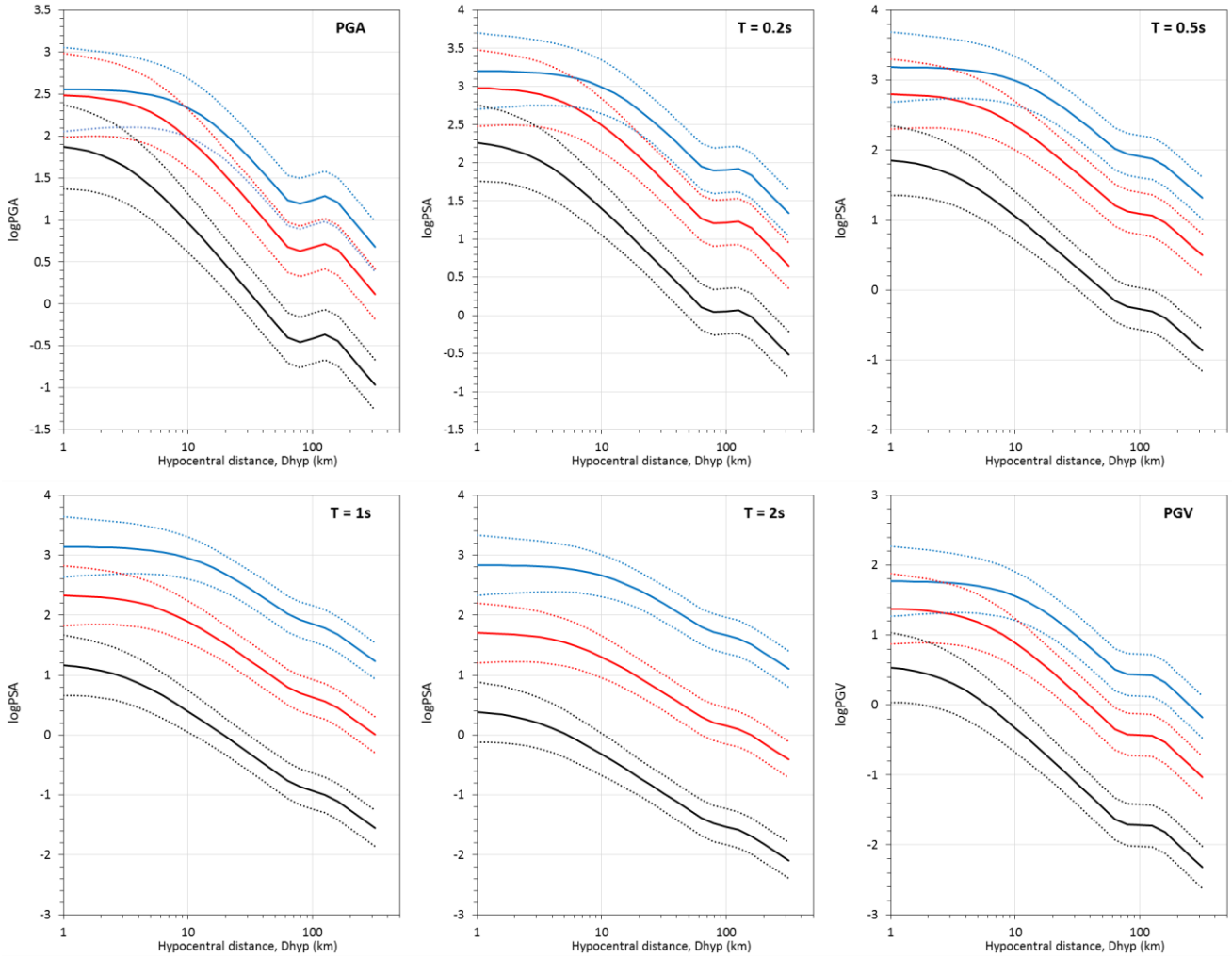

Figure 28 Western Alberta GMPE suite for M4.0 (black), M5.5 (red) and M7.0 (blue). Solid lines represent the center branch and dotted lines indicate high and low branches.

7.0 PROBABILISTIC INDUCED SEISMIC HAZARD ANALYSIS

We assess the seismic hazard associated with induced events in Fox Creek region, using a Monte-Carlo simulation technique. Predicting the seismic hazard from induced events is conceptually different from estimating the seismic hazard for tectonic earthquakes. This is because the spatio-temporal patterns of induced earthquakes are largely dependent on economic forces and public policy decisions. Therefore, induced seismicity rates are inherently variable and nonstationary. In order to capture the spatio-temporal variations in induced seismicity, we perform annual hazard analysis for 2013, 2014 and 2015, considering the active seismic zones within each year.

An open-source software, *EqHaz* (Assatourians and Atkinson, 2013) is used for the analysis. EqHaz consists of three sequential modules: *EqHaz1* generates a synthetic earthquake catalogue using the source zone geometries and magnitude recurrence statistics; *EqHaz2* calculates ground motions received at a site for the simulated catalog, and produces mean-hazard curves for a given set of spectral periods to generate uniform hazard spectrum; and *EqHaz3* compiles statistics on maximum amplitudes for a return period to deaggregate contributions from different sources.

We simulate a 247,500-year (100 x 2475yr) induced seismicity catalog, considering the associated zone geometries and magnitude recurrence parameters determined in previous sections. The probability density function of earthquake magnitude is defined using the Guttenber-Richter model, which is truncated at a maximum magnitude that might be induced.

The maximum magnitude (Mmax) of induced events is an important parameter in hazard analysis, and can have impact on the final results. There are alternative methods to estimate maximum magnitude for induced events. For example, McGarr (2014) suggested that Mmax is controlled by the cumulative injected fluid volume. In a recent study, however, Atkinson et al. (2016) indicated that the claimed relationship between maximum magnitude and injected fluid volume may not be applicable to earthquakes induced by hydraulic fracturing in the western Canadian sedimentary basin. They propose that the size of the available fault surface that is in a critical state of stress may control the maximum magnitude. Shapiro et al. (2011) claimed that maximum magnitude is limited only by the size of the fault upon which slip is initiated, and Sumy et al. (2014) argued that larger tectonic events may be triggered due to Coulomb stress transfer. Petersen et al. (2015) suggested using a large range of uncertainty to characterize maximum magnitude.

We perform a sensitivity analysis to understand the effect of Mmax on induced seismicity hazard in Fox Creek region. For this purpose, we use the 2015 induced seismicity model, assuming three alternative Mmax values of M5.0, M6.0 and M7.0. We choose M5.0 as the lower limit of maximum magnitude, following the assumption that the Mmax should be larger than the magnitude of the largest observed induced earthquake in the region: M4.6 17 August 2015 Fort St. John earthquake. The upper bound of Mmax=7.0 is deduced to consider the possibility of triggering large tectonic

earthquakes to ensure consistency with the 5th generation national seismic hazard model for western Alberta.

Figures 29 and 30 illustrate the sensitivity of hazard results to the choice of maximum magnitude, for two annual rates of exceedance (0.2% and 0.04%). Regions indicated by gray lines show induced seismicity zones. As shown, Mmax has a significant impact on the hazard level over the study region. For the town of Fox Creek, for instance, the peak ground acceleration (PGA) and short-period spectral accelerations increase by about a factor three, when Mmax is changed from M5 to M7. The influence of Mmax is even stronger for long spectral periods, particularly at low annual rates, as illustrated in Figure 31.

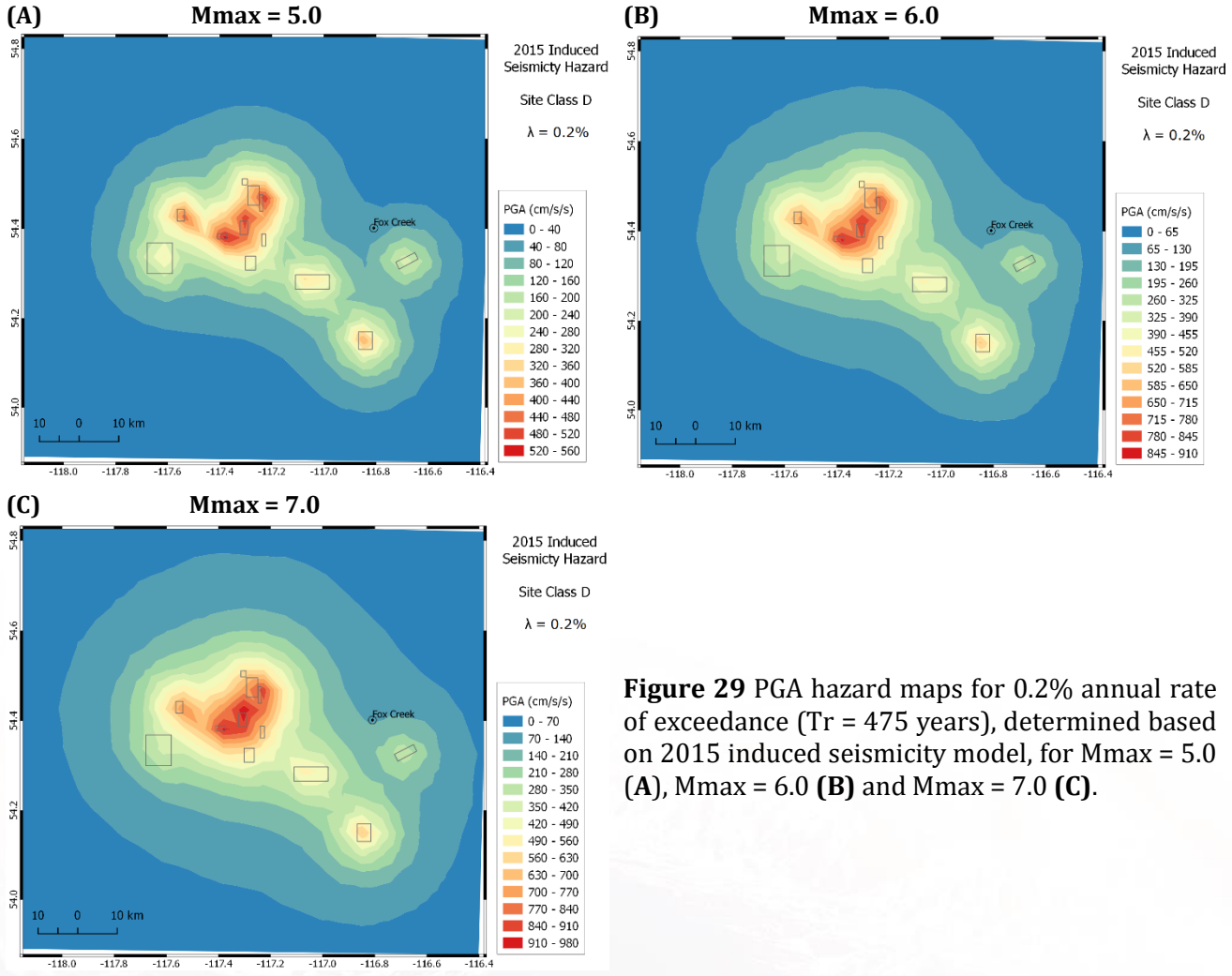

Figure 29 PGA hazard maps for 0.2% annual rate of exceedance (Tr = 475 years), determined based on 2015 induced seismicity model, for Mmax = 5.0 (**A**), Mmax = 6.0 **(B)** and Mmax = 7.0 **(C)**.

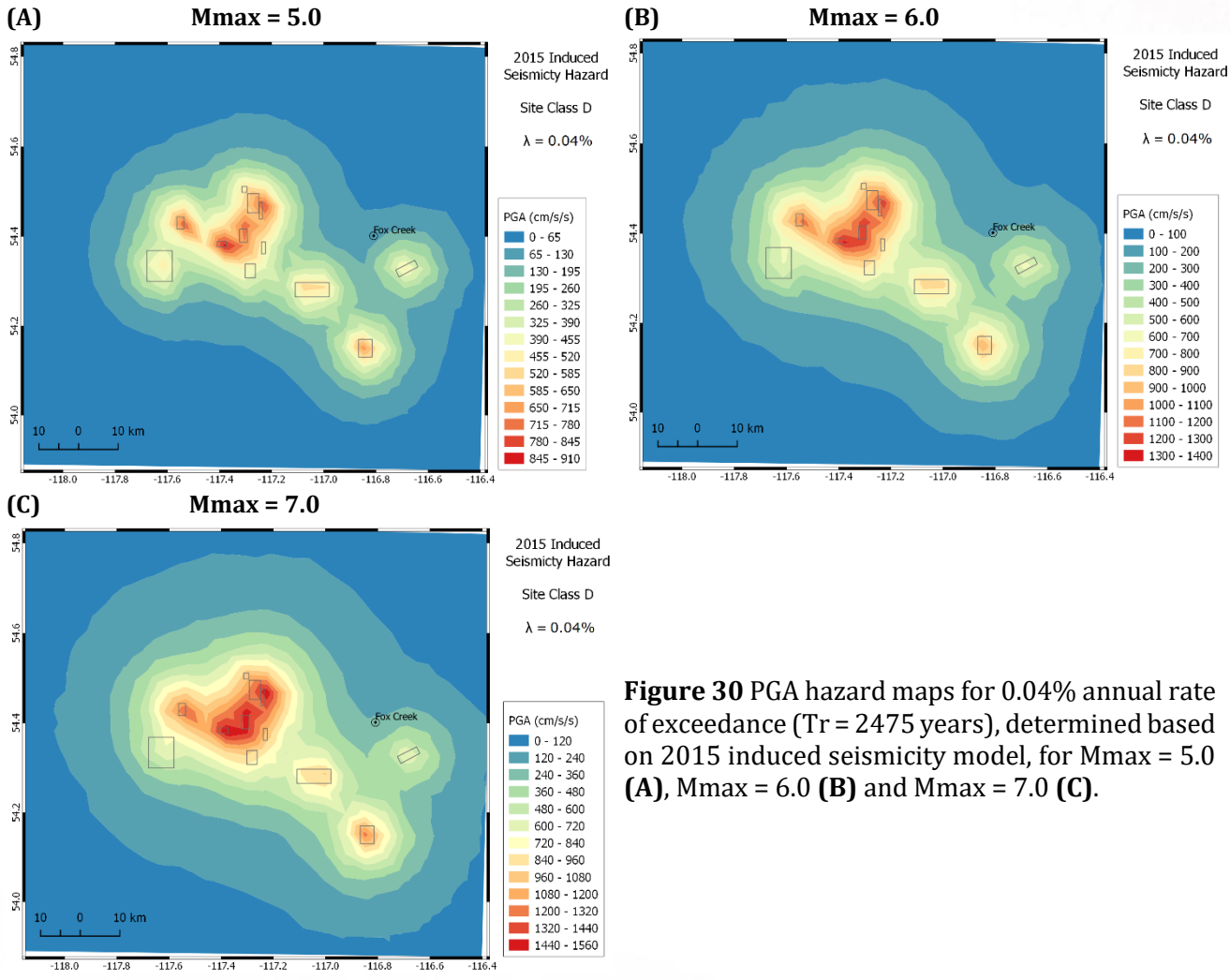

Figure 30 PGA hazard maps for 0.04% annual rate of exceedance (Tr = 2475 years), determined based on 2015 induced seismicity model, for Mmax = 5.0 **(A)**, Mmax = 6.0 **(B)** and Mmax = 7.0 **(C)**.

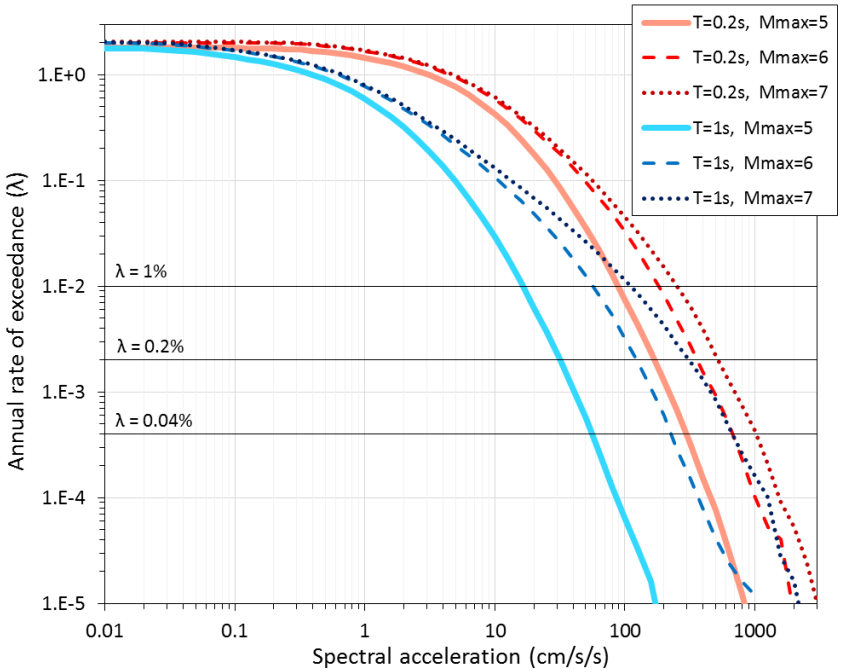

Figure 31 Hazard curves for Fox Creek, determined based on 2015 induced seismicity model, for alternative maximum magnitude estimates.

Minimum magnitude (Mmin) is also an important parameter that may have influence on hazard results. In hazard calculation of tectonic events, earthquakes of M<5 are typically not considered in analysis because such events do not generally cause damage based on an implicit assumption of typical focal depths for natural events (Atkinson et al., 2015). However, induced events are much shallower than natural events on average, and therefore may cause stronger ground motions at close epicentral distances (Hough, 2014; Atkinson, 2015). It is not known what minimum magnitude of induced earthquake might be capable of causing damage, and thus contributing to hazard (Atkinson et al., 2015). Here, we conduct a sensitivity analysis to understand the impact of Mmin on hazard results in Fox Creek region. In this respect, we consider two alternative values of Mmin: M3.5 and M4.0. We perform hazard analysis using the 2015 induced seismicity model, for each Mmin value. We use a maximum magnitude of Mmax=6.0 in this exercise.

Figure 32 shows hazard maps for the alternative Mmin values, at two annual rates of interest (0.2% and 0.04%). The choice of minimum magnitude appears to have negligible effect on the hazard level for low annual rates of exceedance. This is also illustrated in Figure 33, which depicts the hazard curves for the town of Fox Creek, for the two Mmin values. For high annual rates, however, minimum magnitude have some impact on the hazard level, as shown in Figure 33.

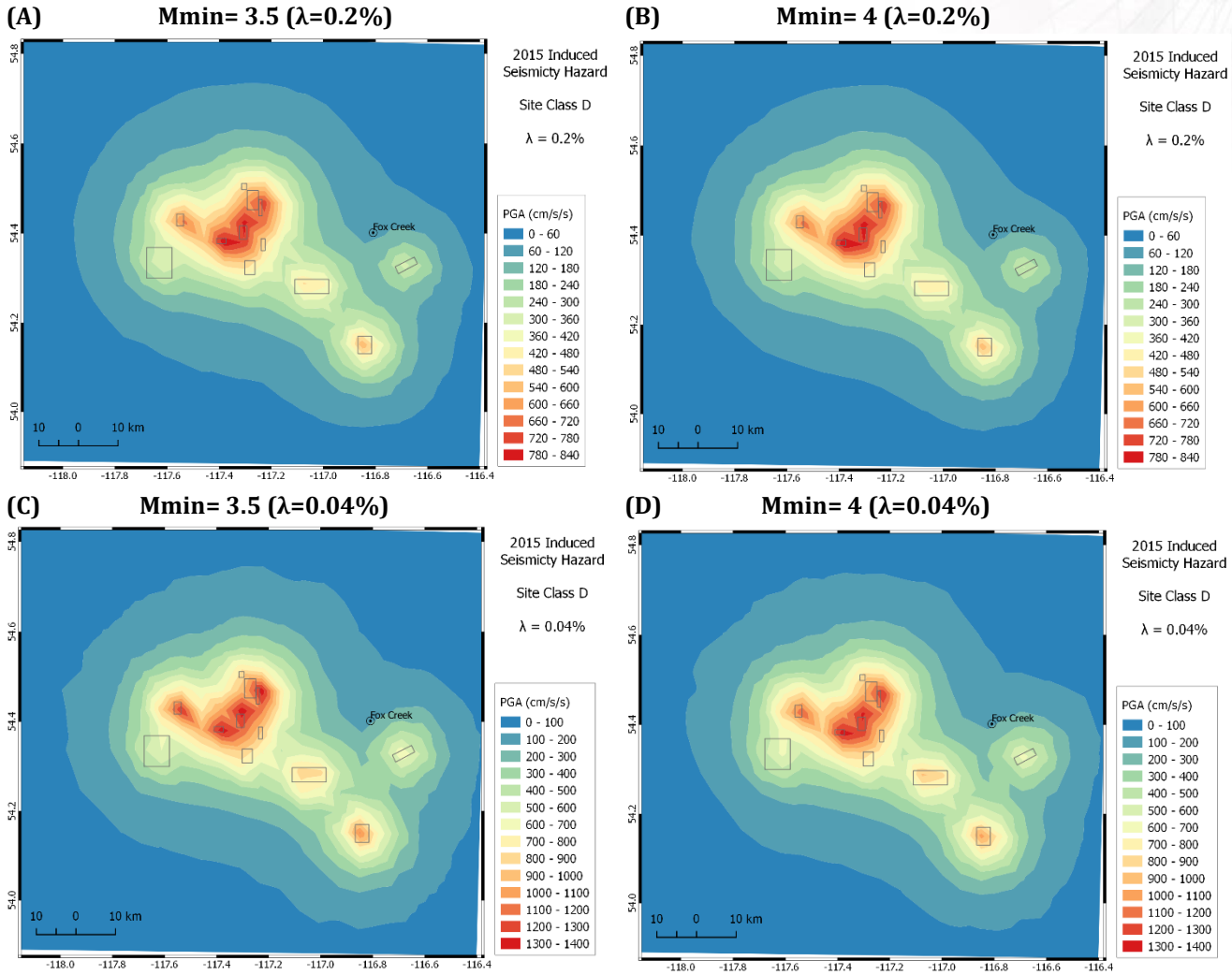

Figure 32 PGA hazard maps for 0.2% and 0.04% annual rate of exceedance, determined based on 2015 induced seismicity model, for Mmin = 3.5 and Mmin = 4.0.

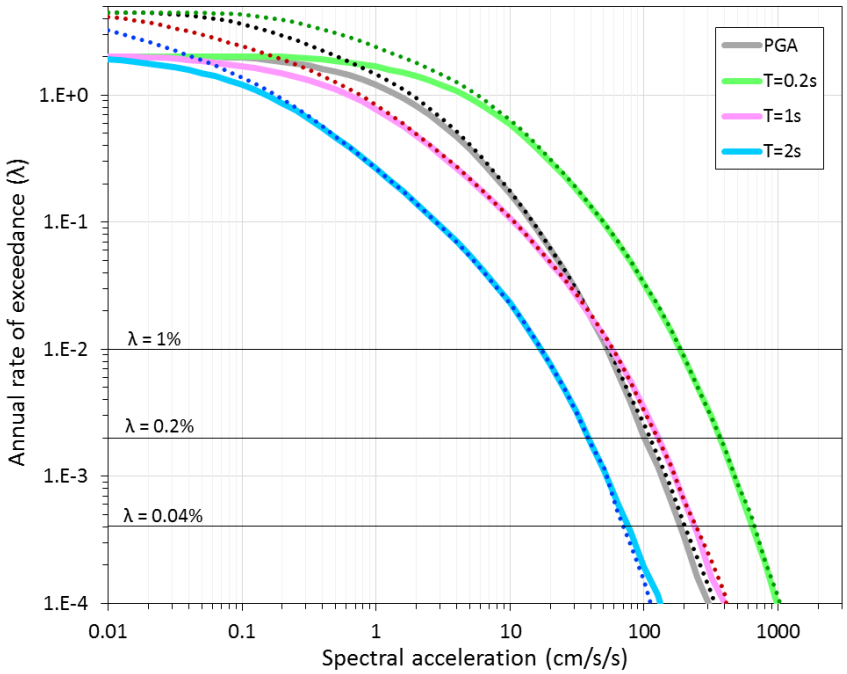

Figure 33 Hazard curves for Fox Creek, determined based on 2015 induced seismicity model, for Mmin=3.5 (dotted) and Mmin=4.0 (solid). Color-coded lines represent hazard curves for peak ground acceleration and response spectra at different periods.

Considering the observations made on the sensitivity of hazard results on Mmax, we use a logic-tree format to account for its uncertainty in annual hazard calculations. We assume maximum magnitudes of M5.0, M6.0 and M7.0 with weights of 0.3, 0.5 and 0.2, respectively. We weight the probability distribution of Mmax toward low-to-moderate values. We acknowledge that this is a subjective judgement that we hope to be able to refine in the future when more information becomes available. It is also worth noting that a M7.0 induced earthquake corresponds to slip on a 60km-long fault segment with a hypocenter located within the identified induced seismicity zones. A fault of such size has not been mapped in the Fox Creek region. Detailed mapping of the existing faults would allow for a more accurate characterization of induced seismicity sources and corresponding Mmax, in future updates of the hazard maps. We consider earthquakes with a minimum magnitude of M4.0 in hazard analysis, assuming that smaller events do not cause damage. A summary of key model parameters used in catalog simulation (*EqHaz1*) is listed in Table 3.

Table 3 List of key model parameters used in catalog simulation

Parameter	Value*
Minimum magnitude, M_{min}	M4.0 (1.0)
Maximum magnitude, M_{max}	Center: M6.0 (0.5) Low: M5.0 (0.3) High: M7.0 (0.2)
Source depth, d	Center: 3.5 km (0.6) Low: 2.5 km (0.2) High: 4.5 km (0.2) with 0.5 km vertical perturbations in each branch

* The values given in parenthesis represent weights for each alternative value.

We examine the focal depth distribution of induced events in the compiled composite catalog to constrain the depths of synthetic events to be generated for hazard analysis. We deduce that induced events occur at 2.5 km to 4.5 km depths with weights listed Table 3. Note that the focal depths of M>6 earthquakes are expected to be in the range of nominal depths for tectonic events (about 10 km). However, *EqHaz* software does not have the ability to variate focal depths with event magnitude, and shallow-depth assumption is implemented for all magnitudes. This may result in overestimation of seismic hazard from large events at distances less than 10 km, which should be considered when interpreting the seismic hazard maps.

Figure 34 shows an example synthetic catalog generated based on the 2015 induced seismicity model parameters for a 100-year time window. The spatial distribution of events agrees well with the geometry of the zones used in simulations. As expected, the majority of the events are between M4.0 and M5.0, and larger events generally occur in relatively more active zones.

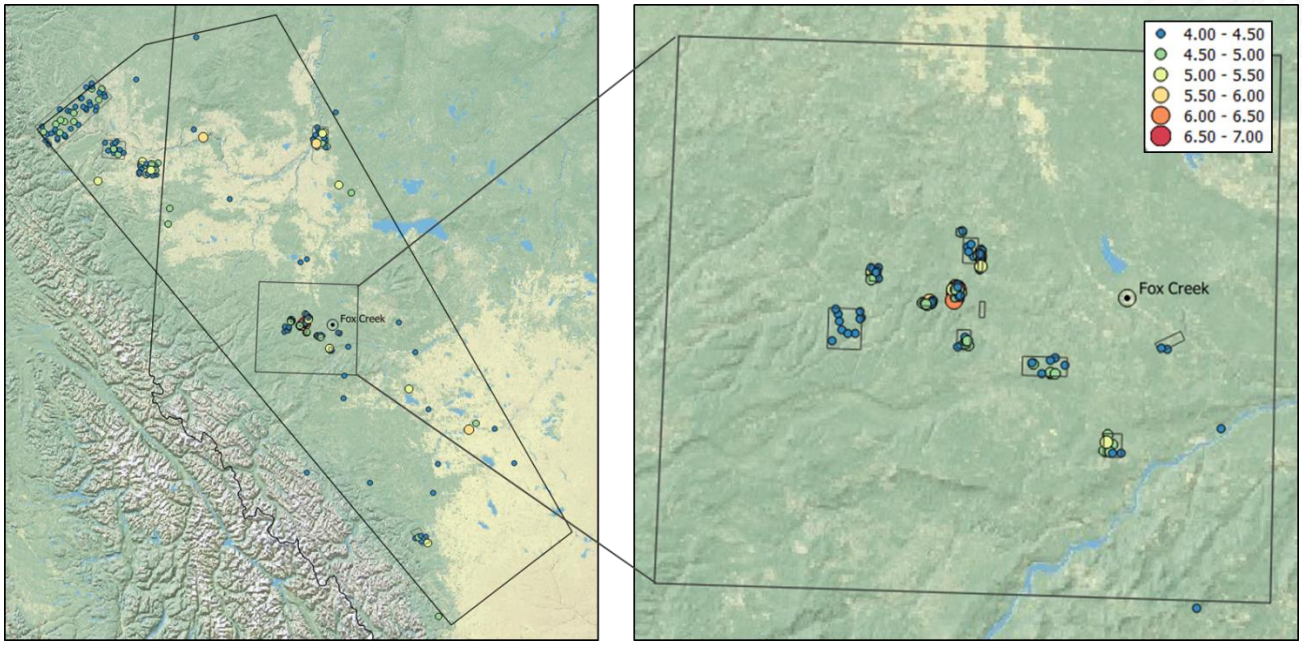

Figure 34 A 100-year synthetic catalog generated based on 2015 induced seismicity model parameters.

We conduct hazard analysis via *EqHaz2* module, using synthetic catalogs generated from 2013, 2014 and 2015 induced seismicity models. Figure 35 shows hazard curves for induced and natural seismicity for the town of Fox Creek. Natural seismicity hazard curves are determined based on the 5th generation national hazard model of Halchuk et al. (2015). For a given level of spectral acceleration, the annual rate of exceedances from induced events (based on the 2015 model) are larger than that of tectonic events, as shown in Figure 36. This suggests that the overall hazard in Fox Creek is dominated by the induced seismic hazard. This is in accord with the findings of Atkinson et al. (2015).

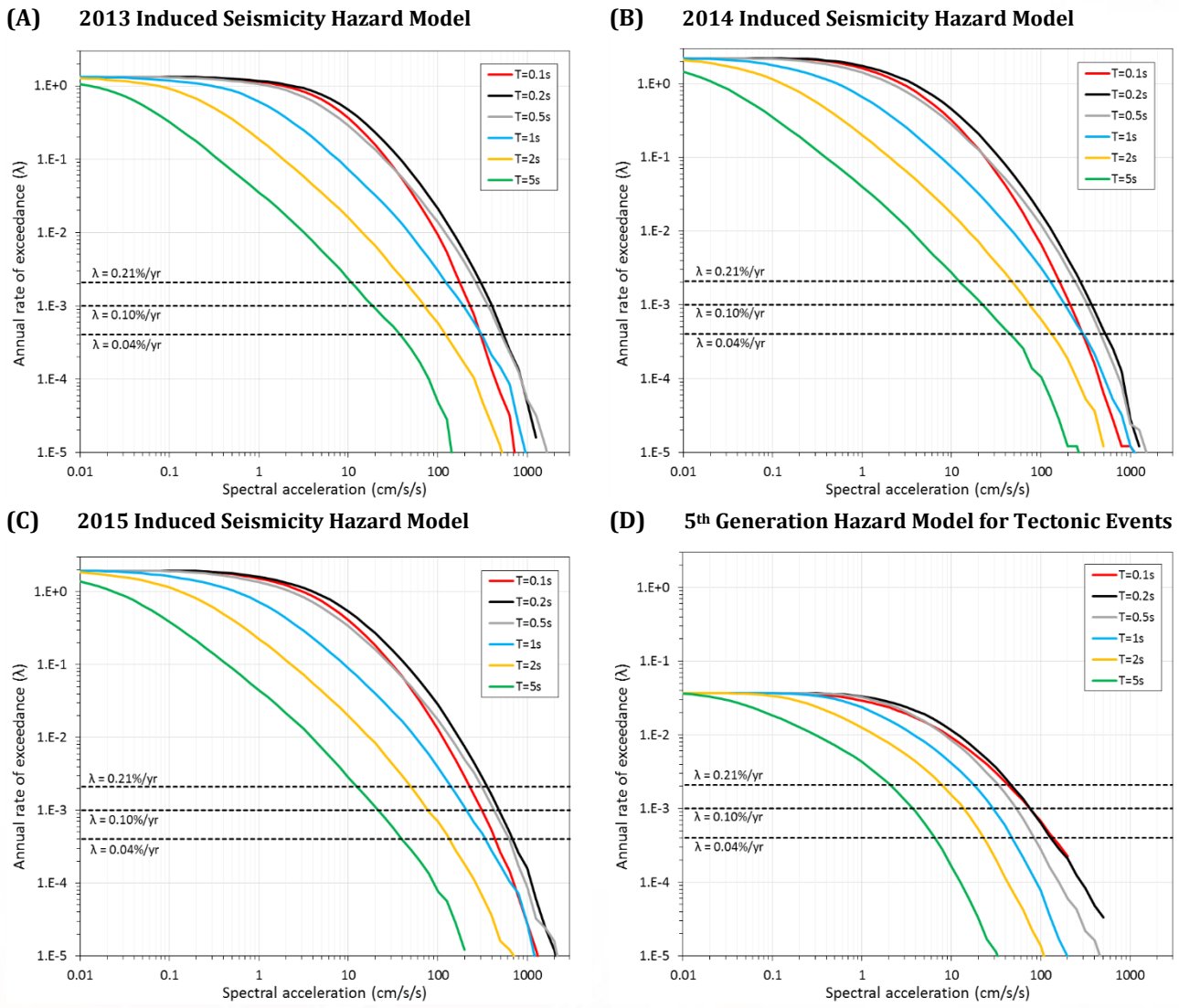

Figure 35 Hazard curves for Fox Creek, determined based on 2013 **(A)**, 2014 **(B)** and 2015 **(C)** induced seismicity models. Panel **(D)** shows the hazard curves for tectonic events based on the 5th generation hazard model (Halchuk et al., 2015).

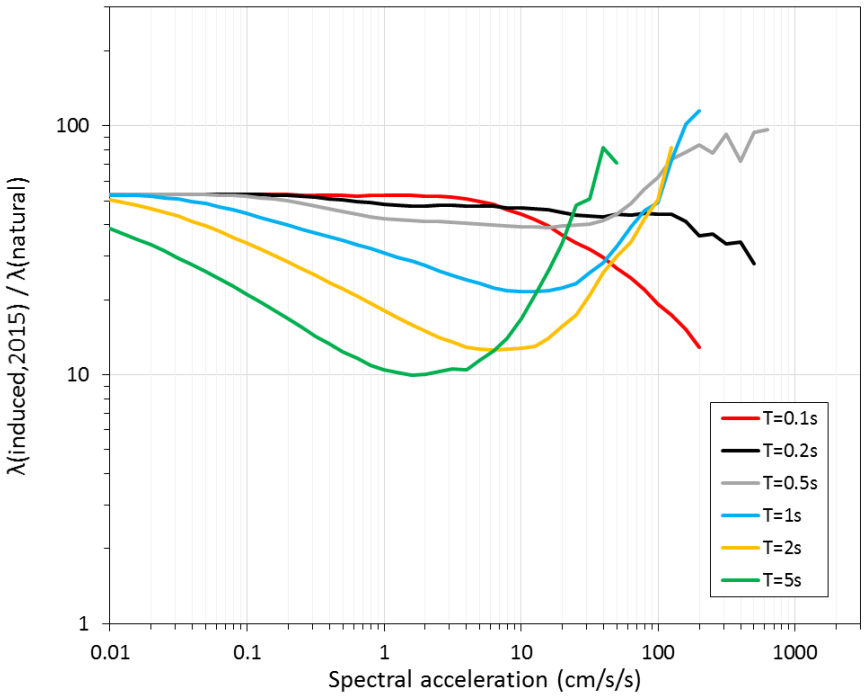

Figure 36 Ratio of the annual rate of exceedances for induced events (based on 2015 model) to that for tectonic events (based on 5th generation national seismic hazard model), for Fox Creek at different spectral periods.

We perform hazard calculations for 530 grid points over Fox Creek region and calculate the spectral accelerations at each grid point for two alternative annual rates of engineering interest: 0.2% (Tr = 475 year) and 0.04% (Tr = 2475 year). The latter corresponds to the value that is recommended in National Building Code 2015 for the calculation of the design spectrum to be considered in structural design. As an example, Figure 37 and 38 shows PGA hazard maps for the two annual rates. Higher resolution hazard maps for PGA and spectral acceleration are provided in the Appendix.

It should be noted that hazard maps should not be interpreted as shake maps. Shake maps show the distribution of ground shaking created by a single observed or scenario event over a region. However, hazard maps show the distribution of ground shaking that is expected to occur in an area for a given probability level, considering the contributions from all earthquake magnitudes and distances to the hazard at each point on the map. Contours delineate regions likely to experience similar ground motions.

(A) 2013

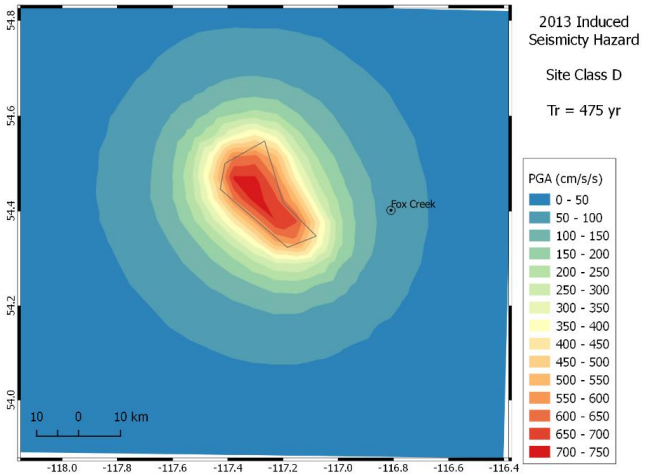

(B) 2014

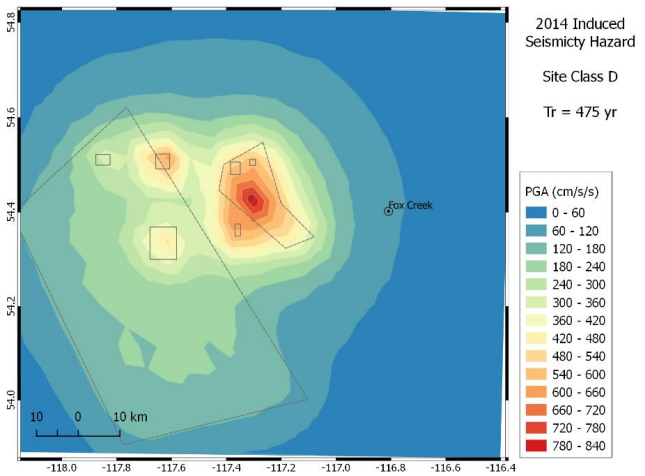

(C) 2015

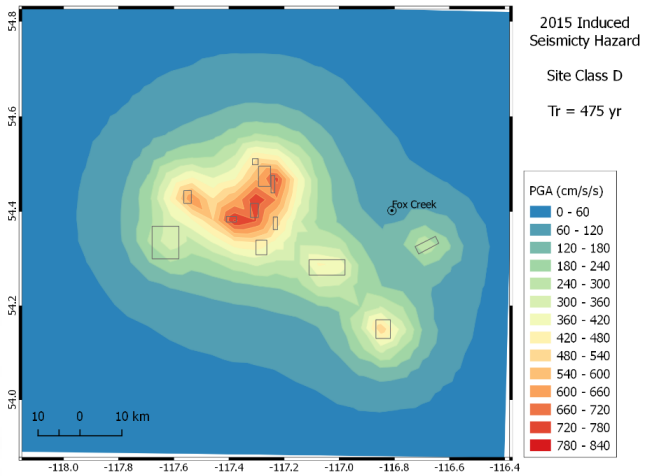

Figure 37 PGA hazard maps for 0.2% annual rate of exceedance (Tr = 475 years) determined based on 2013 **(A)**, 2014 **(B)** and 2015 **(C)** induced seismicity models. Regions indicated by gray lines show induced seismicity zones. Higher resolution hazard maps for PGA and spectral acceleration are provided in the Appendix.

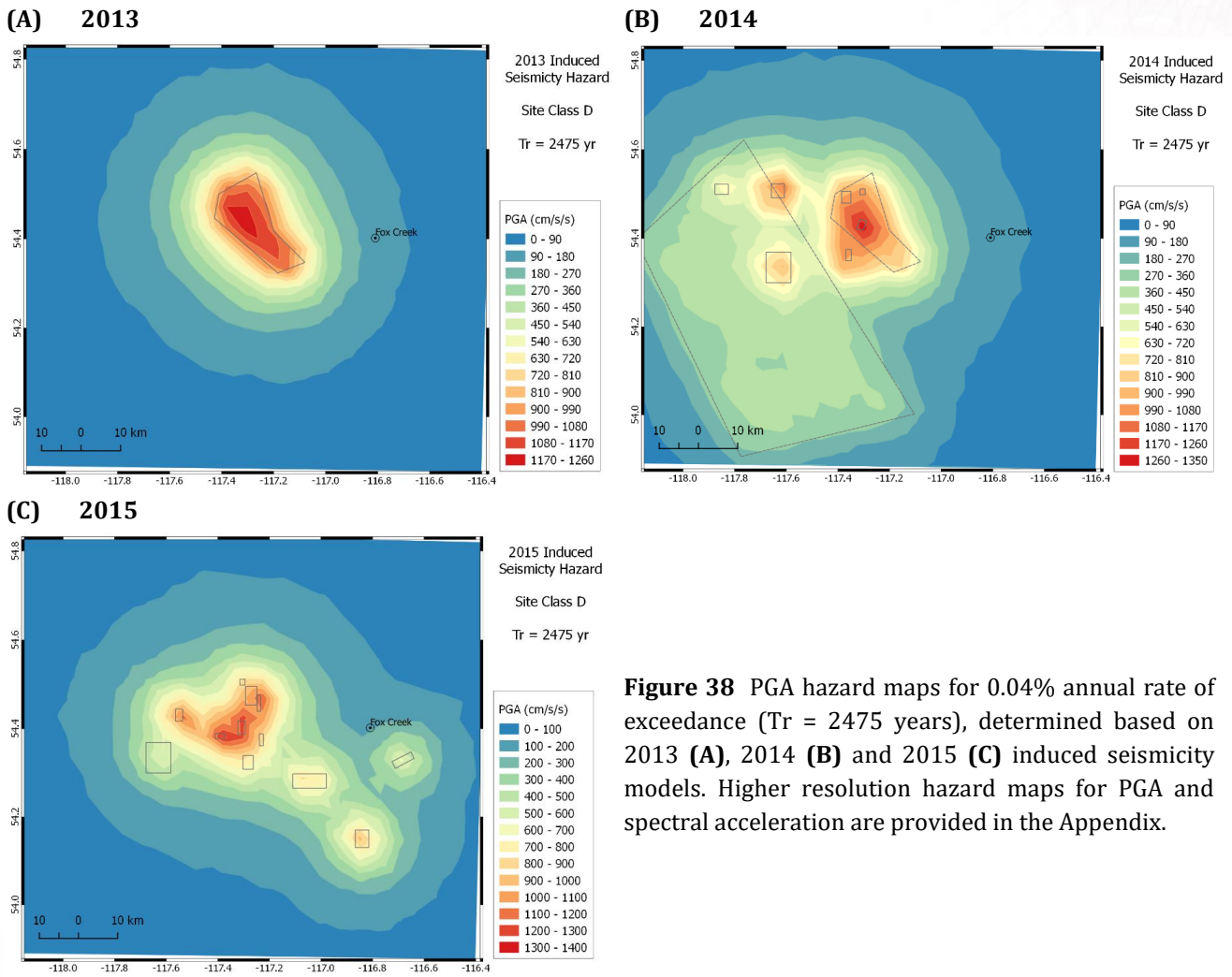

Figure 38 PGA hazard maps for 0.04% annual rate of exceedance (Tr = 2475 years), determined based on 2013 **(A)**, 2014 **(B)** and 2015 **(C)** induced seismicity models. Higher resolution hazard maps for PGA and spectral acceleration are provided in the Appendix.

7.1 DEAGGREGATION OF SEISMIC HAZARD FOR FOX CREEK

We calculate the contributions of induced seismicity sources to the overall hazard in Fox Creek for different magnitude and distance bins using the third module of EqHaz. Figures 39 and 40 illustrate example deaggreagion plots for PSA0.2s and PSA1.0s, at 0.2% and 0.04% annual rates, respectively. Plots are generated to show hazard contributions from local sources within 40 km distance. Induced seismicity sources at larger distances have negligibly small contribution to the overall hazard in Fox Creek. Deaggregation plots for PGA and spectral acceleration at different periods are provided in the Appendix.

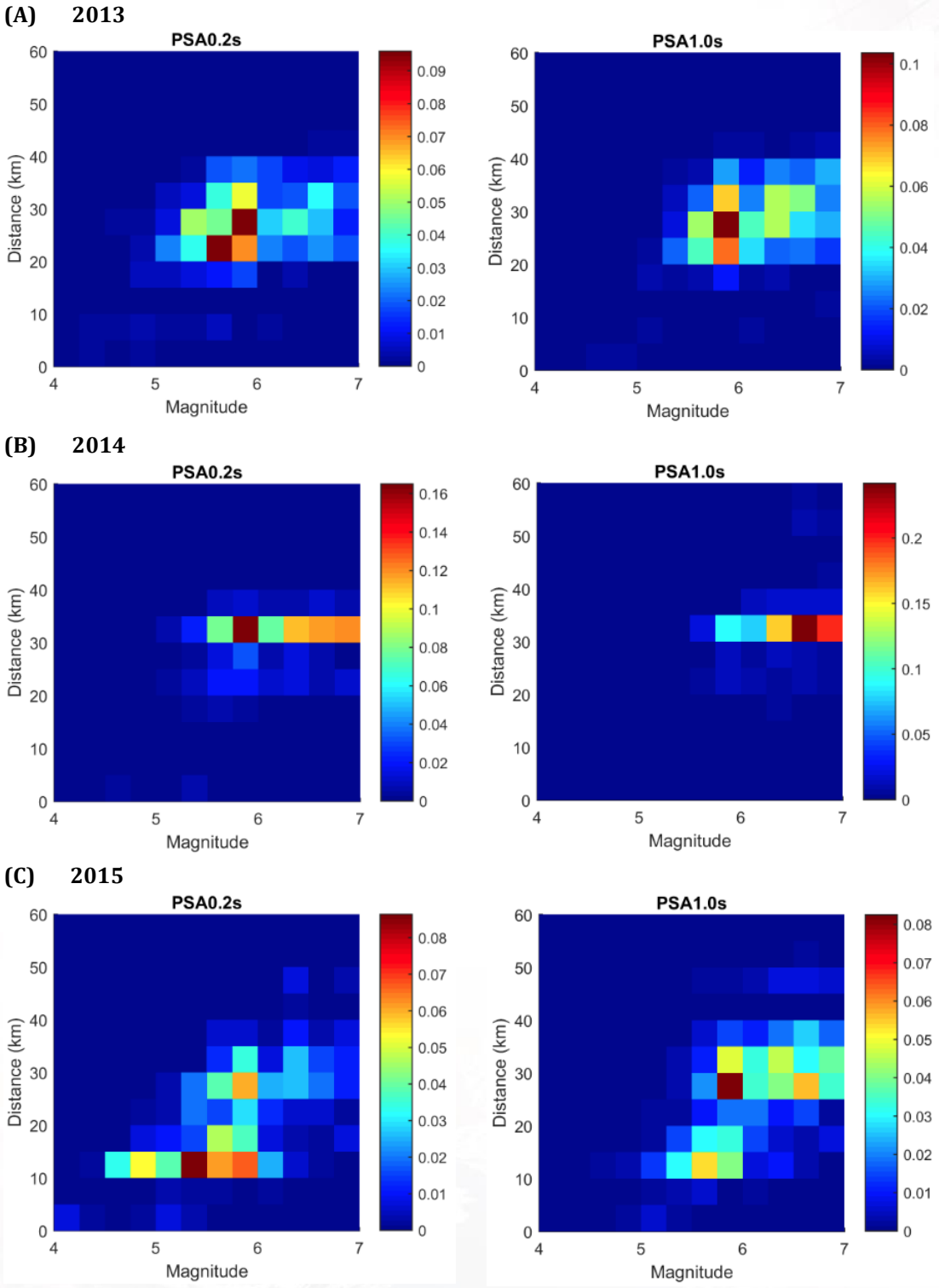

Figure 39. Deaggregation of seismic hazard in Fox Creek for annual rate of 0.2%. Rows show deaggregation plots for 2013 **(A)**, 2014 **(B)** and 2015 **(C)** induced seismicity models.

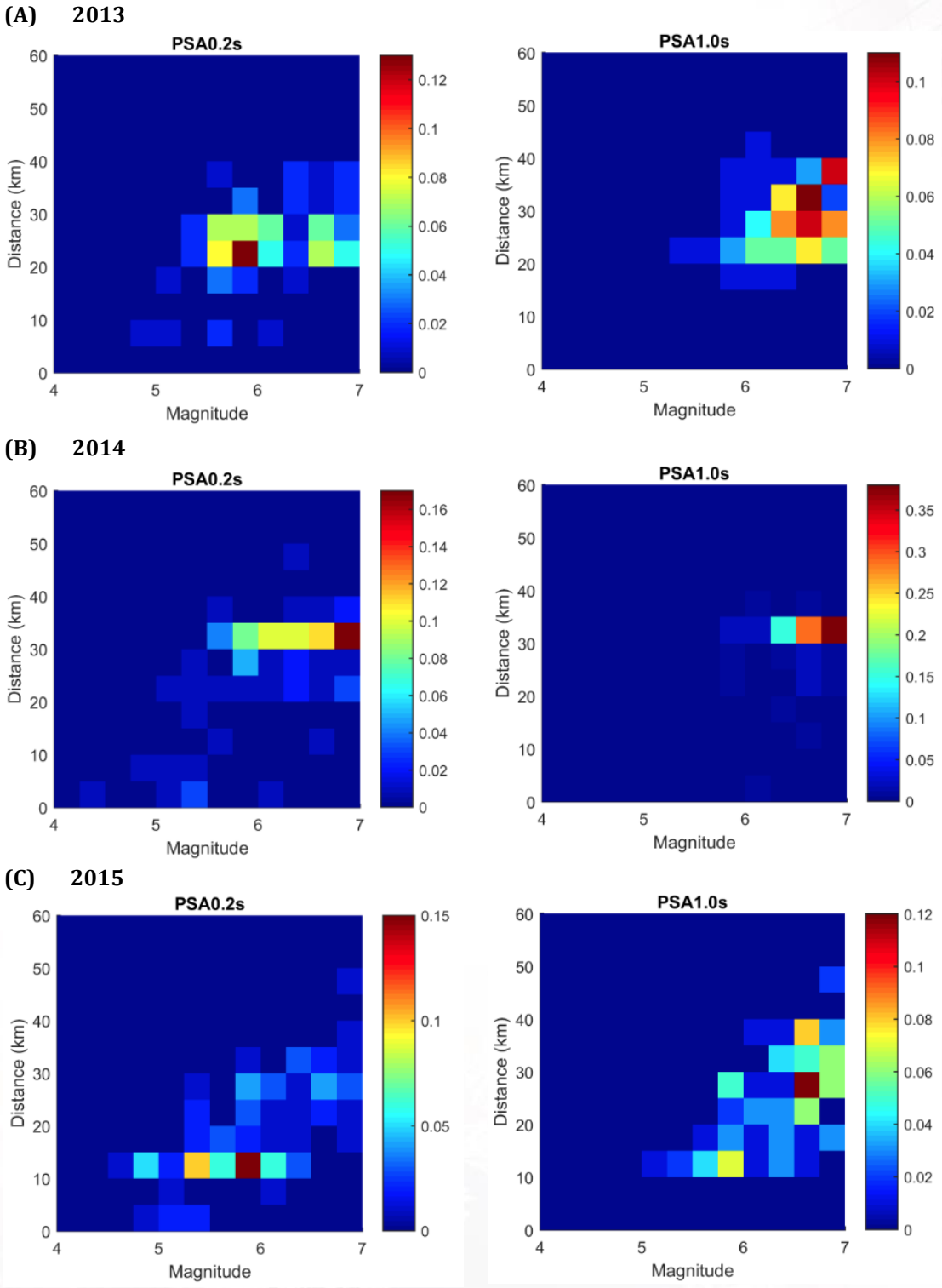

Figure 40. Deaggregation of seismic hazard in Fox Creek for annual rate of 0.04%. Rows show deaggregation plots for 2013 **(A)**, 2014 **(B)** and 2015 **(C)** induced seismicity models.

8.0 SUMMARY

We conducted probabilistic hazard analysis for induced seismicity in Fox Creek, Alberta, to generate hazard maps for peak ground acceleration and response spectra at periods of engineering interest. In this respect, we first compiled a composite induced seismicity catalog spanning from January 2013 to January 2016. Six input catalogs were merged, removing duplicate and suspected blast events from the catalogs. The reported magnitudes were converted to moment magnitude scale to obtain a uniform induced seismicity catalog.

Using the compiled catalog, seismic activities were examined in time and space domains to understand the spatio-temporal variation of induced seismicity in Fox Creek region. We mimic the temporal variation of induced seismicity by performing annual hazard analysis for three years (2013, 2014 and 2015), separately. Based on the inspection of clustered activities, we identified source zones that were active in each year. We then inspected temporal seismicity in each zone to identify earthquake sequences. Magnitudes of completeness (Mc), activity rates and b-values were determined for each sequence, to characterize the magnitude recurrence relationship. We observed large variation of b-values (from 0.5 to 2.7) between difference sequences. In order to model the probability distribution of magnitudes robustly in hazard analysis, we associated each sequence to a pre-defined b-value (default b-value of 1, mild b-value of 0.6 and steep b-value of 1.6) based on a hypothesis testing approach.

Additionally, we adjusted two published ground motion prediction equations (GMPEs) to the observed ground motions in the western Alberta to develop a GMPE suite that was used in induced seismicity hazard calculations for Fox Creek region.

We evaluated the seismic hazard associated with induced events in Fox Creek region, using a Monte-Carlo simulation technique. Sensitivity analyses revealed that the maximum magnitude of induced earthquakes can have significant impact on the hazard results, whereas the minimum magnitude has negligible effect. A logic-tree approach is adopted to account for uncertainties in maximum magnitude, focal depth, b-values and GMPEs.

Annual hazard analyses were performed for 2013, 2014 and 2015, considering the active zones in each year. Induced seismicity hazard maps were generated for PGA and PSA at variable spectral periods, for two alternative annual rates of engineering interest (0.2% and 0.04%). The induced seismicity hazard for Fox Creek is deaggregated to identify the sources and event magnitudes that most contribute to the overall hazard in Fox Creek.

It is important to acknowledge that the presented hazard models of induced seismicity are largely based on statistical analysis of the observed activity rates, using a standard tectonic seismicity PSHA methodology for each year. Due to the nature of the PSHA, a number of assumptions had to be made regarding the earthquake catalogs, rates, recurrences, locations, maximum magnitudes, and ground motions to perform hazard analysis for induced events. Further research can improve

on the present hazard calculations. The research topics include determining the appropriate b-values, and fine-tuning declustering methods, mapping of existing faults in the region, maximum magnitudes, testing the GMPE suite for larger events, characterization of site effects in Fox Creek region, further examination of uncertainties in ground motion prediction using a richer empirical data, and creating shake maps that show how the ground motions distribute from real and scenario events. Future research could also consider the development of seismic hazard assessment methods that do not require the use of stationary Poisson earthquake rates and allow variation with time which more accurately characterizes the nature of induced seismicity.

9.0 REFERENCES

Assatourians, K., and G. M. Atkinson (2013). EqHaz—An open-source probabilistic seismic hazard code based on the Monte Carlo simulation approach, *Seismol. Res. Lett.* 84, 516–524,

Atkinson, G. M. (2015). Ground-motion prediction equation for small-to-moderate events at short hypocentral distances, with application to induced seismicity hazards, *Bull. Seismol. Soc. Am.* 105, 981–992.

Atkinson, G. M., and S. I. Kaka (2007). Relationships between felt intensity and instrumental ground motion in the central United States and California, *Bull. Seismol. Soc. Am.,* 97, 497–510.

Atkinson G. M., and J. Adams (2013). Ground motion prediction equations for application to the 2015 Canadian national seismic hazard maps, *Canadian Journal of Civil Engineering*, 40, 988–998.

Atkinson, G. M. and D. M. Boore (2014). The attenuation of Fourier amplitudes for rock sites in eastern North America, *Bull. Seismol. Soc. Am.* 104, 513–528.

Atkinson, G. M., D. W. Greig, and E. Yenier (2014). Estimation of moment magnitude (**M**) for small events (M <4) on local networks, *Seismol. Res. Lett.,* 85, 1116–1124.

Atkinson, G. M., H. Ghofrani, and K. Assatourians (2015). Impact of induced seismicity on the evaluation of seismic hazard: some preliminary considerations, *Seismol. Res. Lett.,* 86, 1009–1021.

Atkinson, G. M., D. W. Eaton, H. Ghofrani, D. Walker, B. Cheadle, R. Schultz, R. Shcherbakov, K. Tiampo, J. Gu, R. M. Harrington, Y. Liu, M. van der Baan, and H. Kao (2016). Hydraulic fracturing and seismicity in the Western Canada Sedimentary Basin, *Seismol. Res. Lett.,* 87, 1–17.

Boore, D. M. (2003). Simulation of ground motion using the stochastic method, *Pure and Applied Geophysics*, 160, 635-376.

Boore, D. M. and W. B. Joyner (1997). Site amplifications for generic rock sites, *Bull. Seism. Soc. Am.* 87, 327-341.

Boore, D. M., J. P. Stewart, E. Seyhan, and G. M. Atkinson (2014b). NGA-West2 equations for predicting response spectral accelerations for shallow crustal earthquakes, Earthquake Spectra, 30, 1057-1085.

Eaton J. P. (1992). Determination of amplitude and duration magnitudes and site residuals from short-period seismographs in northern California. *Bull. Seismol. Soc. Am.* 82, 533–579.

Halchuk, S., T. I. Allen, J. Adams, and G.C. Rogers (2014). Fifth Generation Seismic Hazard Model Input Files as Proposed to Produce Values for the 2015 National Building Code of Canada, Geological Survey Canada, Open File 7576.

Hough, S. (2014). Shaking from injection-induced earthquakes in the central and eastern United States, *Bull. Seismol. Soc. Am.* 104, 2619–2626.

Hutton, L. K., and D. M. Boore (1987). The ML scale in southern California. *Bull. Seismol. Soc. Am.*, 77, 2074–2094.

McGarr, A. (2014). Maximum magnitude earthquakes induced by fluid injection, *J. Geophys. Res.* 119, 1008–1019.

Novakovic, M., and G. M. Atkinson (2015). Preliminary evaluation of ground motions from earthquakes in Alberta, *Seismol. Res. Lett.* 86, 1086–1095.

Petersen, M. D., C. S. Mueller, M. P. Moschetti, S. M. Hoover, J. L. Rubinstein, A. L. Llenos, A. J. Michael, W. L. Ellsworth, A. F. McGarr, A. A. Holland, and J. G. Anderson (2015). Incorporating Induced Seismicity in the 2014 United States National Seismic Hazard Model—Results of 2014 Workshop and Sensitivity Studies, *U.S. Geological Survey*, Open-File Report 2015-1070.

Richter, C. F. (1935). An instrumental earthquake magnitude scale. *Bull. Seismol. Soc. Am.*, 25, 1–31.

Richter, C. F. (1958). *Elementary Seismology*, W. H. Freeman and Co., San Francisco, California, 578 pp.

Shapiro, S. A., O. S. Kruger, C. Dinske, and C. Langenbruch (2011). Magnitudes of induced earthquakes and geometric scales of fluid-stimulated rock volumes, Geophysics 76,WC55–WC63.

Sumy, D. F., E. S. Cochran, K. M. Keranen, M. Wei, and G. A. Abers (2014). Observations of static Coulomb stress triggering of the November 2011 M5.7 Oklahoma earthquake sequence, *J. Geophys. Res.* 119, 1904–1923.

Yenier, E., and G. M. Atkinson (2015). An equivalent point-source model for stochastic simulation of earthquake ground motions in California, *Bull. Seismol. Soc. Am.* 105, 1989–2009

Yenier E., D. Baturan, A. Law, and G. M. Atkinson (2016). A local magnitude (ML) formula for western Alberta, GeoConvention, Calgary, Alberta, Canada.

10.0 APPENDICES

10.1 HAZARD MAPS FOR 2013 INDUCED SEISMICITY MODEL (0.21%/YR)

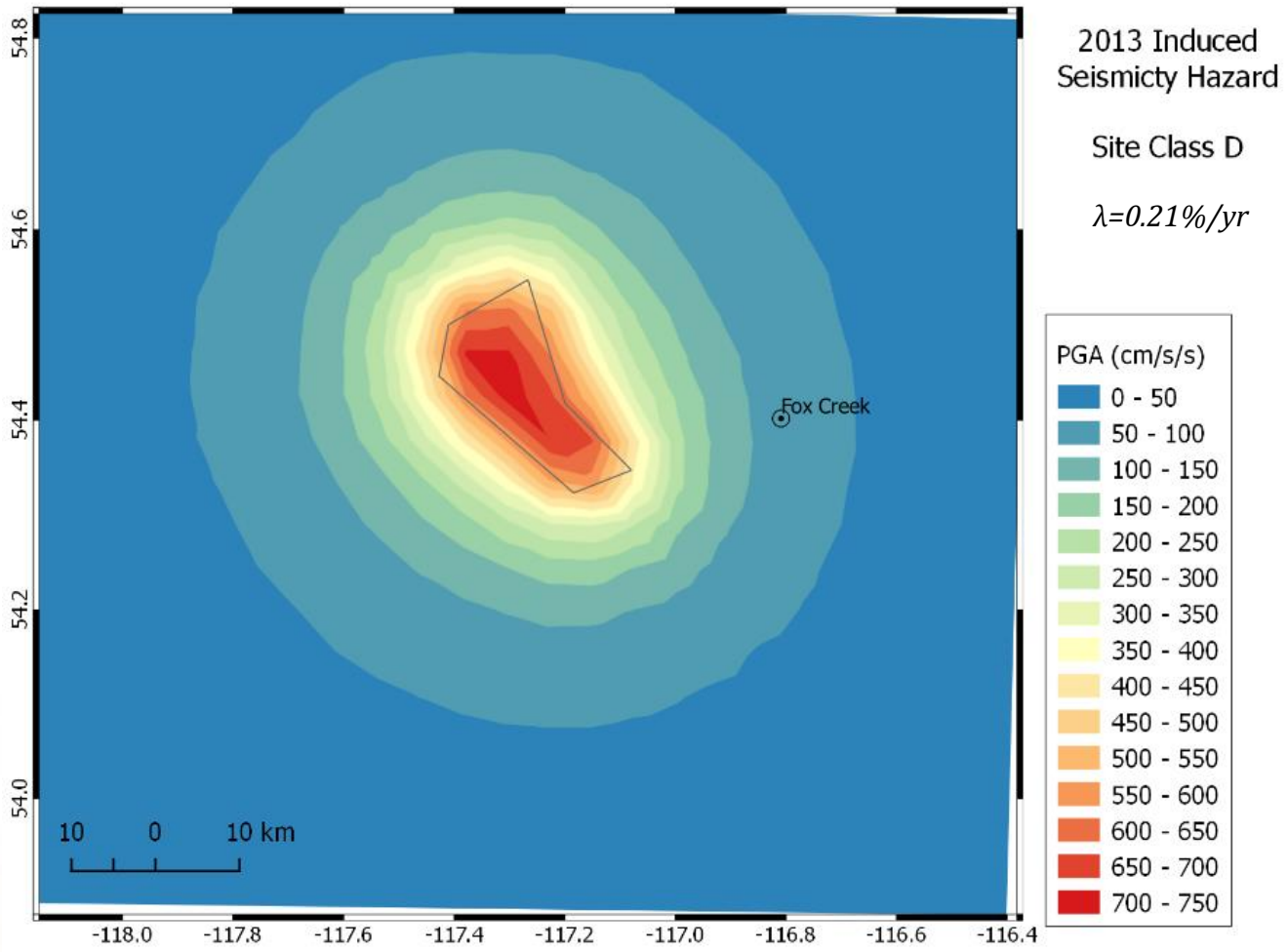

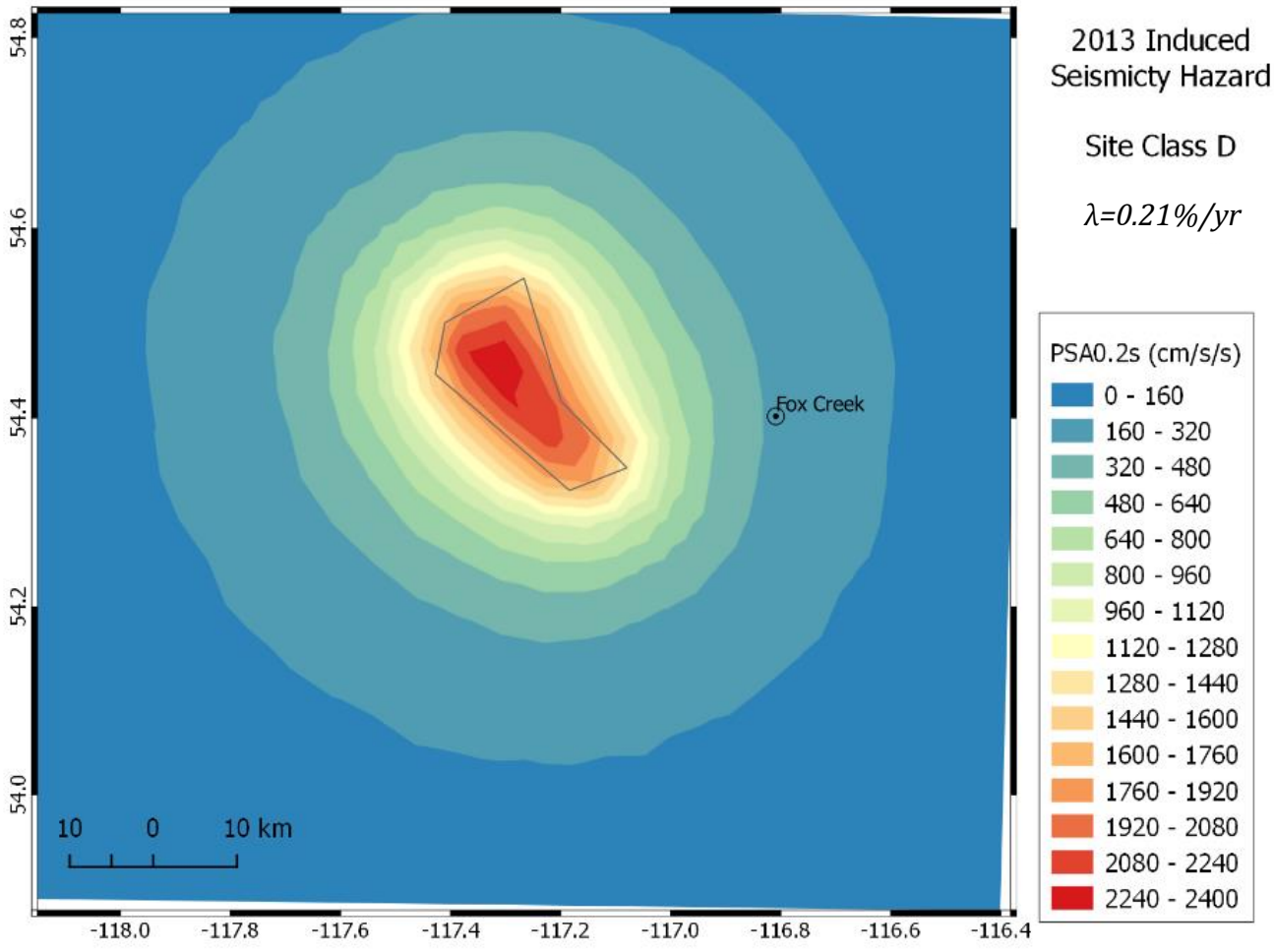
2013 Induced
Seismicty Hazard
Site Class D
λ=0.21%/yr
PSA0.2s (cm/s/s)
0 - 160
160 - 320
320 - 480
480 - 640
640 - 800
800 - 960
960 - 1120
1120 - 1280
1280 - 1440
1440 - 1600
1600 - 1760
1760 - 1920
1920 - 2080
2080 - 2240
2240 - 2400
Fox Creek
10 0 10 km
54.8
54.6
54.4
54.2
54.0
-118.0
-117.8
-117.6
-117.4
-117.2
-117.0
-116.8
-116.6
-116.4

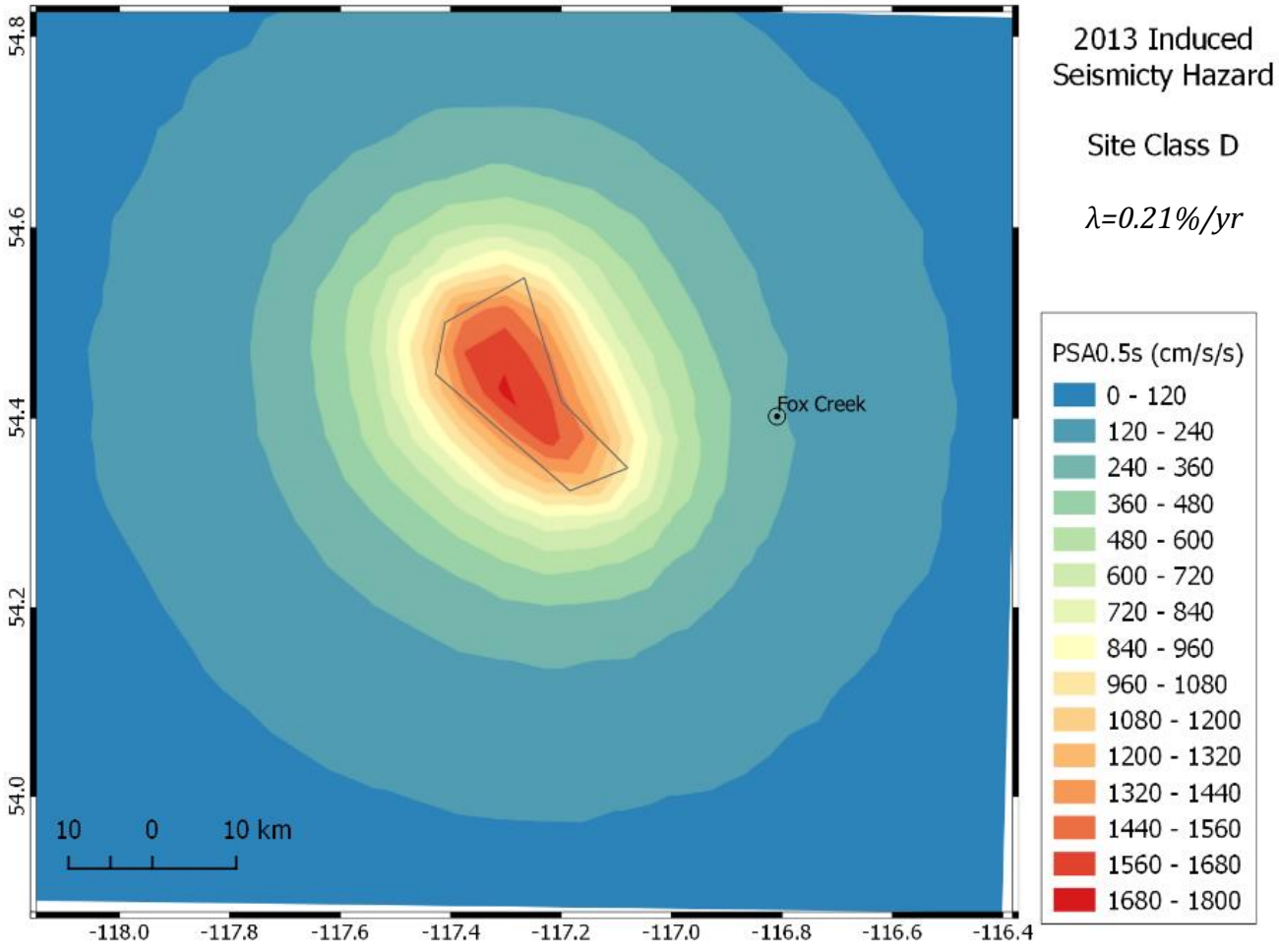
2013 Induced Seismicty Hazard
Site Class D
λ=0.21%/yr
PSA0.5s (cm/s/s)
0 - 120
120 - 240
240 - 360
360 - 480
480 - 600
600 - 720
720 - 840
840 - 960
960 - 1080
1080 - 1200
1200 - 1320
1320 - 1440
1440 - 1560
1560 - 1680
1680 - 1800
Fox Creek
10 0 10 km
54.8
54.6
54.4
54.2
54.0
-118.0
-117.8
-117.6
-117.4
-117.2
-117.0
-116.8
-116.6
-116.4

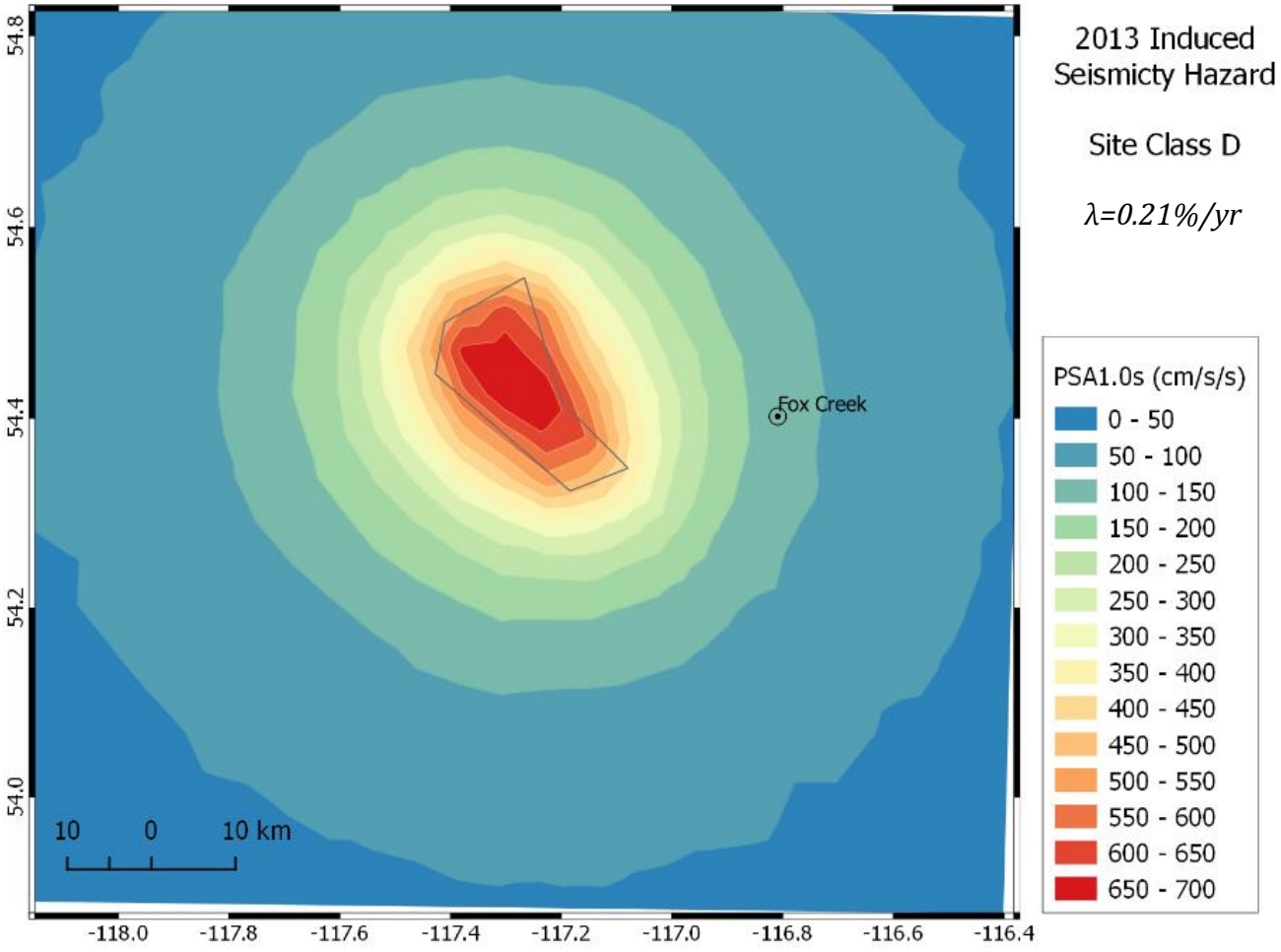
2013 Induced Seismicty Hazard
Site Class D
λ=0.21%/yr
PSA1.0s (cm/s/s)
0 - 50
50 - 100
100 - 150
150 - 200
200 - 250
250 - 300
300 - 350
350 - 400
400 - 450
450 - 500
500 - 550
550 - 600
600 - 650
650 - 700
Fox Creek
10 0 10 km
54.8
54.6
54.4
54.2
54.0
-118.0
-117.8
-117.6
-117.4
-117.2
-117.0
-116.8
-116.6
-116.4

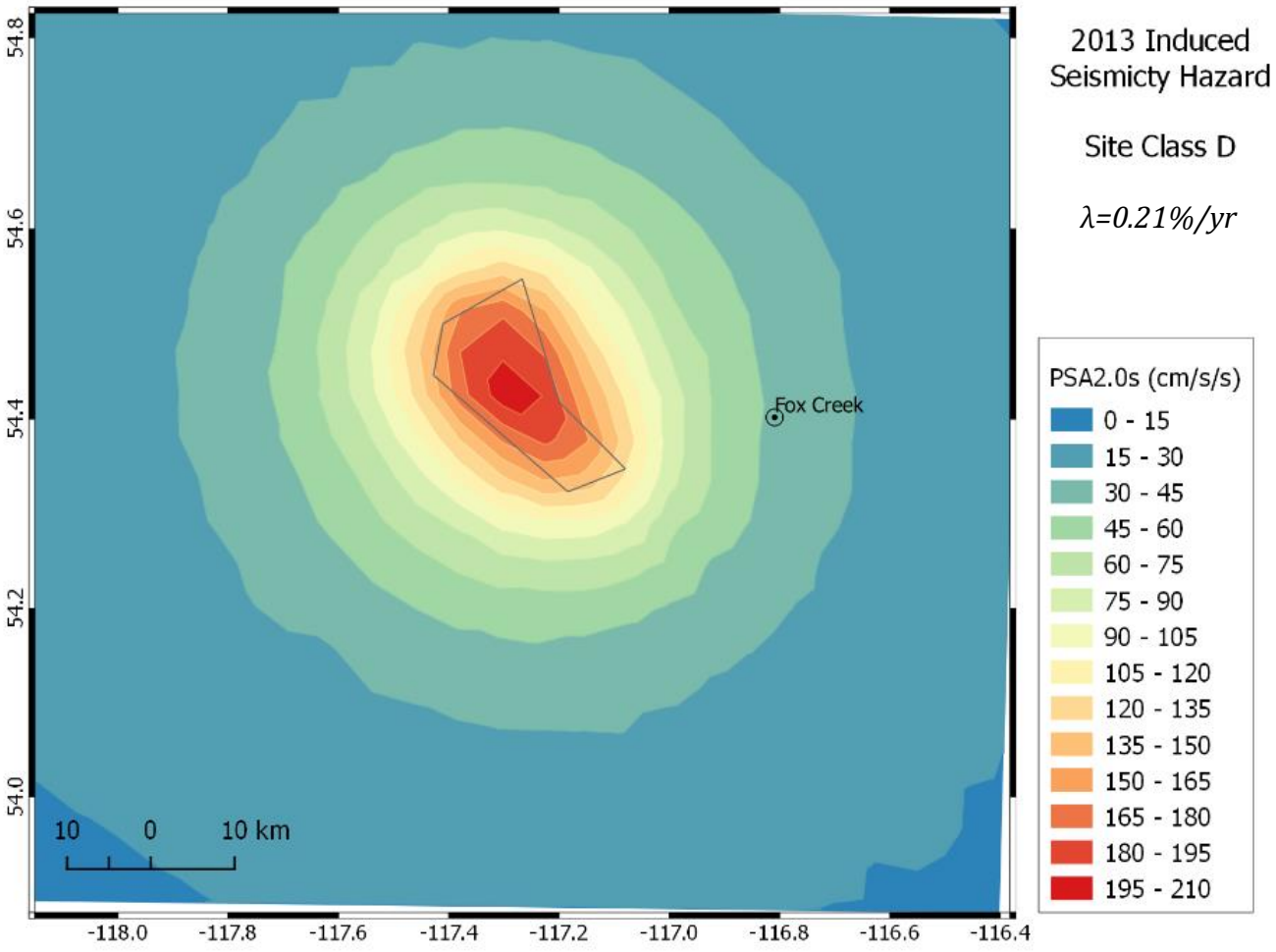
2013 Induced Seismicty Hazard
Site Class D
λ=0.21%/yr
PSA2.0s (cm/s/s)
0 - 15
15 - 30
30 - 45
45 - 60
60 - 75
75 - 90
90 - 105
105 - 120
120 - 135
135 - 150
150 - 165
165 - 180
180 - 195
195 - 210
Fox Creek
10 0 10 km
54.8
54.6
54.4
54.2
54.0
-118.0
-117.8
-117.6
-117.4
-117.2
-117.0
-116.8
-116.6
-116.4

10.2 HAZARD MAPS FOR 2014 INDUCED SEISMICITY MODEL (0.21%/YR)

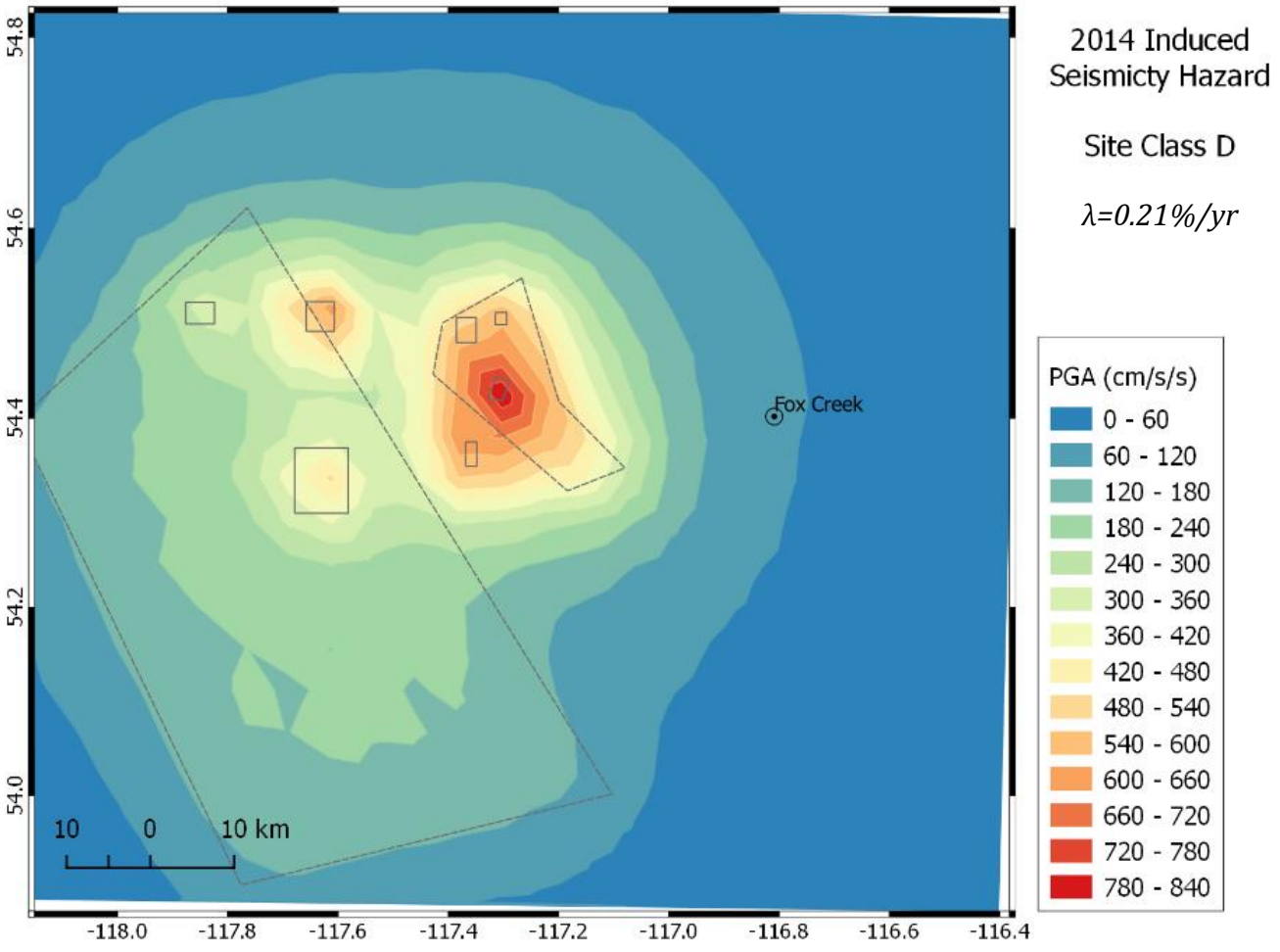

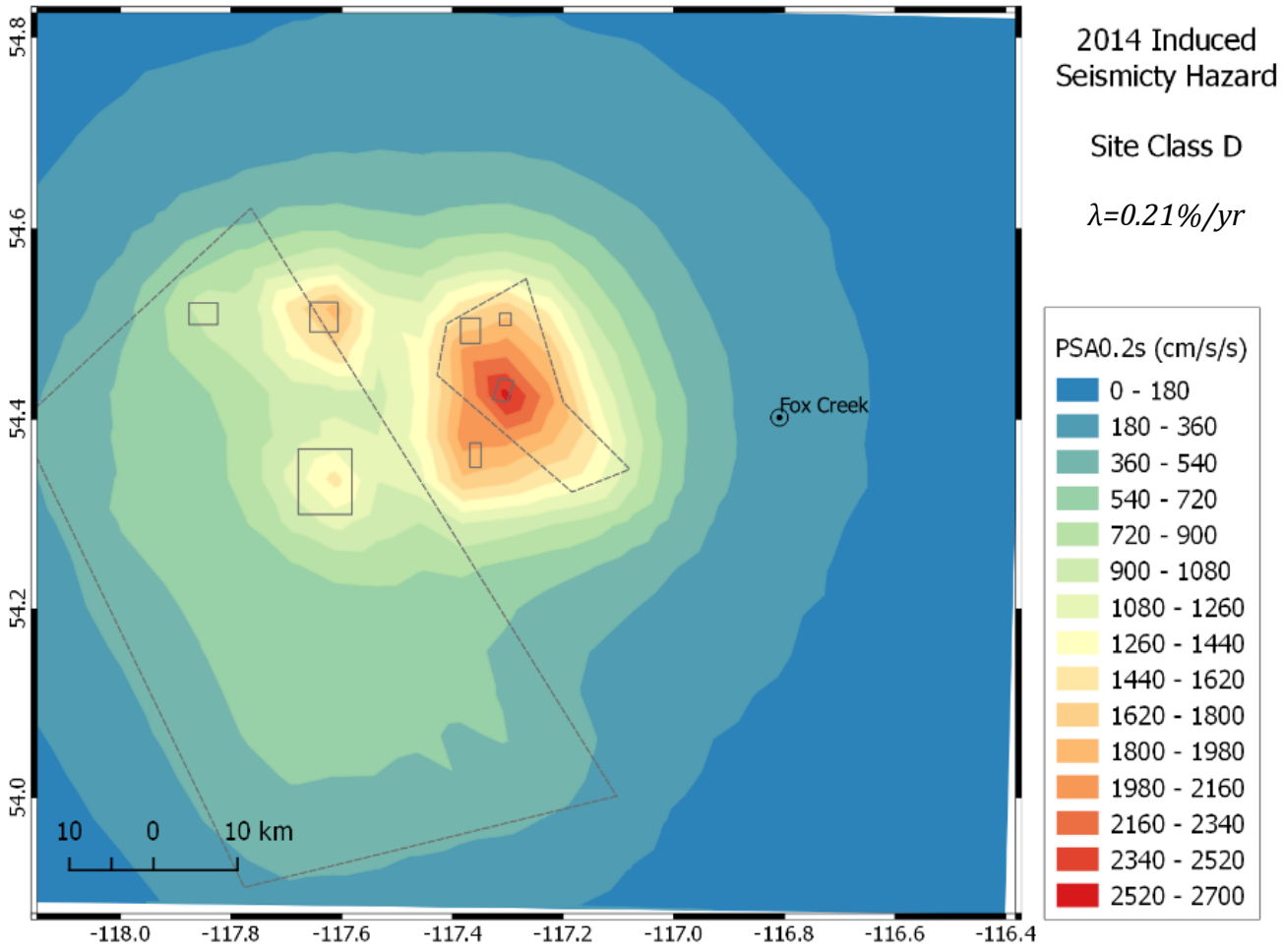
2014 Induced
Seismicty Hazard
Site Class D
λ=0.21%/yr
PSA0.2s (cm/s/s)
0 - 180
180 - 360
360 - 540
540 - 720
720 - 900
900 - 1080
1080 - 1260
1260 - 1440
1440 - 1620
1620 - 1800
1800 - 1980
1980 - 2160
2160 - 2340
2340 - 2520
2520 - 2700
Fox Creek
10 0 10 km
54.8
54.6
54.4
54.2
54.0
-118.0
-117.8
-117.6
-117.4
-117.2
-117.0
-116.8
-116.6
-116.4

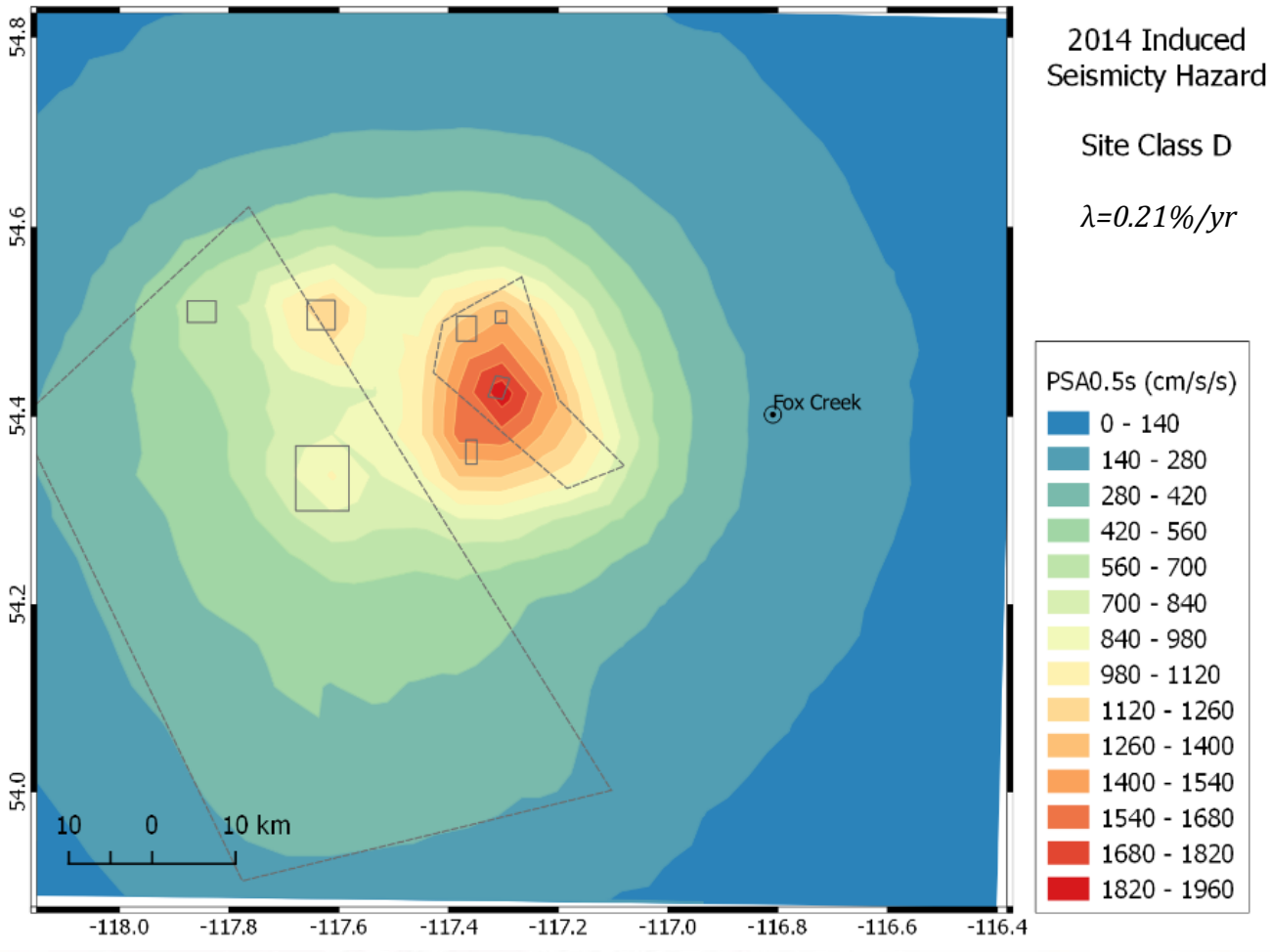
2014 Induced
Seismicty Hazard
Site Class D
λ=0.21%/yr
Fox Creek
PSA0.5s (cm/s/s)
0 - 140
140 - 280
280 - 420
420 - 560
560 - 700
700 - 840
840 - 980
980 - 1120
1120 - 1260
1260 - 1400
1400 - 1540
1540 - 1680
1680 - 1820
1820 - 1960
10 0 10 km
54.8
54.6
54.4
54.2
54.0
-118.0
-117.8
-117.6
-117.4
-117.2
-117.0
-116.8
-116.6
-116.4

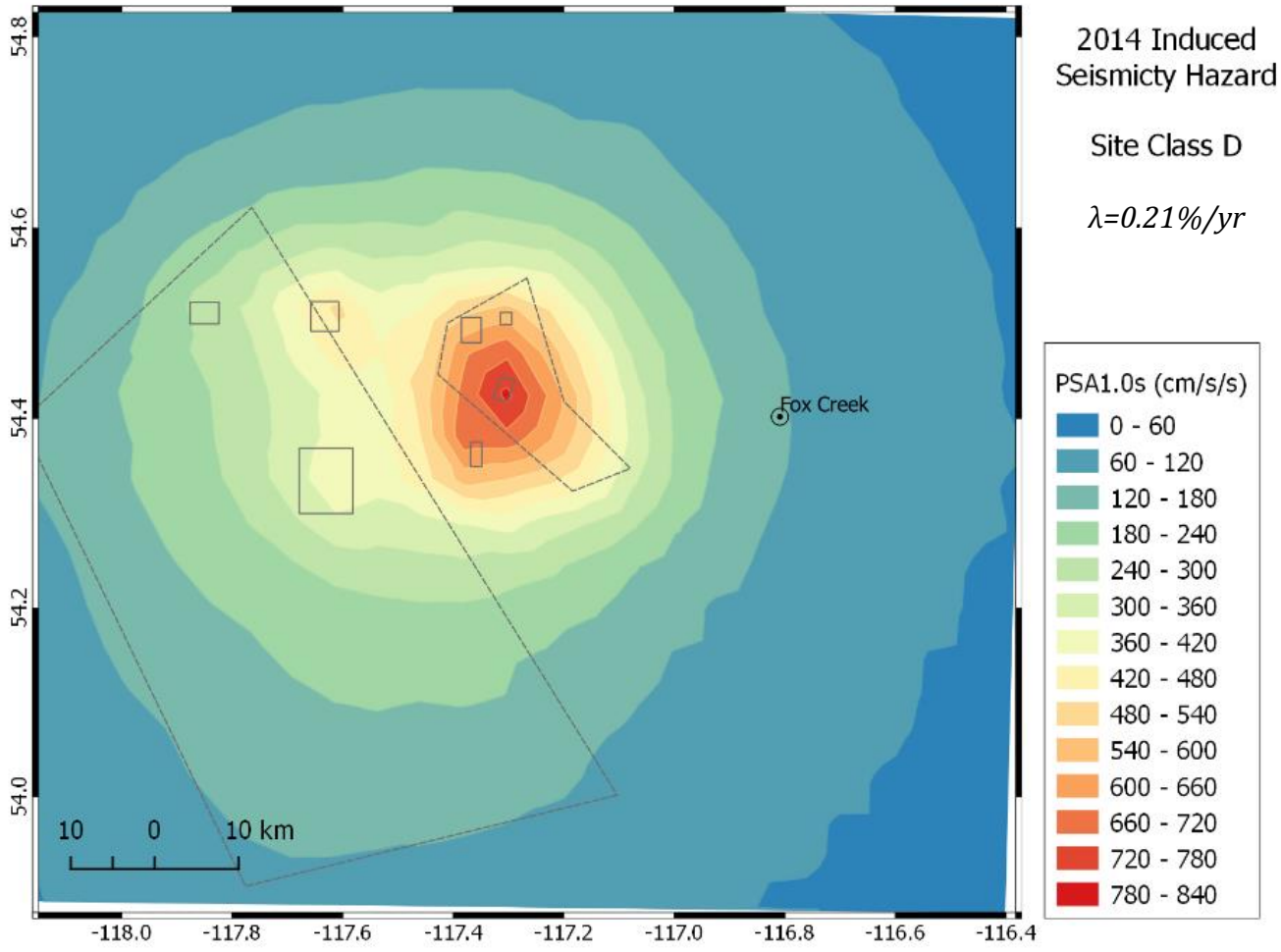
2014 Induced
Seismicty Hazard
Site Class D
λ=0.21%/yr
PSA1.0s (cm/s/s)
0 - 60
60 - 120
120 - 180
180 - 240
240 - 300
300 - 360
360 - 420
420 - 480
480 - 540
540 - 600
600 - 660
660 - 720
720 - 780
780 - 840
Fox Creek
10 0 10 km
54.8
54.6
54.4
54.2
54.0
-118.0
-117.8
-117.6
-117.4
-117.2
-117.0
-116.8
-116.6
-116.4

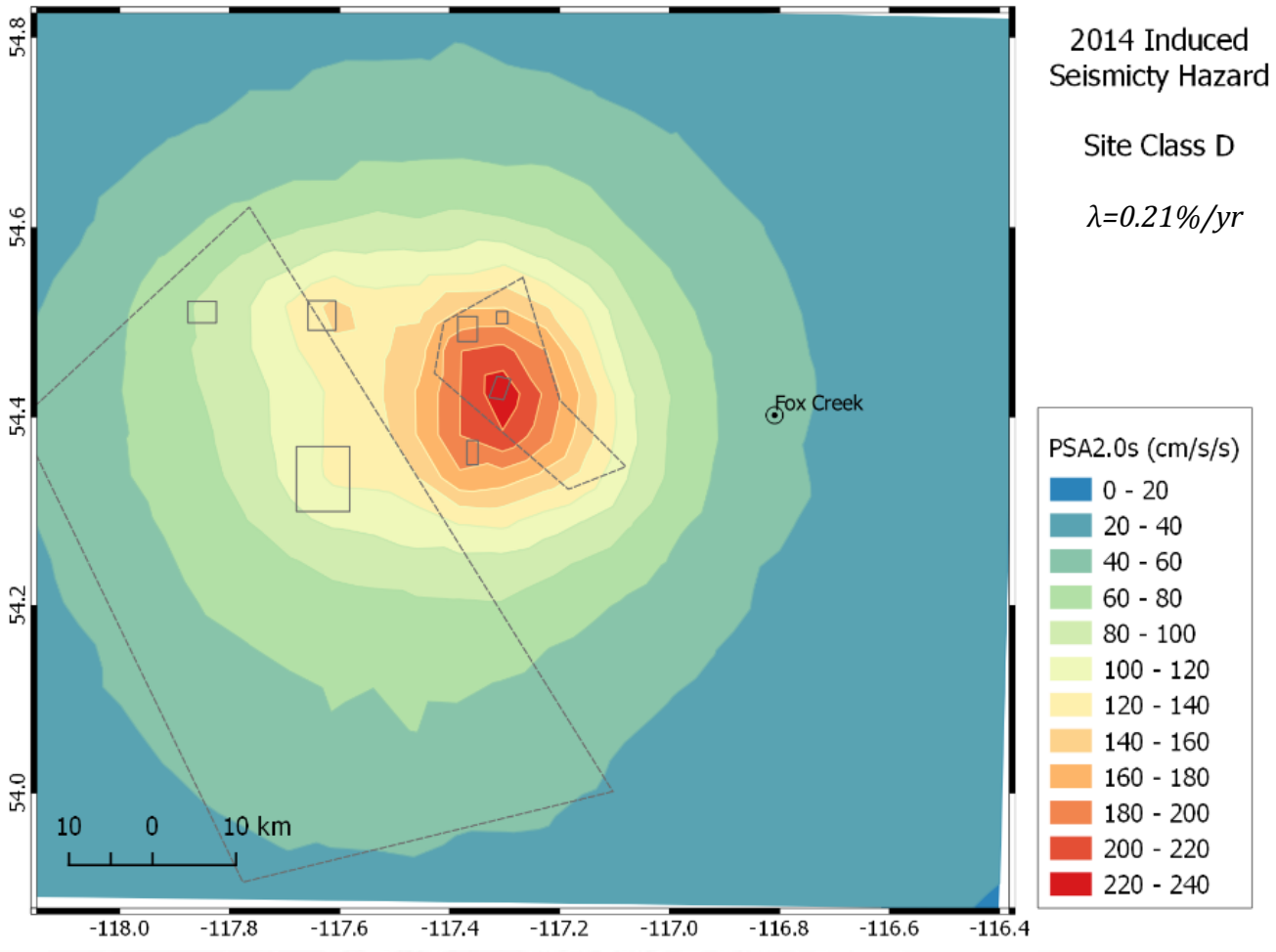
2014 Induced Seismicty Hazard
Site Class D
λ=0.21%/yr
Fox Creek
PSA2.0s (cm/s/s)
0 - 20
20 - 40
40 - 60
60 - 80
80 - 100
100 - 120
120 - 140
140 - 160
160 - 180
180 - 200
200 - 220
220 - 240
10 0 10 km
54.8
54.6
54.4
54.2
54.0
-118.0
-117.8
-117.6
-117.4
-117.2
-117.0
-116.8
-116.6
-116.4

10.3 HAZARD MAPS FOR 2015 INDUCED SEISMICITY MODEL (0.21%/YR)

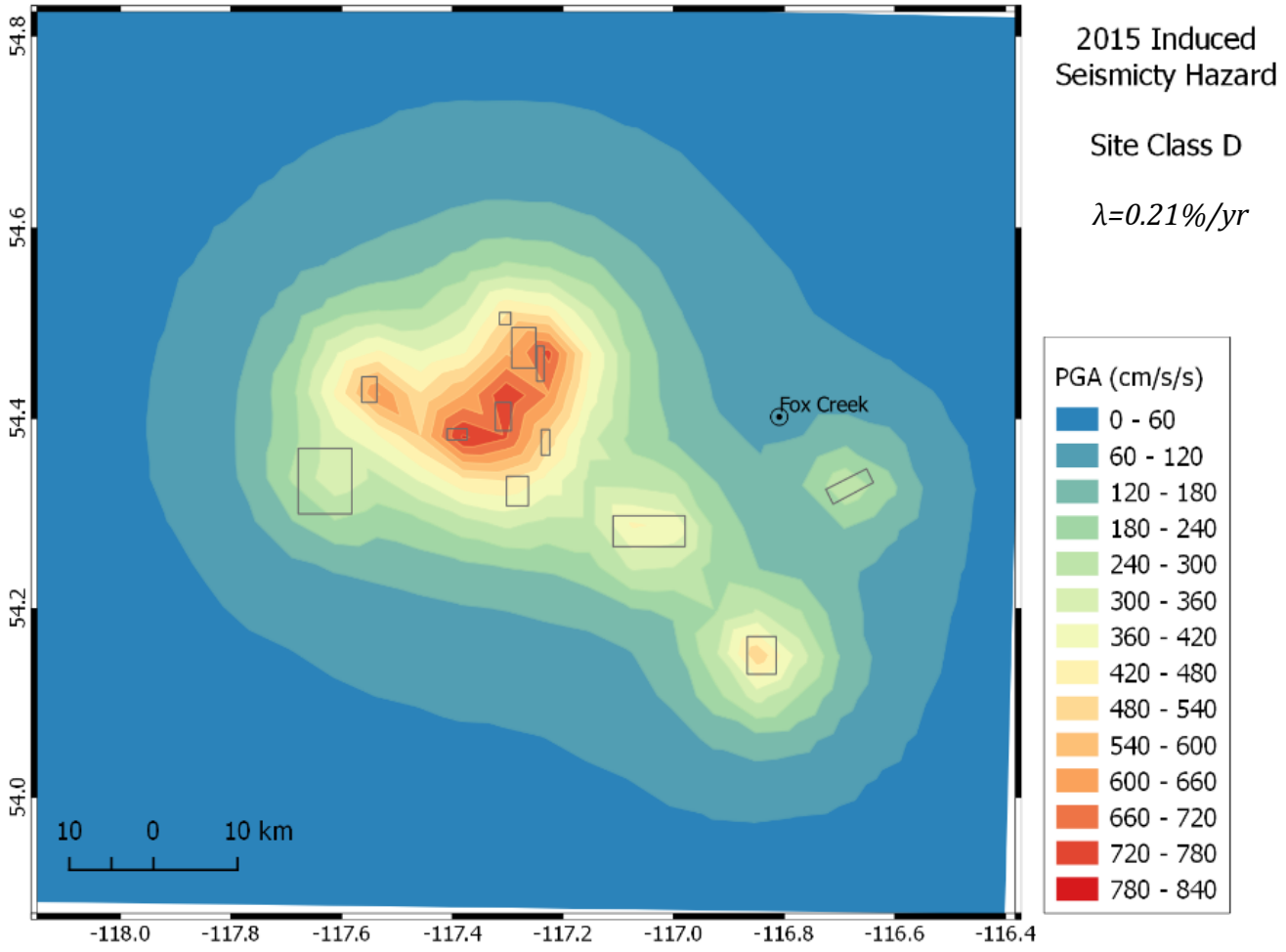

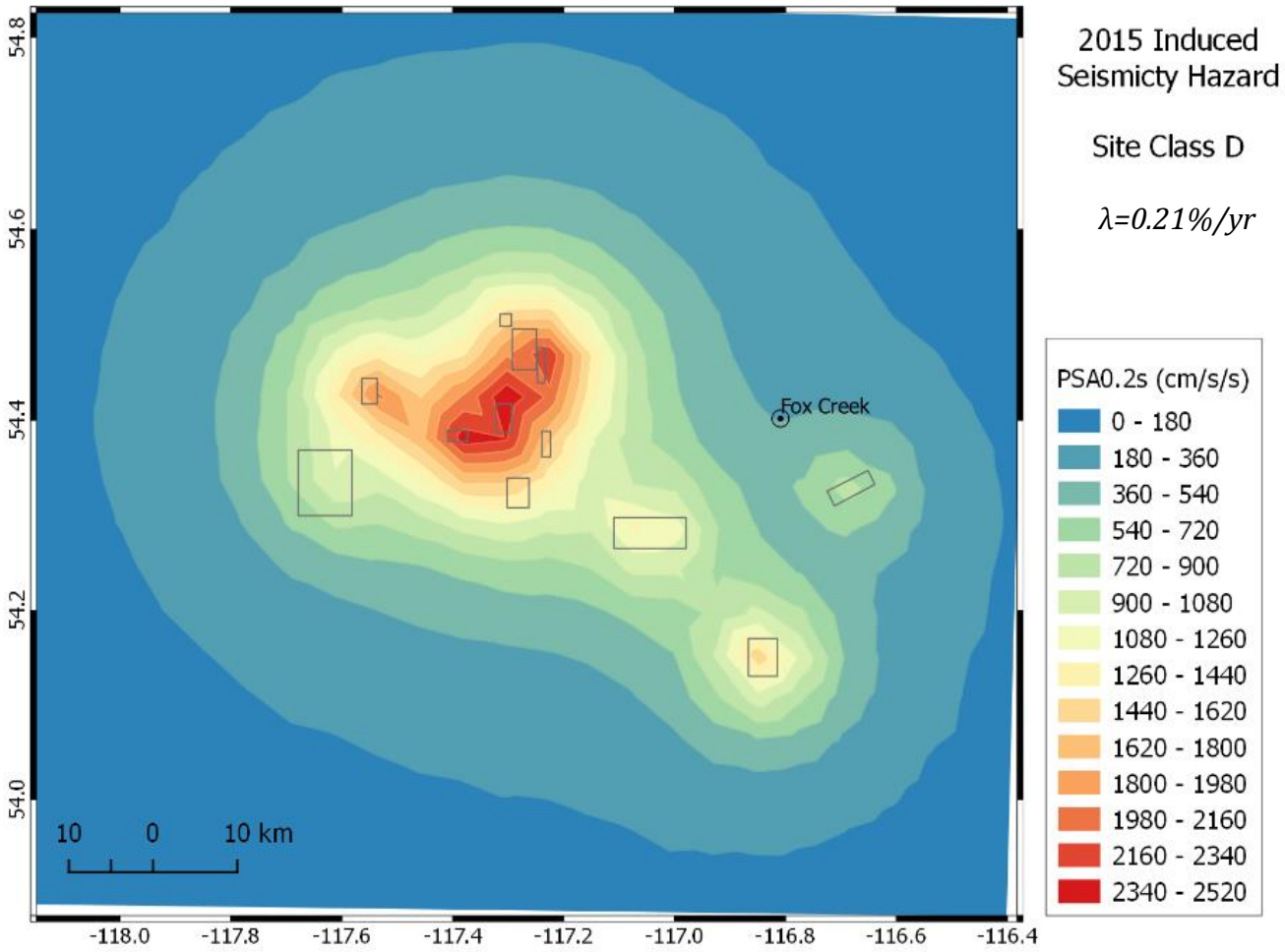
2015 Induced Seismicty Hazard
Site Class D
λ=0.21%/yr
PSA0.2s (cm/s/s)
0 - 180
180 - 360
360 - 540
540 - 720
720 - 900
900 - 1080
1080 - 1260
1260 - 1440
1440 - 1620
1620 - 1800
1800 - 1980
1980 - 2160
2160 - 2340
2340 - 2520
Fox Creek
10 0 10 km
54.8
54.6
54.4
54.2
54.0
-118.0
-117.8
-117.6
-117.4
-117.2
-117.0
-116.8
-116.6
-116.4

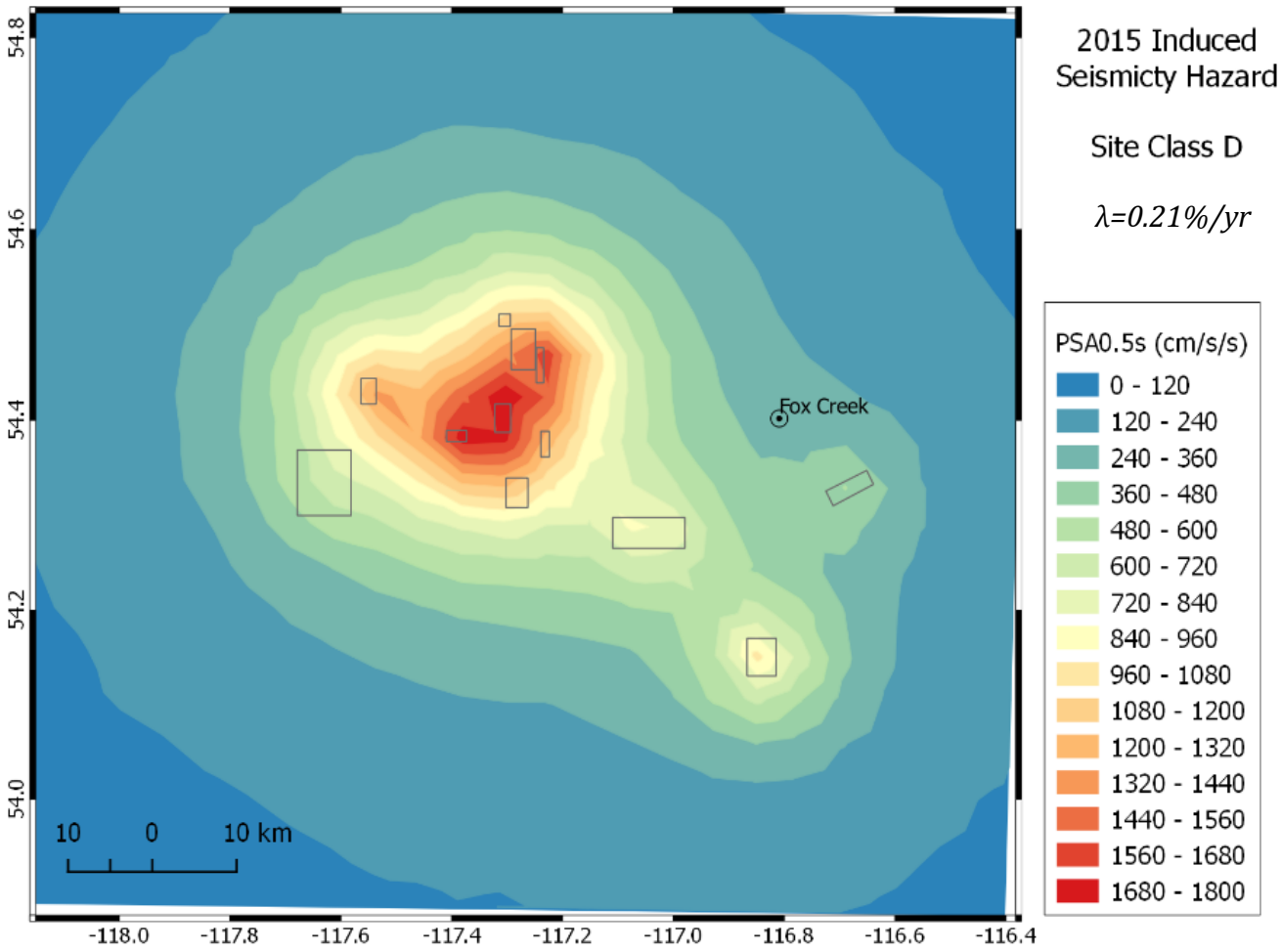
2015 Induced Seismicty Hazard
Site Class D
λ=0.21%/yr
PSA0.5s (cm/s/s)
0 - 120
120 - 240
240 - 360
360 - 480
480 - 600
600 - 720
720 - 840
840 - 960
960 - 1080
1080 - 1200
1200 - 1320
1320 - 1440
1440 - 1560
1560 - 1680
1680 - 1800
Fox Creek
10 0 10 km
54.8
54.6
54.4
54.2
54.0
-118.0
-117.8
-117.6
-117.4
-117.2
-117.0
-116.8
-116.6
-116.4

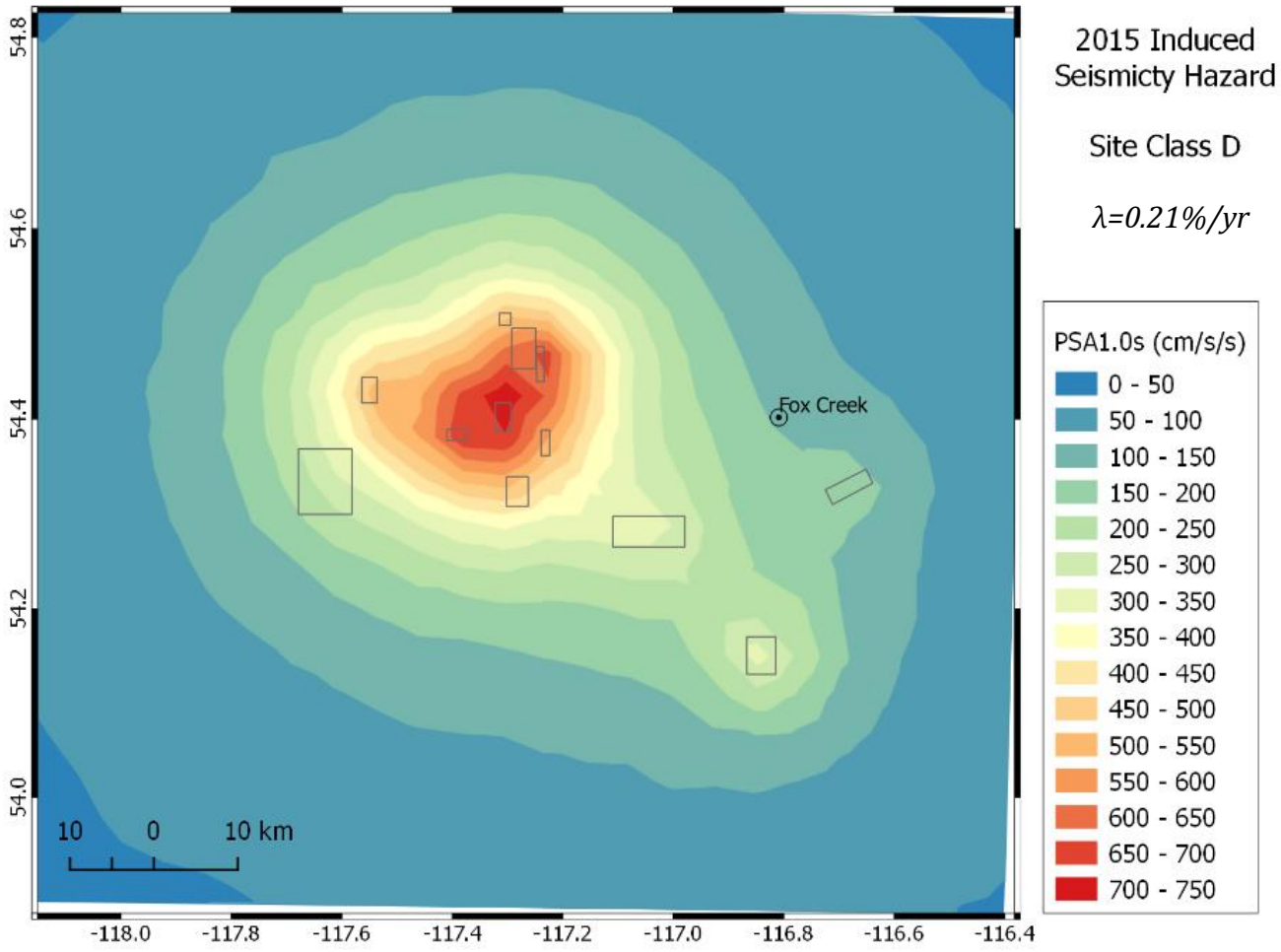
2015 Induced
Seismicty Hazard
Site Class D
λ=0.21%/yr
PSA1.0s (cm/s/s)
0 - 50
50 - 100
100 - 150
150 - 200
200 - 250
250 - 300
300 - 350
350 - 400
400 - 450
450 - 500
500 - 550
550 - 600
600 - 650
650 - 700
700 - 750
Fox Creek
10 0 10 km
54.8
54.6
54.4
54.2
54.0
-118.0
-117.8
-117.6
-117.4
-117.2
-117.0
-116.8
-116.6
-116.4

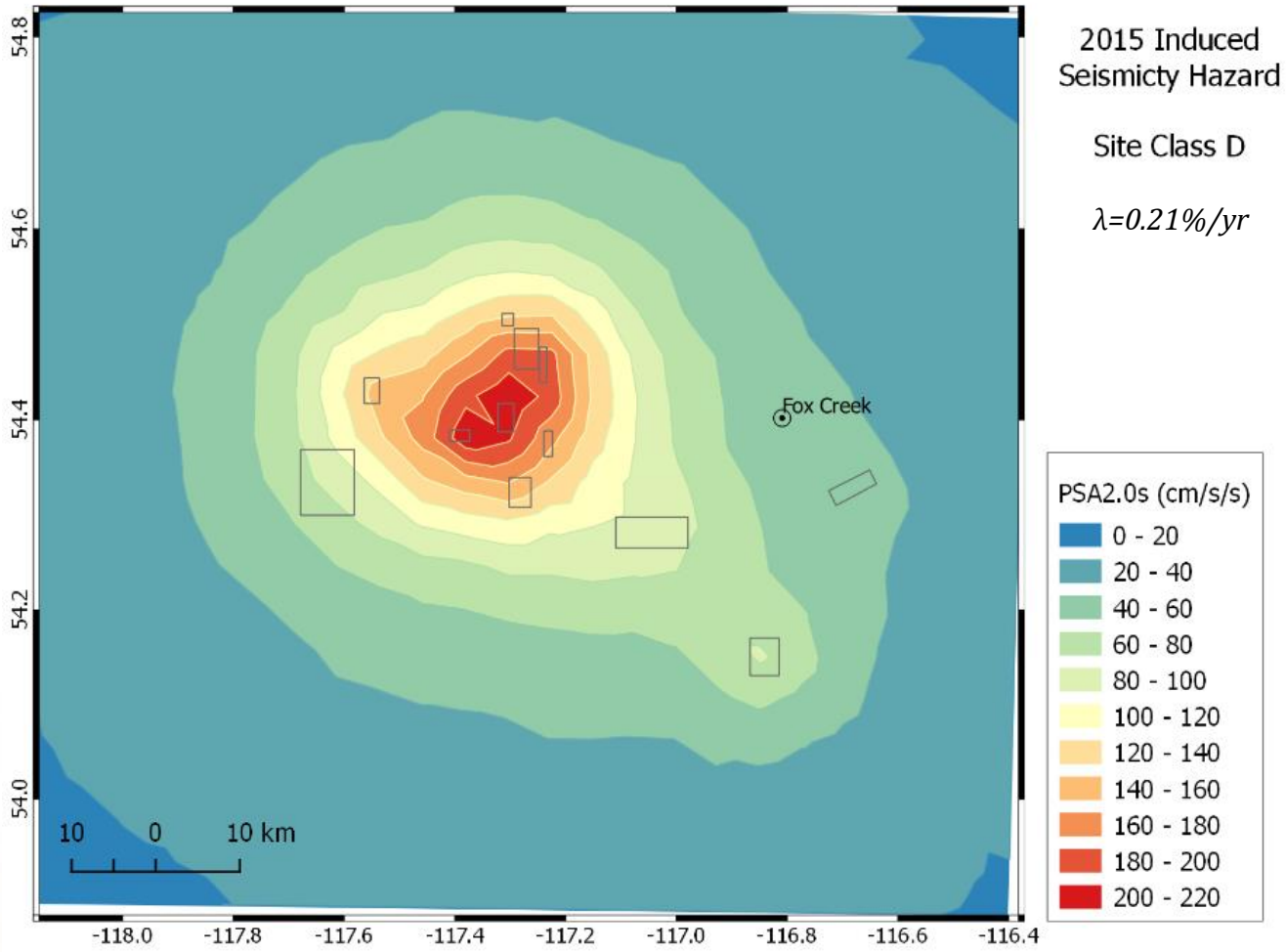
2015 Induced
Seismicty Hazard
Site Class D
λ=0.21%/yr
Fox Creek
PSA2.0s (cm/s/s)
0 - 20
20 - 40
40 - 60
60 - 80
80 - 100
100 - 120
120 - 140
140 - 160
160 - 180
180 - 200
200 - 220
10 0 10 km
54.8
54.6
54.4
54.2
54.0
-118.0
-117.8
-117.6
-117.4
-117.2
-117.0
-116.8
-116.6
-116.4

10.4 HAZARD MAPS FOR 2013 INDUCED SEISMICITY MODEL (0.04%/YR)

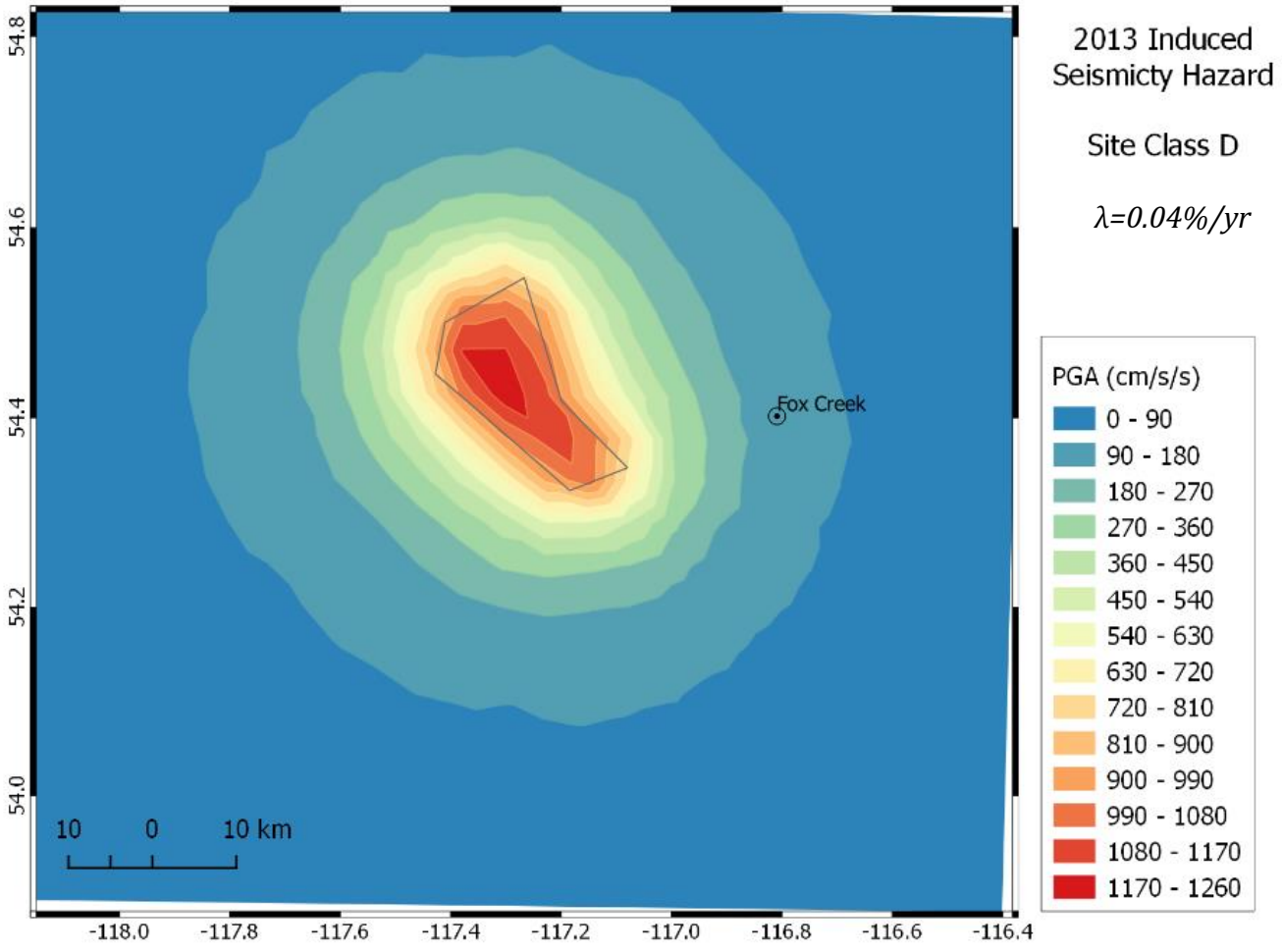

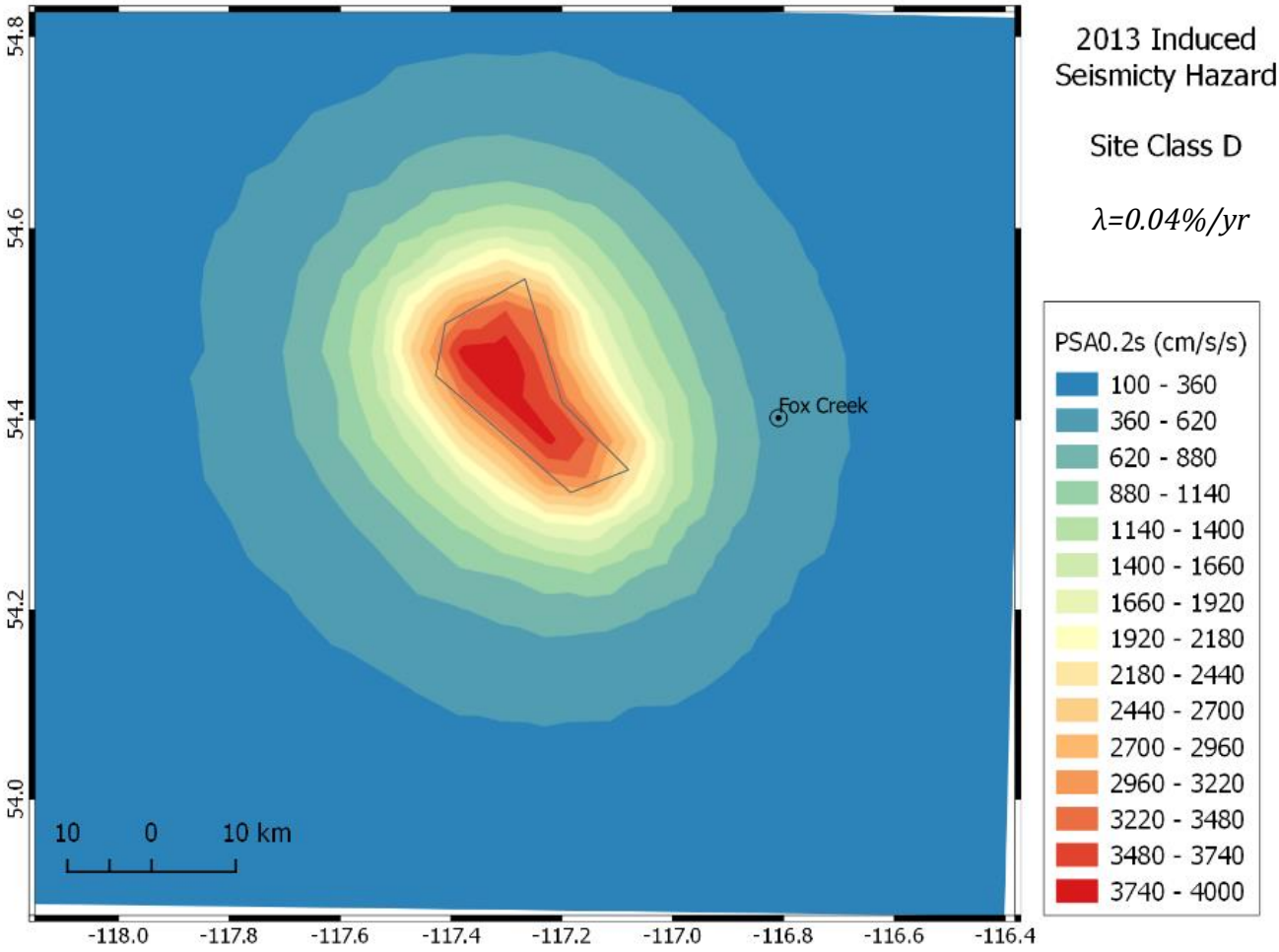
2013 Induced Seismicty Hazard
Site Class D
λ=0.04%/yr
PSA0.2s (cm/s/s)
100 - 360
360 - 620
620 - 880
880 - 1140
1140 - 1400
1400 - 1660
1660 - 1920
1920 - 2180
2180 - 2440
2440 - 2700
2700 - 2960
2960 - 3220
3220 - 3480
3480 - 3740
3740 - 4000
Fox Creek
10 0 10 km
54.8
54.6
54.4
54.2
54.0
-118.0
-117.8
-117.6
-117.4
-117.2
-117.0
-116.8
-116.6
-116.4

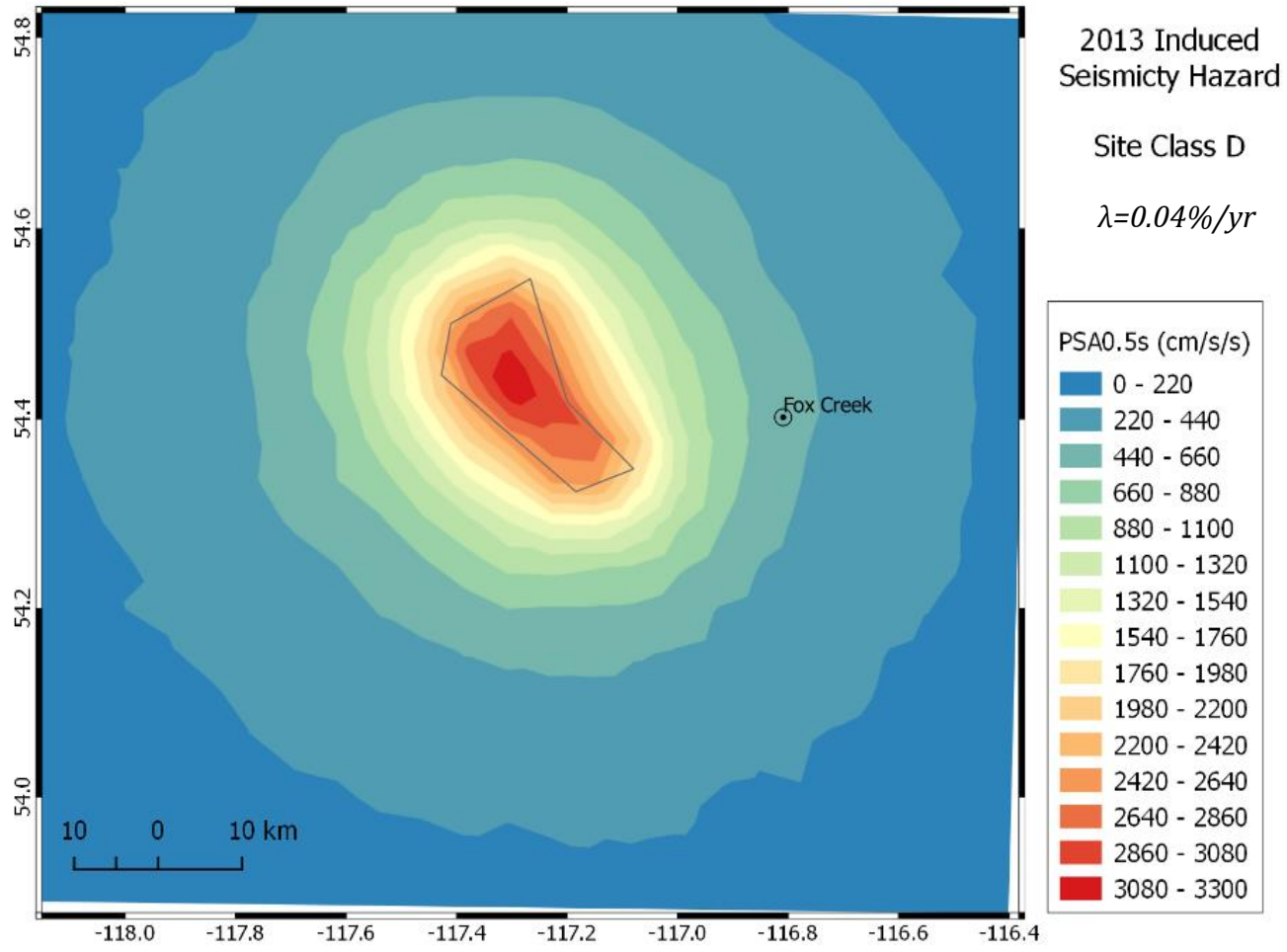
2013 Induced
Seismicty Hazard
Site Class D
λ=0.04%/yr
PSA0.5s (cm/s/s)
0 - 220
220 - 440
440 - 660
660 - 880
880 - 1100
1100 - 1320
1320 - 1540
1540 - 1760
1760 - 1980
1980 - 2200
2200 - 2420
2420 - 2640
2640 - 2860
2860 - 3080
3080 - 3300
Fox Creek
10 0 10 km
54.8
54.6
54.4
54.2
54.0
-118.0
-117.8
-117.6
-117.4
-117.2
-117.0
-116.8
-116.6
-116.4

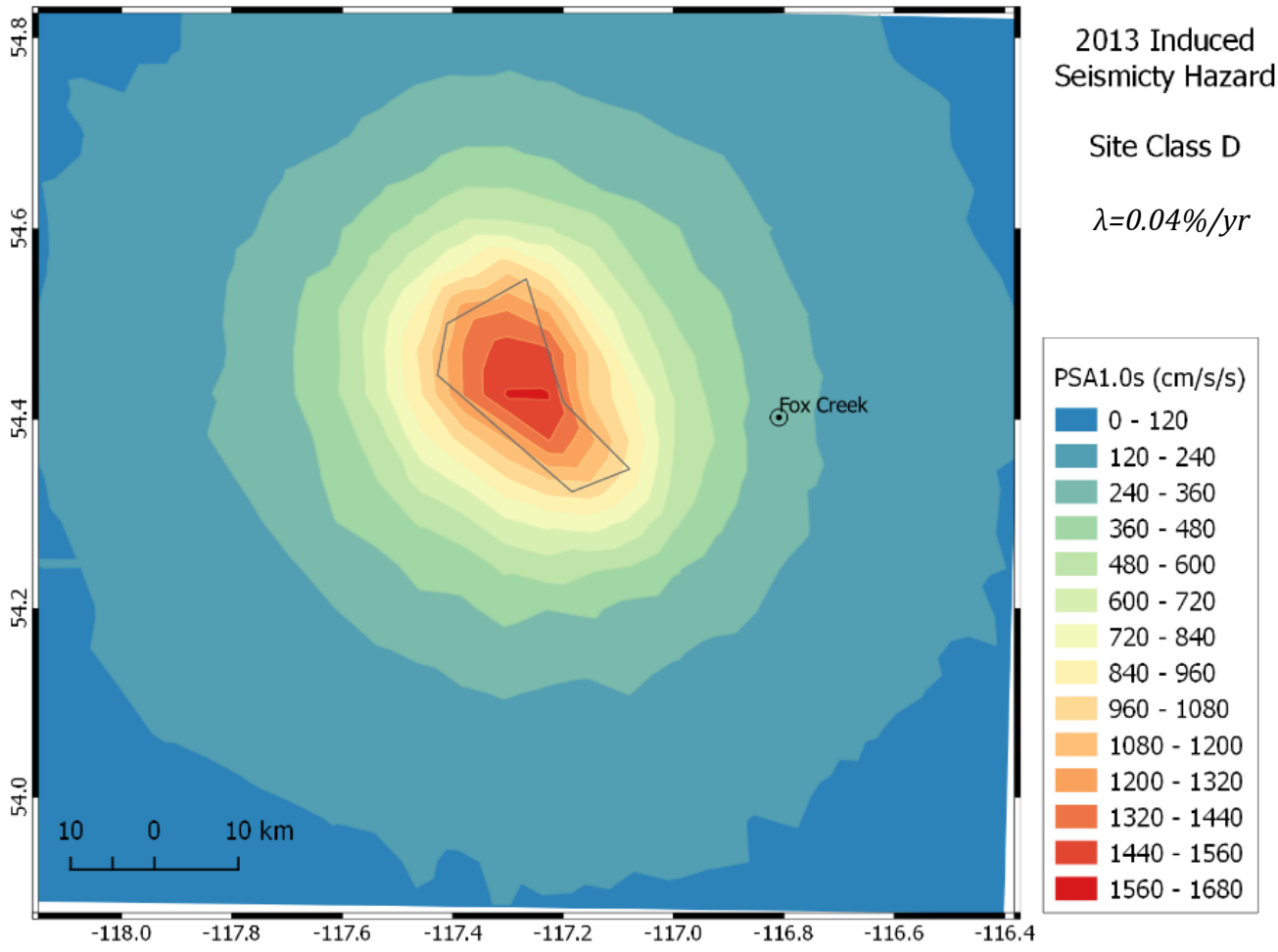
2013 Induced
Seismicty Hazard
Site Class D
λ=0.04%/yr
PSA1.0s (cm/s/s)
0 - 120
120 - 240
240 - 360
360 - 480
480 - 600
600 - 720
720 - 840
840 - 960
960 - 1080
1080 - 1200
1200 - 1320
1320 - 1440
1440 - 1560
1560 - 1680
Fox Creek
10 0 10 km
54.8
54.6
54.4
54.2
54.0
-118.0
-117.8
-117.6
-117.4
-117.2
-117.0
-116.8
-116.6
-116.4

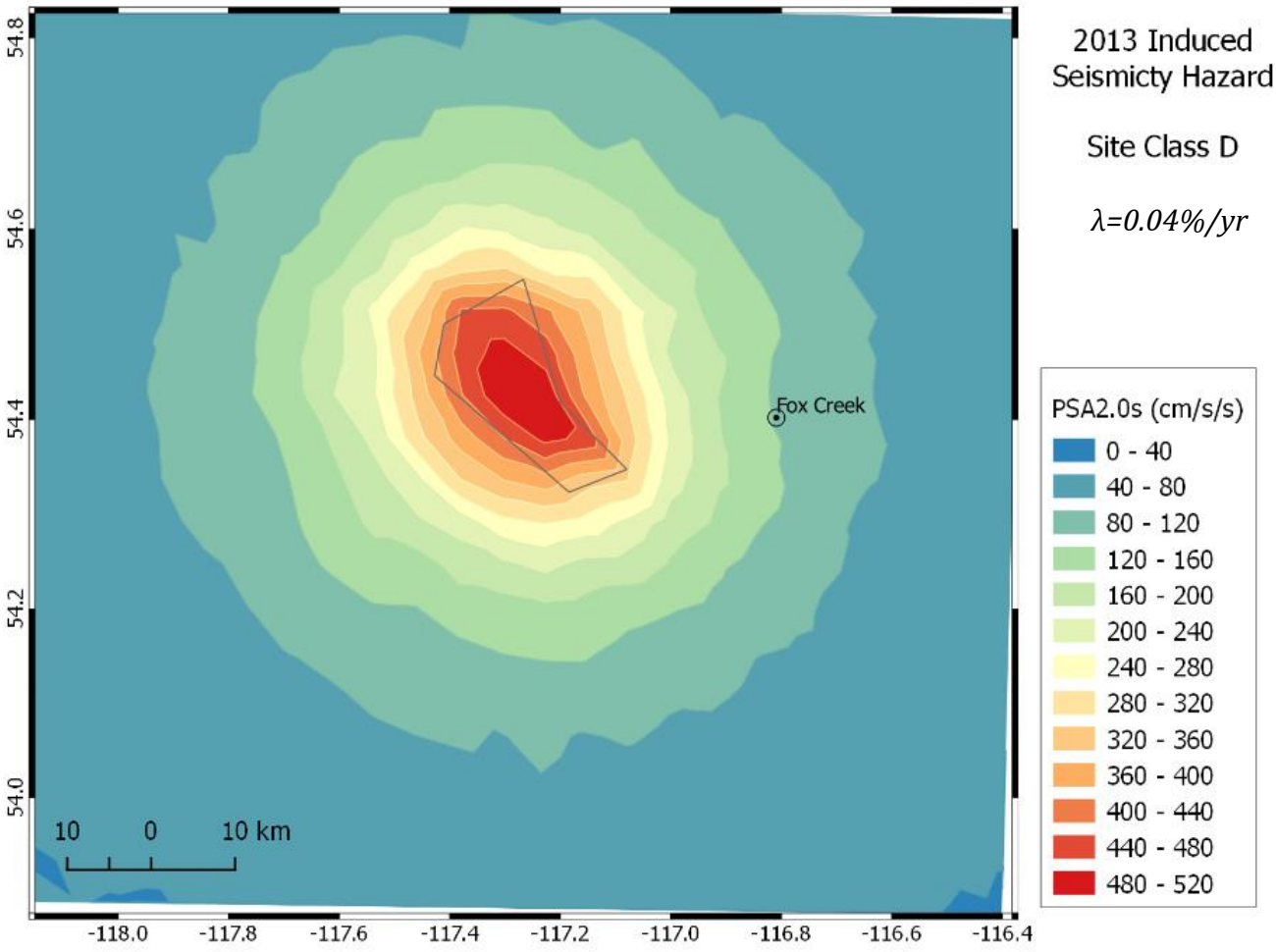
2013 Induced Seismicty Hazard
Site Class D
λ=0.04%/yr
Fox Creek
PSA2.0s (cm/s/s)
0 - 40
40 - 80
80 - 120
120 - 160
160 - 200
200 - 240
240 - 280
280 - 320
320 - 360
360 - 400
400 - 440
440 - 480
480 - 520
10 0 10 km
54.8
54.6
54.4
54.2
54.0
-118.0
-117.8
-117.6
-117.4
-117.2
-117.0
-116.8
-116.6
-116.4

10.5 HAZARD MAPS FOR 2014 INDUCED SEISMICITY MODEL (0.04%/YR)

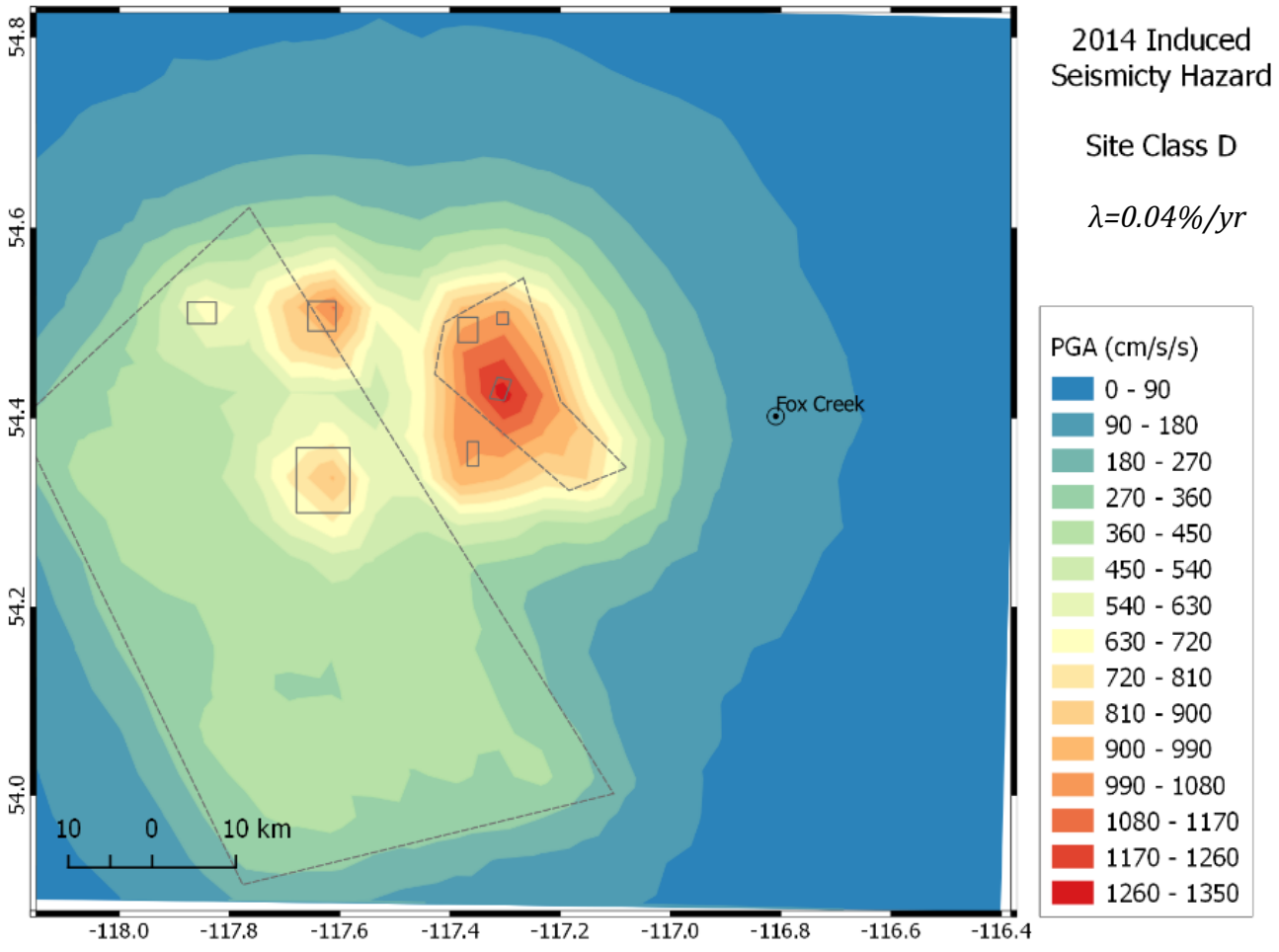

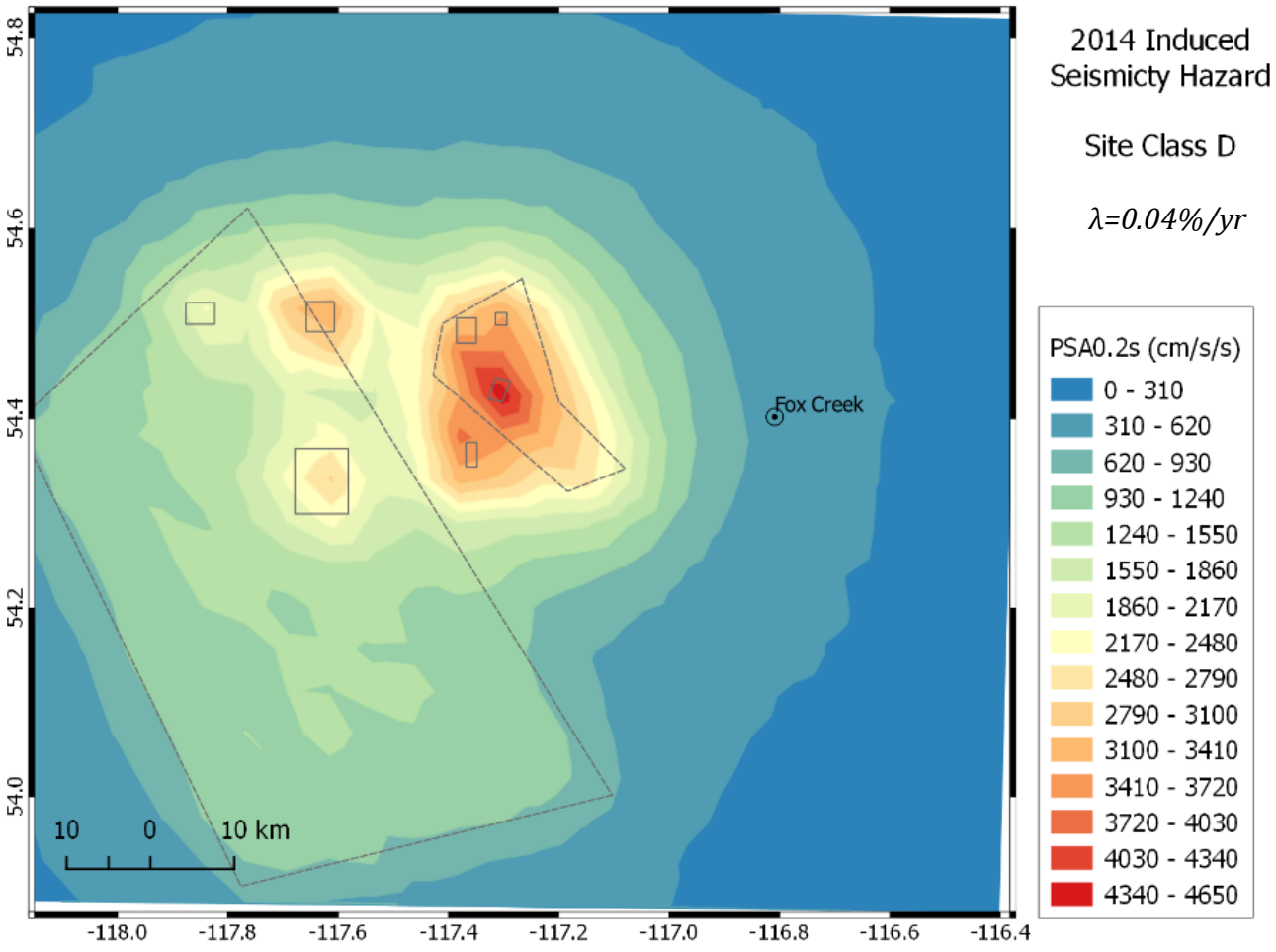
2014 Induced Seismicty Hazard
Site Class D
λ=0.04%/yr
PSA0.2s (cm/s/s)
0 - 310
310 - 620
620 - 930
930 - 1240
1240 - 1550
1550 - 1860
1860 - 2170
2170 - 2480
2480 - 2790
2790 - 3100
3100 - 3410
3410 - 3720
3720 - 4030
4030 - 4340
4340 - 4650
Fox Creek
10 0 10 km
54.8
54.6
54.4
54.2
54.0
-118.0
-117.8
-117.6
-117.4
-117.2
-117.0
-116.8
-116.6
-116.4

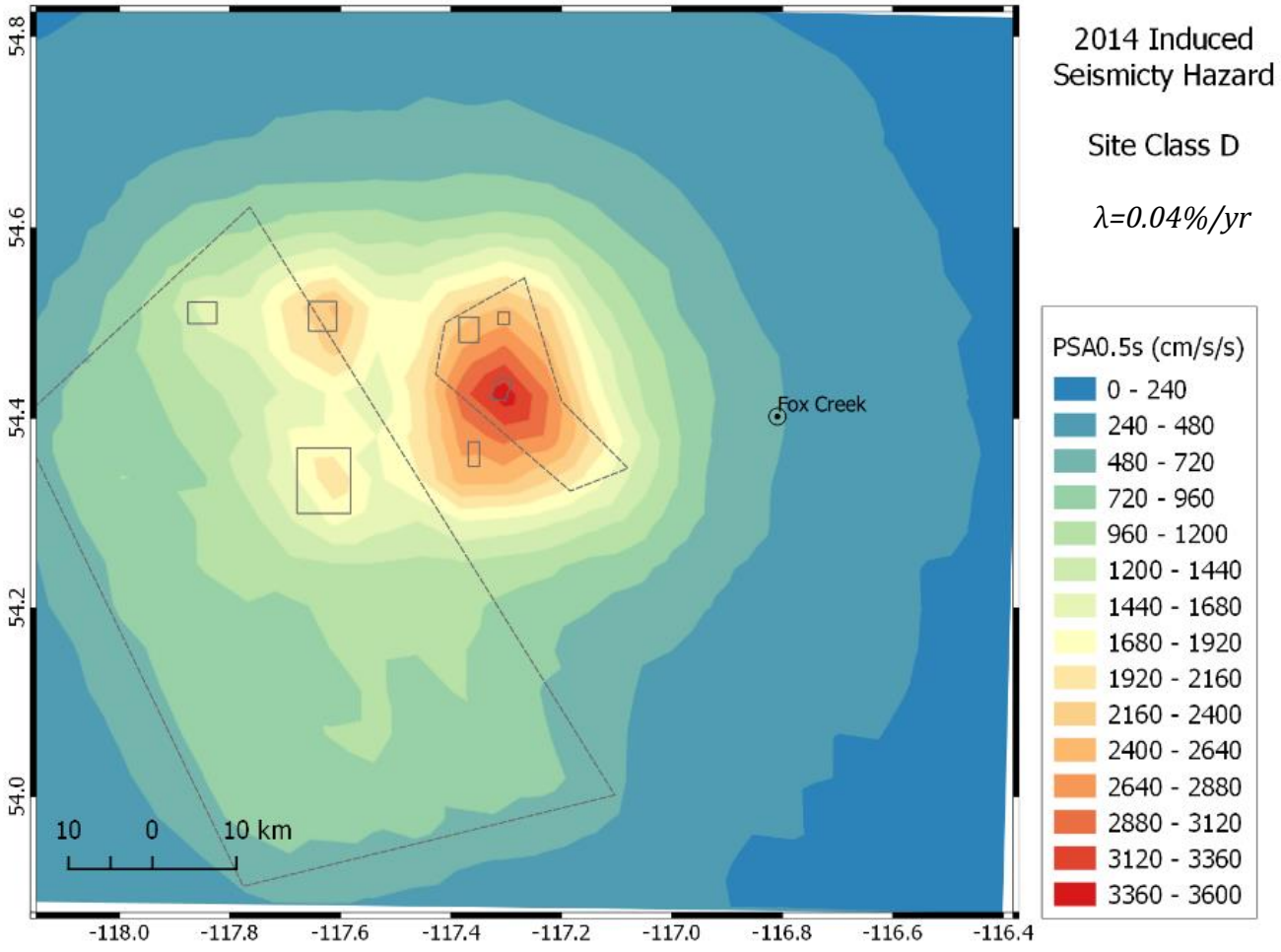
2014 Induced
Seismicty Hazard
Site Class D
λ=0.04%/yr
PSA0.5s (cm/s/s)
0 - 240
240 - 480
480 - 720
720 - 960
960 - 1200
1200 - 1440
1440 - 1680
1680 - 1920
1920 - 2160
2160 - 2400
2400 - 2640
2640 - 2880
2880 - 3120
3120 - 3360
3360 - 3600
Fox Creek
10 0 10 km
54.8
54.6
54.4
54.2
54.0
-118.0
-117.8
-117.6
-117.4
-117.2
-117.0
-116.8
-116.6
-116.4

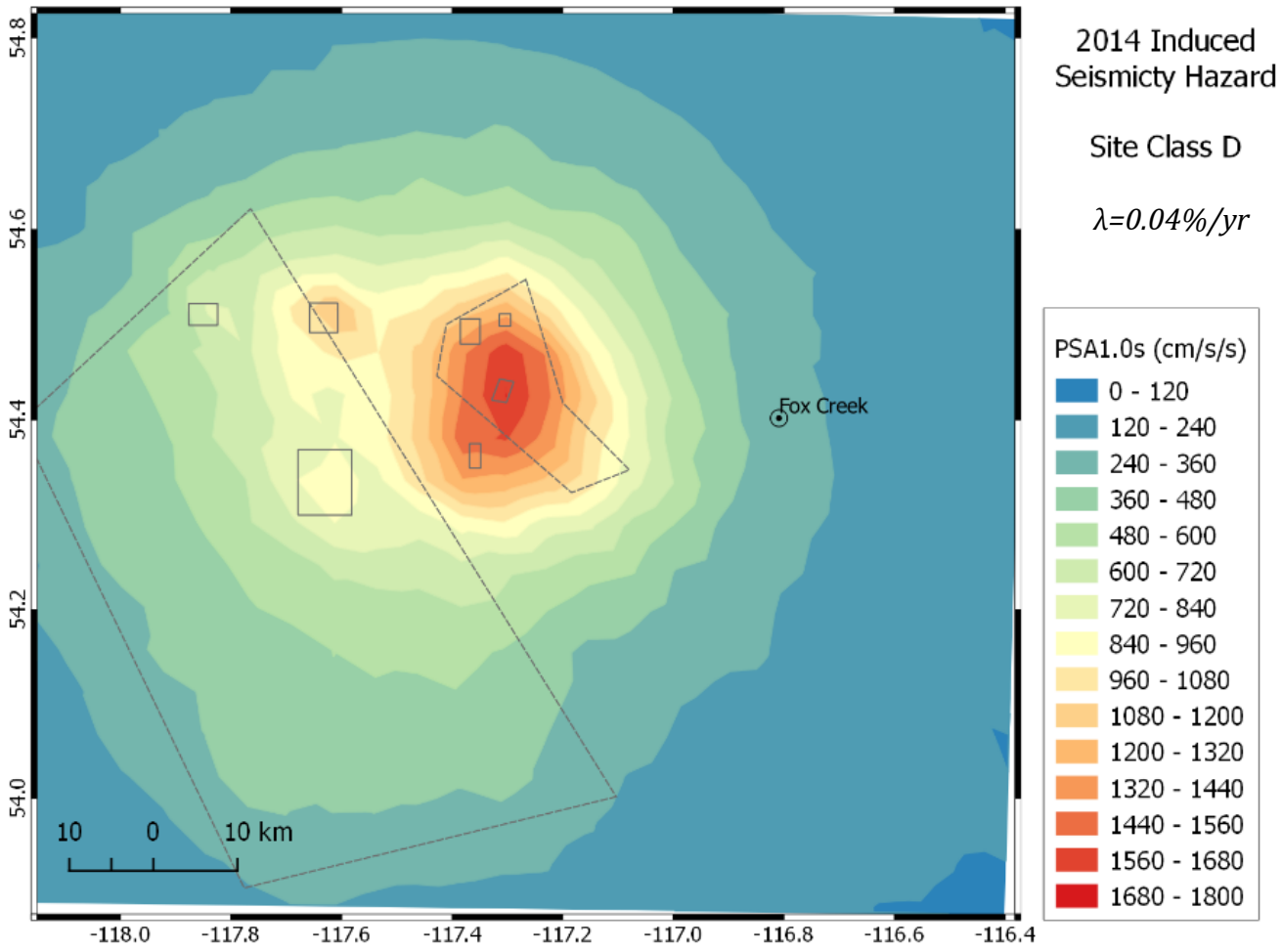
2014 Induced Seismicty Hazard
Site Class D
λ=0.04%/yr
PSA1.0s (cm/s/s)
0 - 120
120 - 240
240 - 360
360 - 480
480 - 600
600 - 720
720 - 840
840 - 960
960 - 1080
1080 - 1200
1200 - 1320
1320 - 1440
1440 - 1560
1560 - 1680
1680 - 1800
Fox Creek
10 0 10 km
54.8
54.6
54.4
54.2
54.0
-118.0
-117.8
-117.6
-117.4
-117.2
-117.0
-116.8
-116.6
-116.4

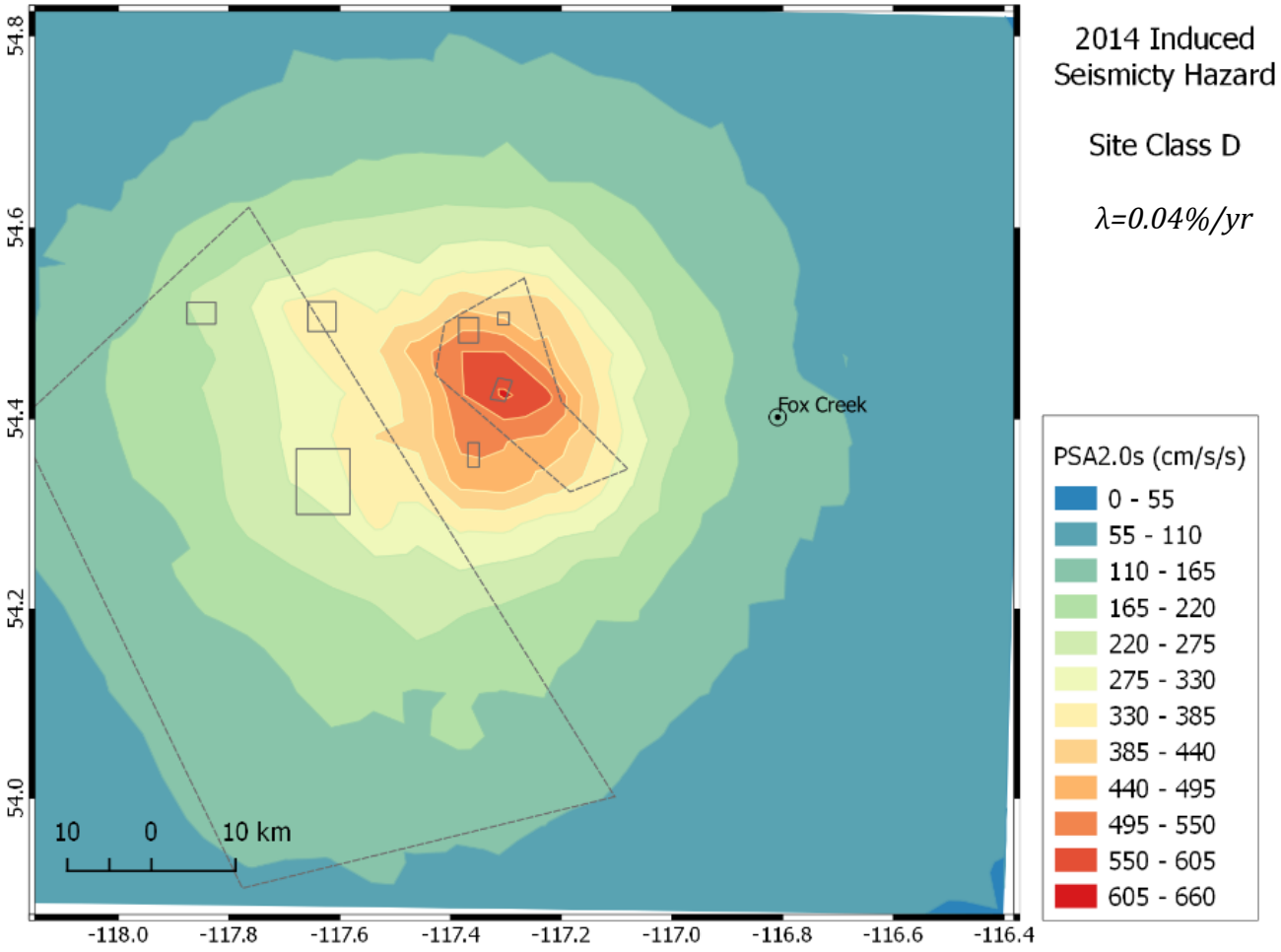
2014 Induced
Seismicty Hazard
Site Class D
λ=0.04%/yr
Fox Creek
PSA2.0s (cm/s/s)
0 - 55
55 - 110
110 - 165
165 - 220
220 - 275
275 - 330
330 - 385
385 - 440
440 - 495
495 - 550
550 - 605
605 - 660
10 0 10 km
54.8
54.6
54.4
54.2
54.0
-118.0
-117.8
-117.6
-117.4
-117.2
-117.0
-116.8
-116.6
-116.4

10.6 HAZARD MAPS FOR 2015 INDUCED SEISMICITY MODEL (0.04%/YR)

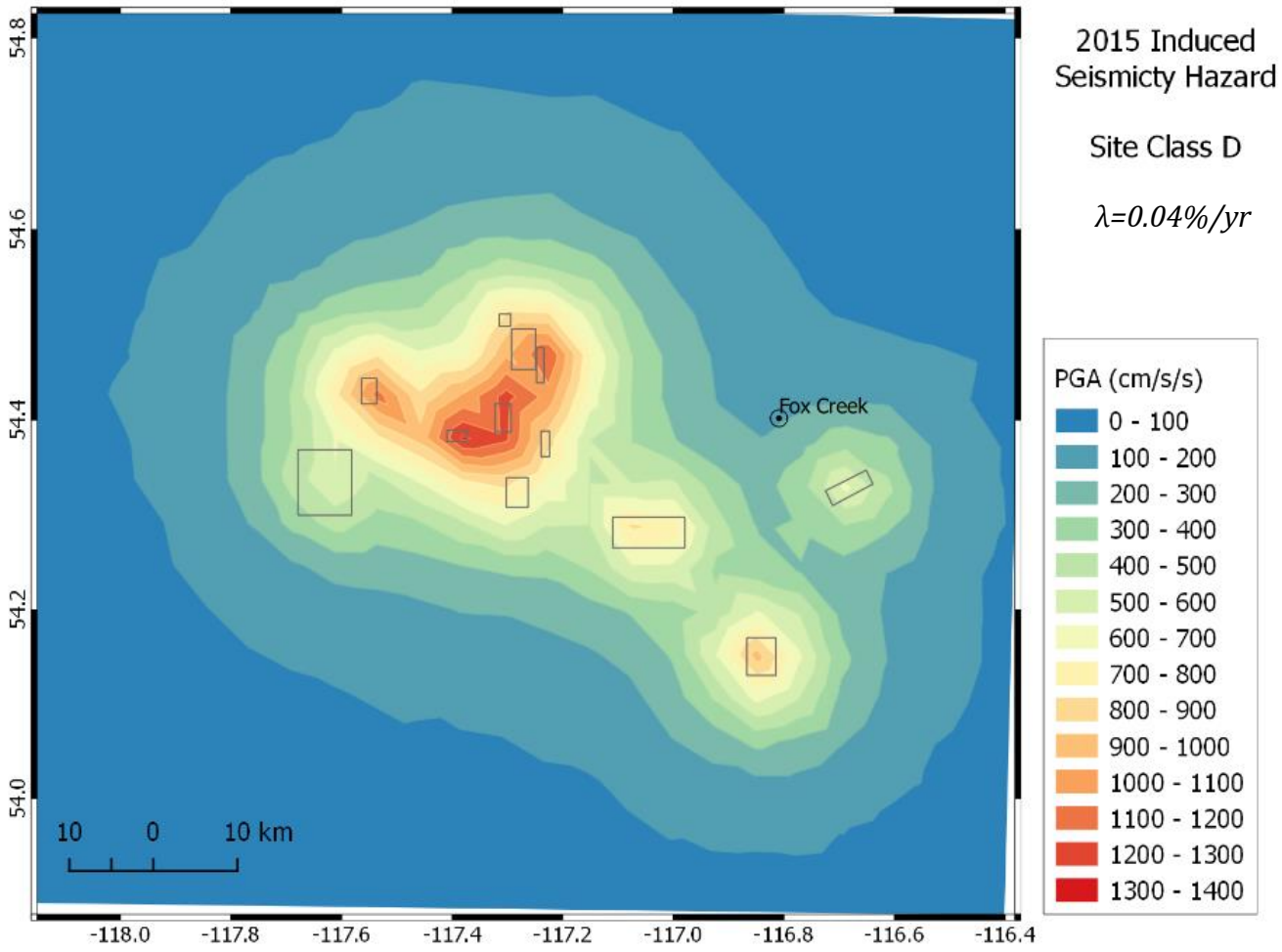

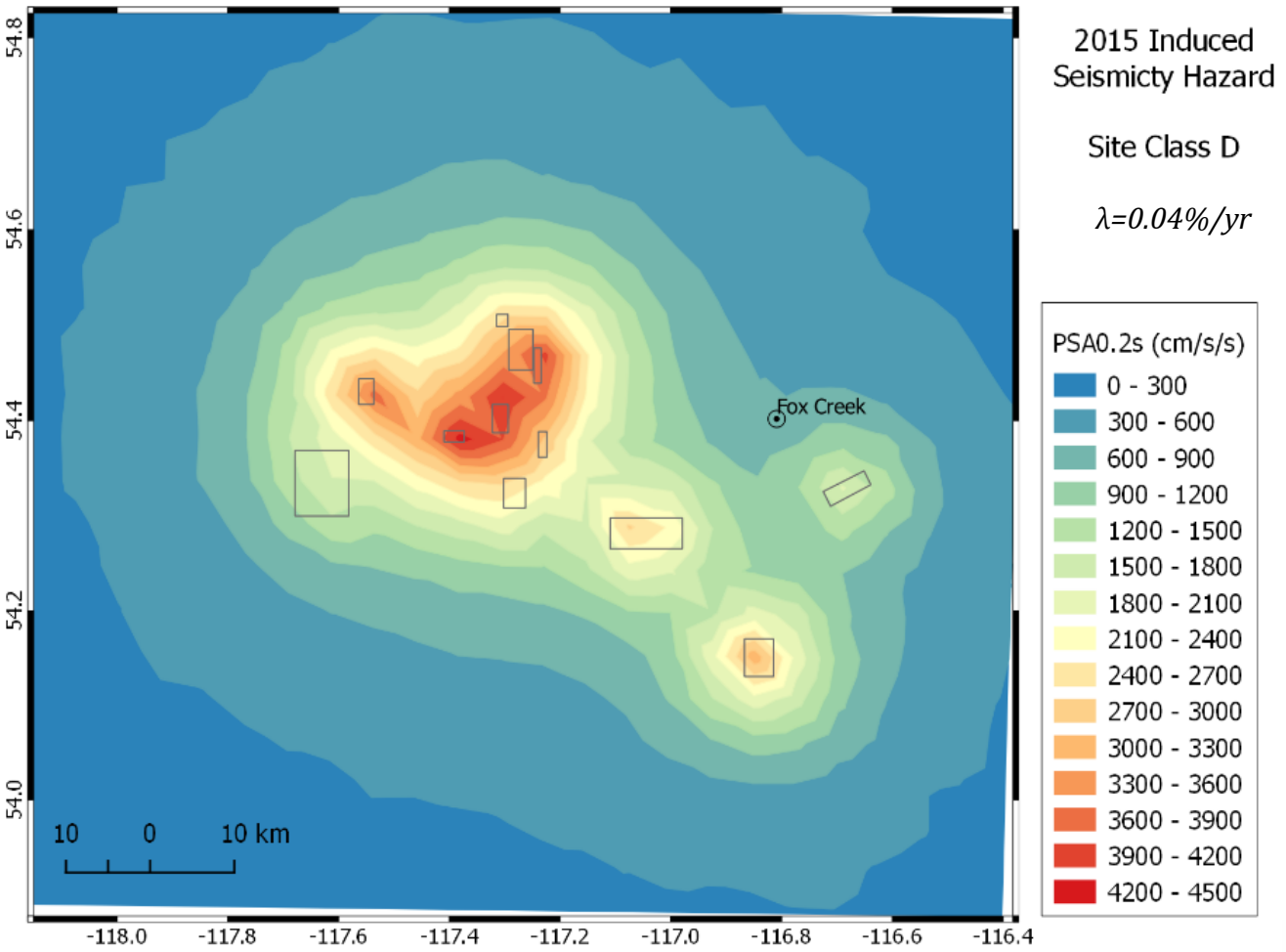
2015 Induced Seismicty Hazard
Site Class D
λ=0.04%/yr
PSA0.2s (cm/s/s)
0 - 300
300 - 600
600 - 900
900 - 1200
1200 - 1500
1500 - 1800
1800 - 2100
2100 - 2400
2400 - 2700
2700 - 3000
3000 - 3300
3300 - 3600
3600 - 3900
3900 - 4200
4200 - 4500
Fox Creek
10 0 10 km
54.8
54.6
54.4
54.2
54.0
-118.0
-117.8
-117.6
-117.4
-117.2
-117.0
-116.8
-116.6
-116.4

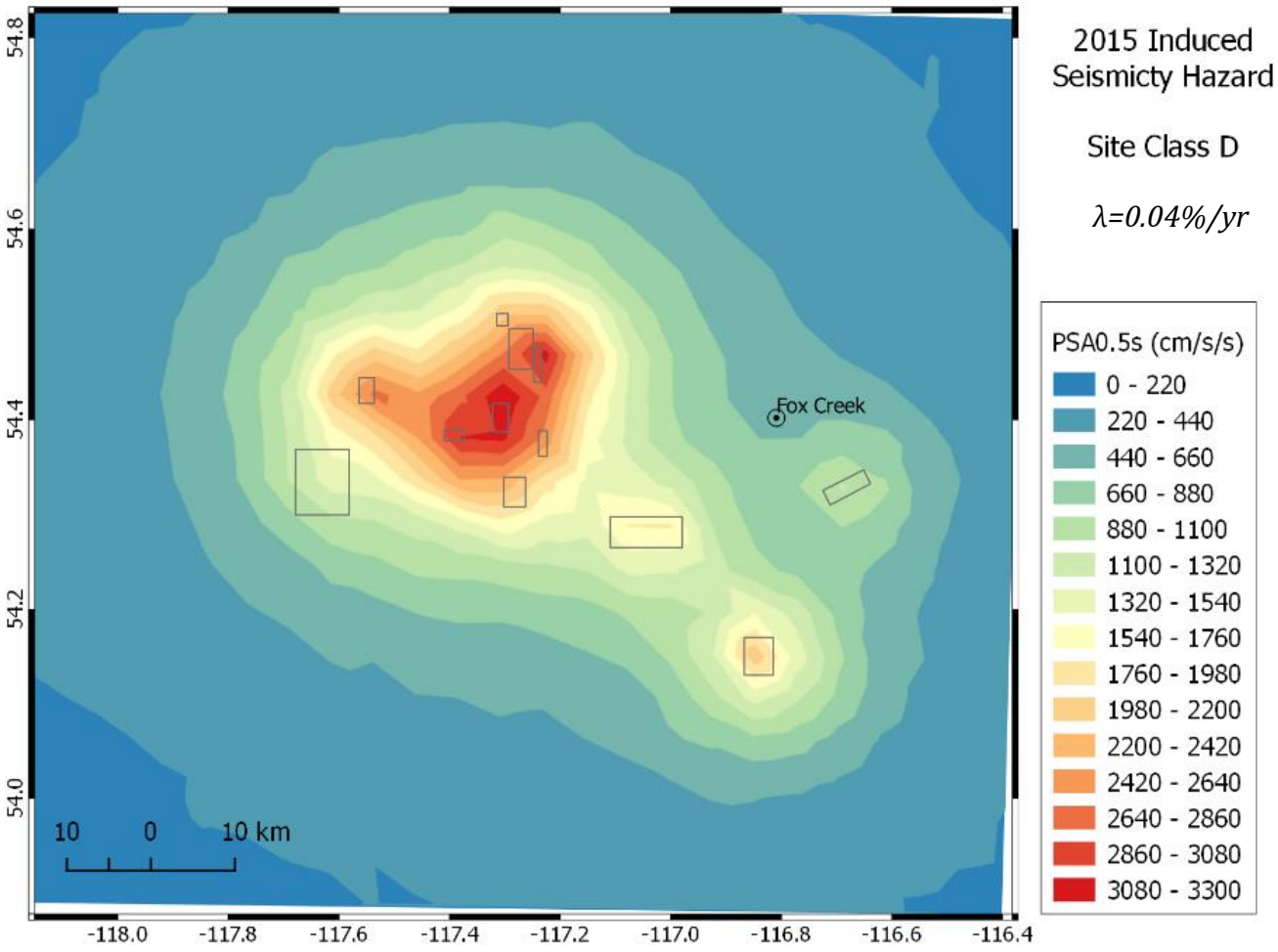
2015 Induced Seismicty Hazard
Site Class D
λ=0.04%/yr
PSA0.5s (cm/s/s)
0 - 220
220 - 440
440 - 660
660 - 880
880 - 1100
1100 - 1320
1320 - 1540
1540 - 1760
1760 - 1980
1980 - 2200
2200 - 2420
2420 - 2640
2640 - 2860
2860 - 3080
3080 - 3300
Fox Creek
10 0 10 km
54.8
54.6
54.4
54.2
54.0
-118.0
-117.8
-117.6
-117.4
-117.2
-117.0
-116.8
-116.6
-116.4

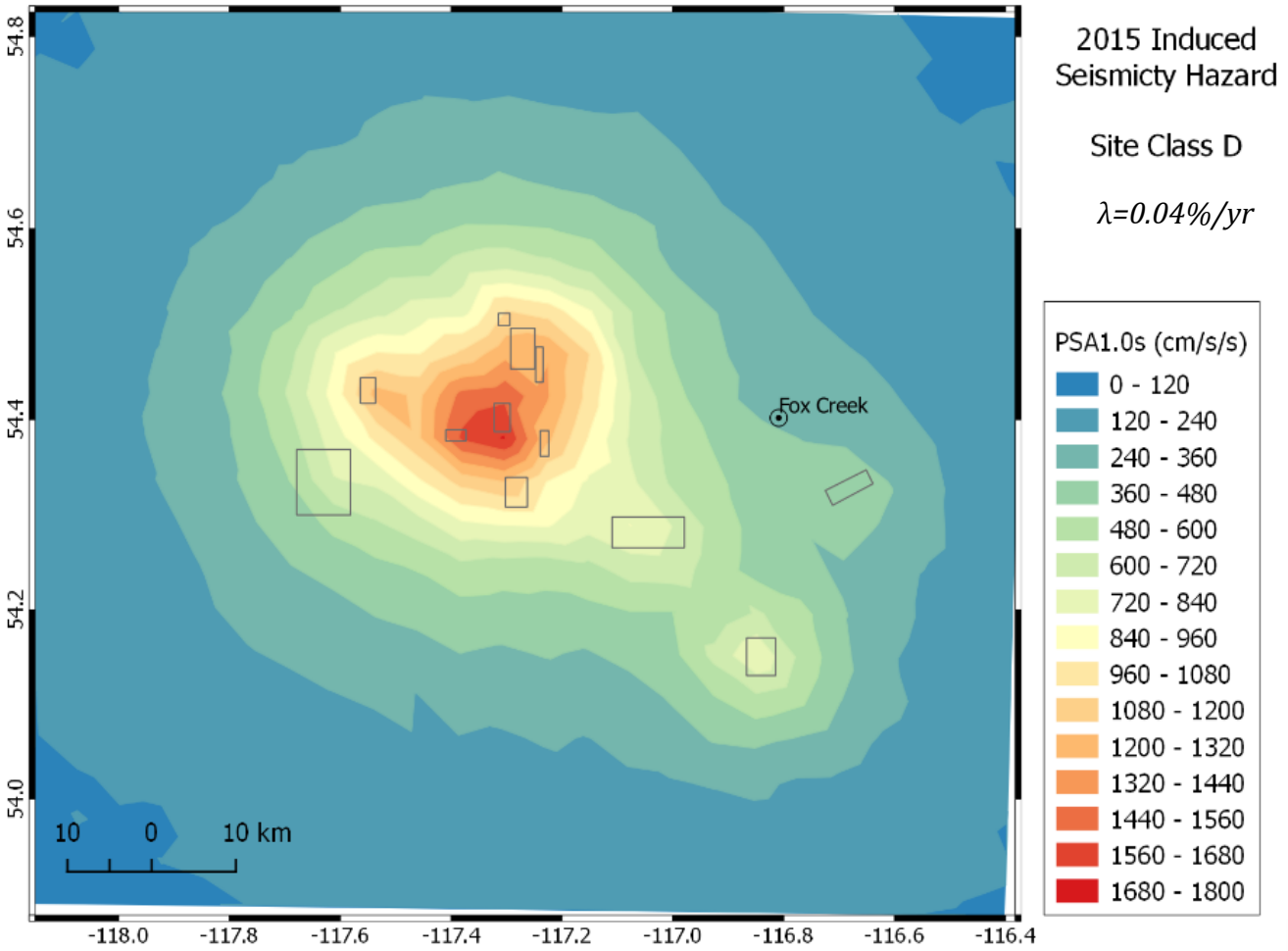
2015 Induced Seismicty Hazard
Site Class D
λ=0.04%/yr
PSA1.0s (cm/s/s)
0 - 120
120 - 240
240 - 360
360 - 480
480 - 600
600 - 720
720 - 840
840 - 960
960 - 1080
1080 - 1200
1200 - 1320
1320 - 1440
1440 - 1560
1560 - 1680
1680 - 1800
Fox Creek
10 0 10 km
54.8
54.6
54.4
54.2
54.0
-118.0
-117.8
-117.6
-117.4
-117.2
-117.0
-116.8
-116.6
-116.4

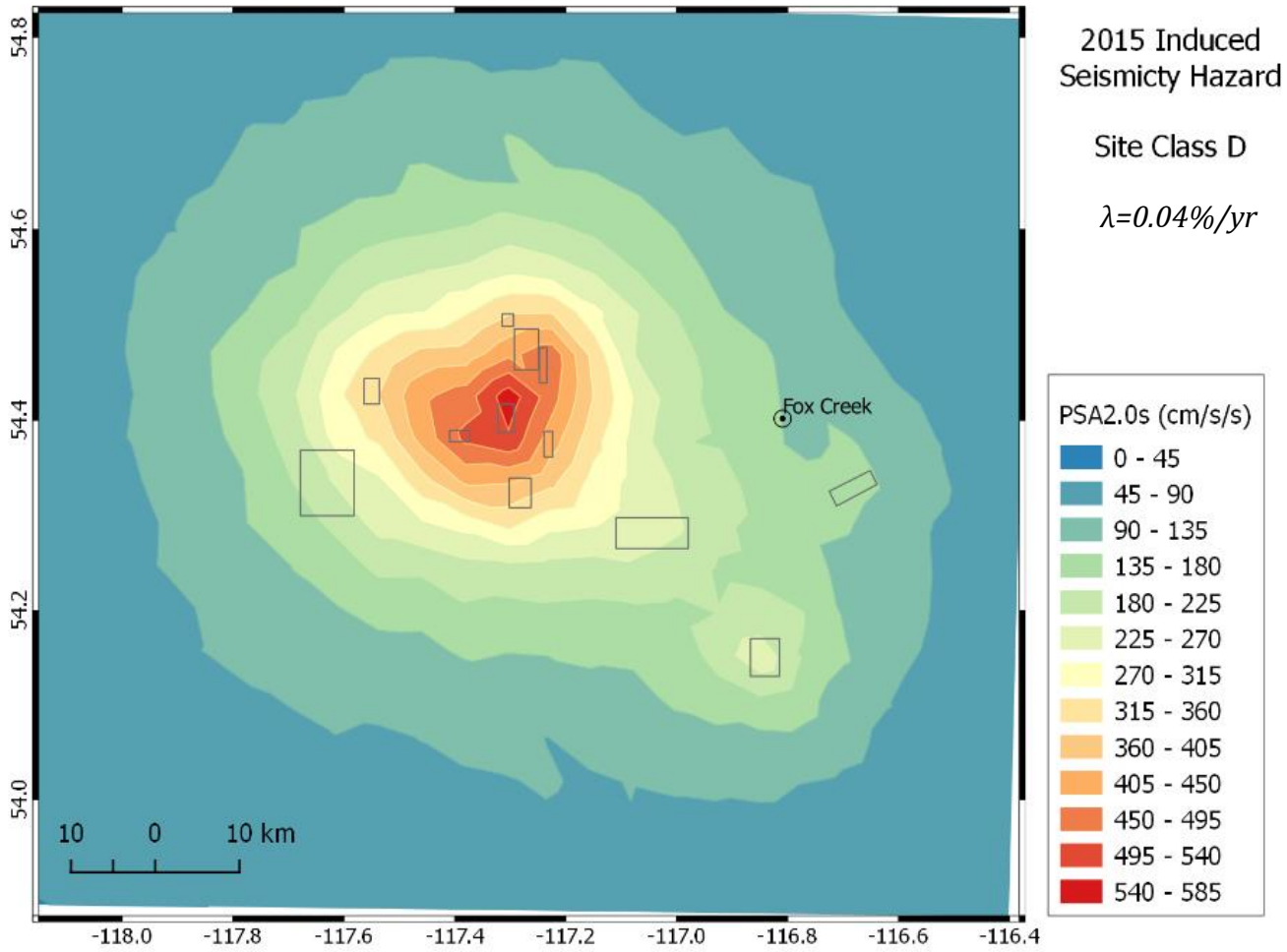
2015 Induced
Seismicty Hazard
Site Class D
λ=0.04%/yr
Fox Creek
PSA2.0s (cm/s/s)
0 - 45
45 - 90
90 - 135
135 - 180
180 - 225
225 - 270
270 - 315
315 - 360
360 - 405
405 - 450
450 - 495
495 - 540
540 - 585
10 0 10 km
54.8
54.6
54.4
54.2
54.0
-118.0
-117.8
-117.6
-117.4
-117.2
-117.0
-116.8
-116.6
-116.4

10.7 DEAGGREGATION OF SEISMIC HAZARD FOR FOX CREEK

2013 Induced Seismicity Model (λ=0.21%/yr)

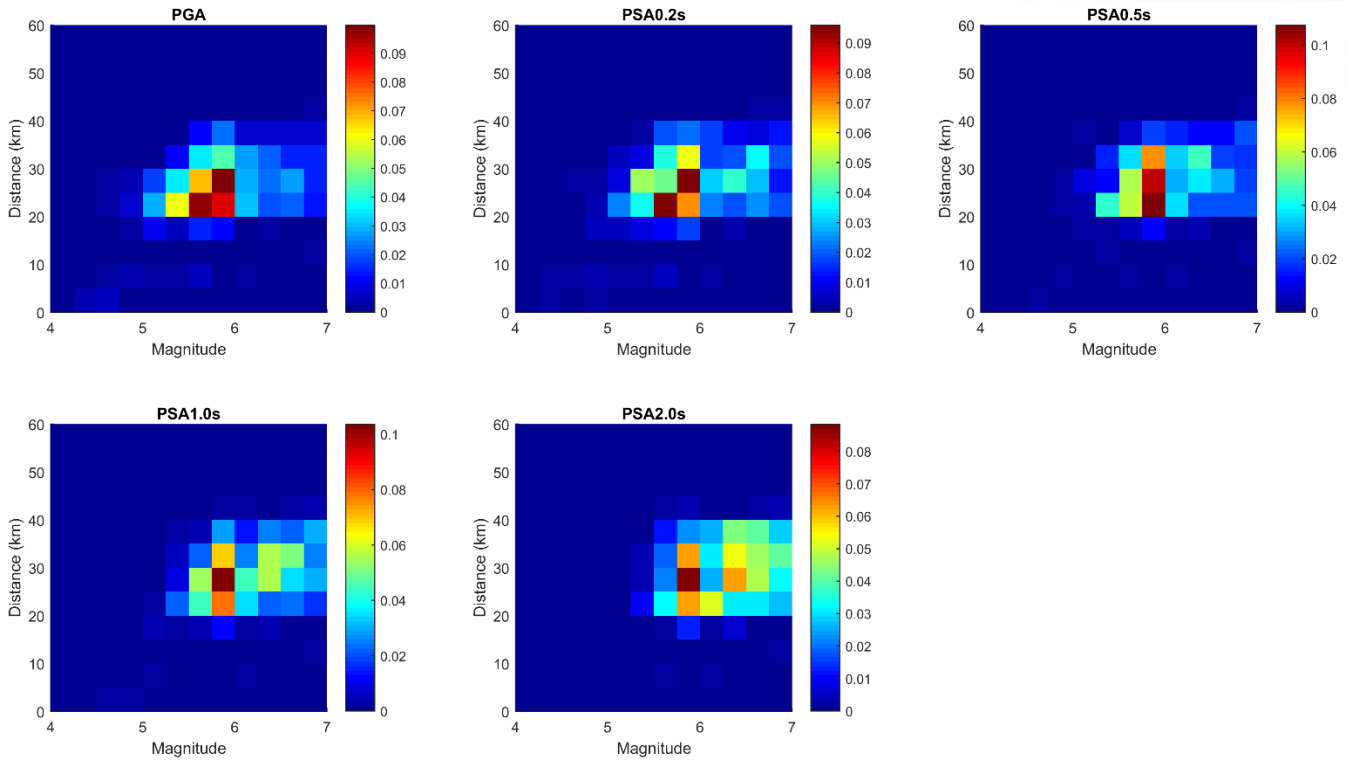

2014 Induced Seismicity Model (λ=0.21%/yr)

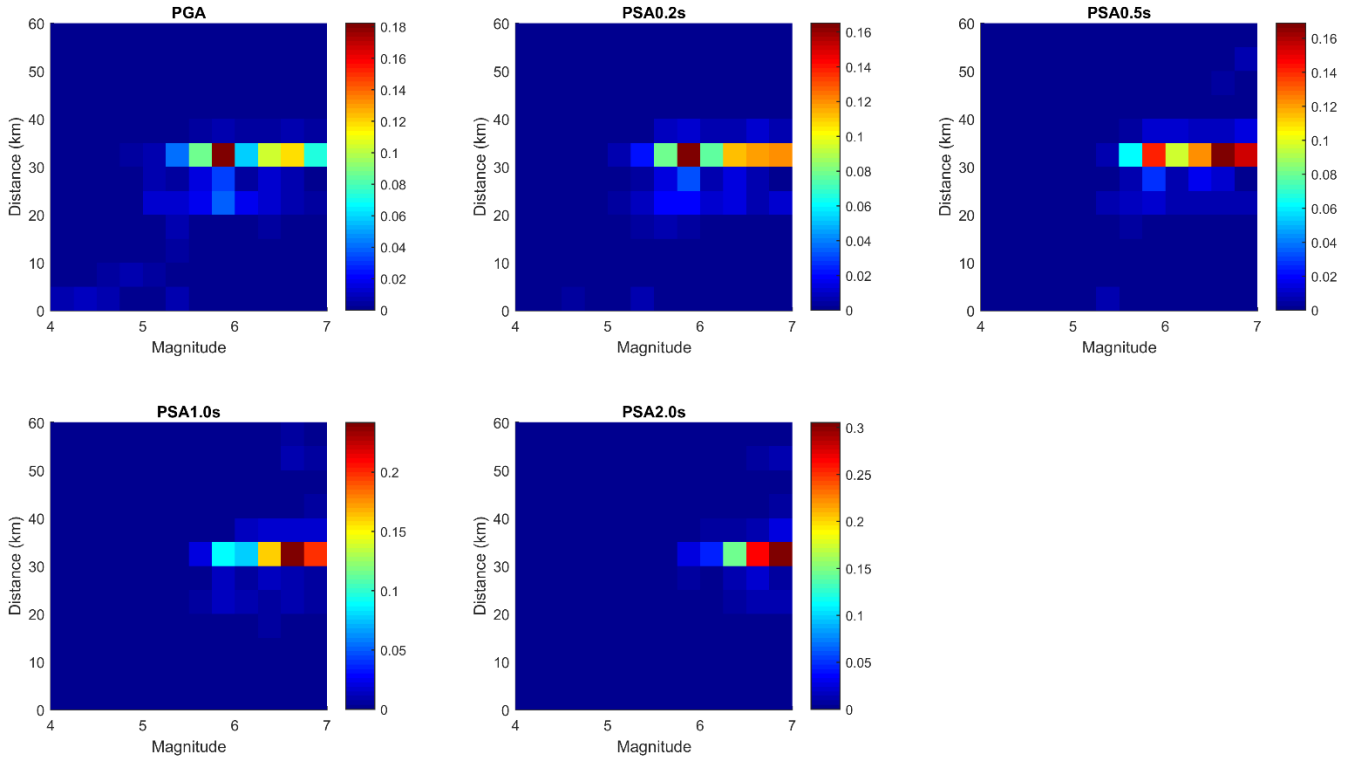

2015 Induced Seismicity Model (λ=0.21%/yr)

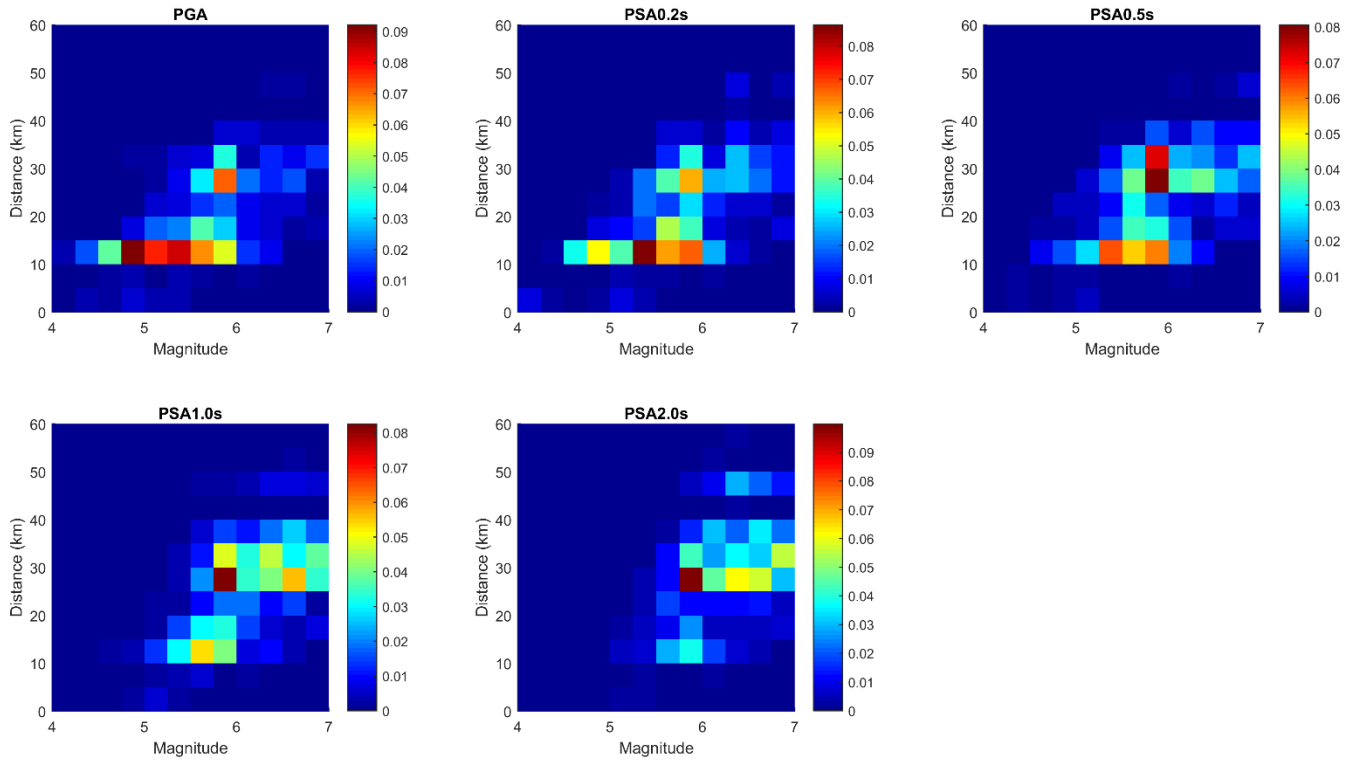

2013 Induced Seismicity Model (λ=0.04%/yr)

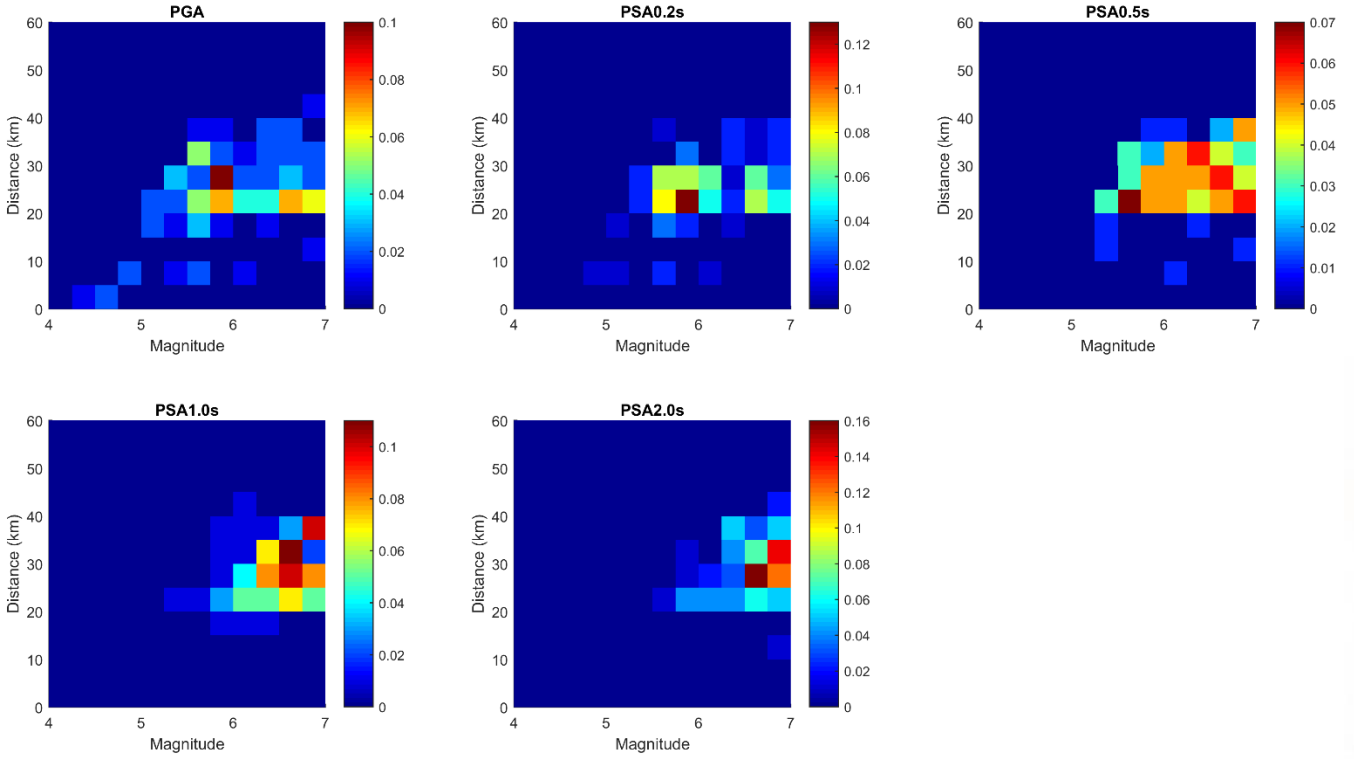

2014 Induced Seismicity Model (λ=0.04%/yr)

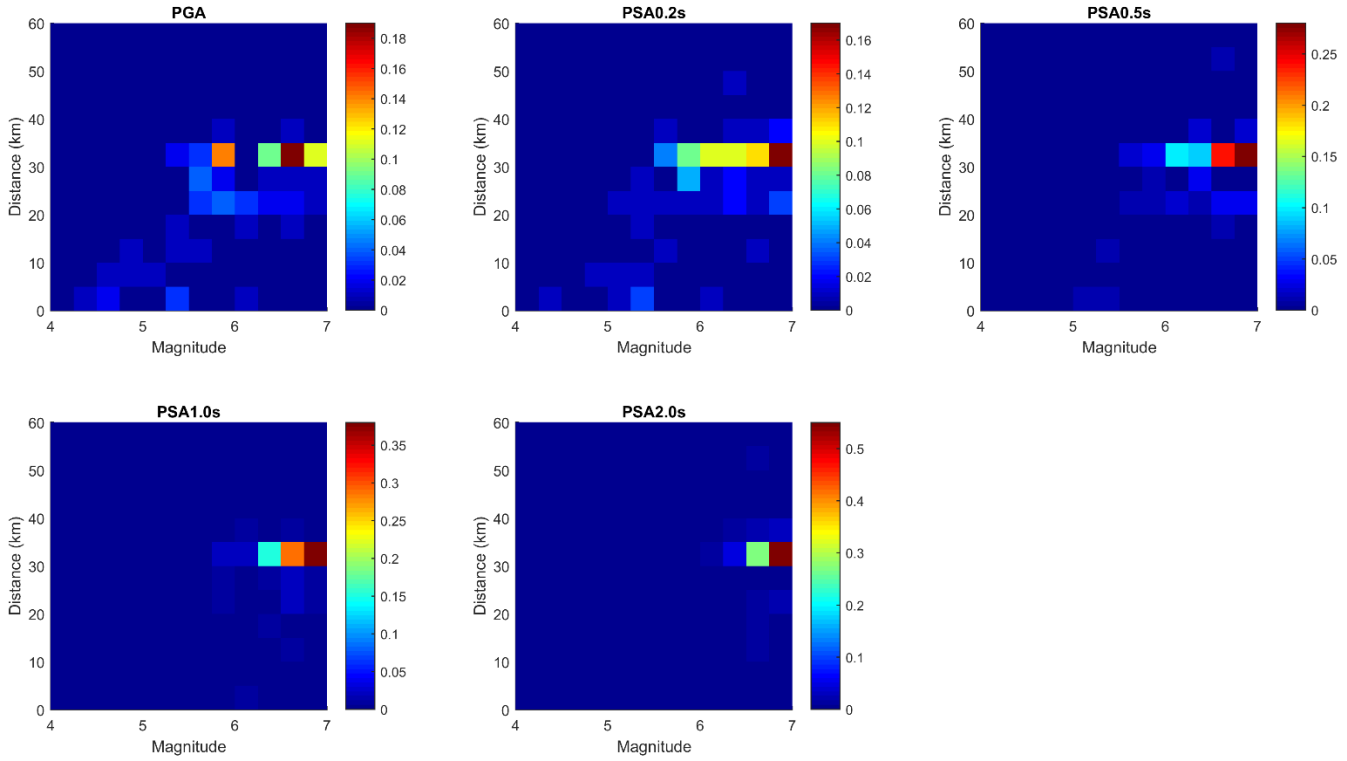

2015 Induced Seismicity Model (λ=0.04%/yr)

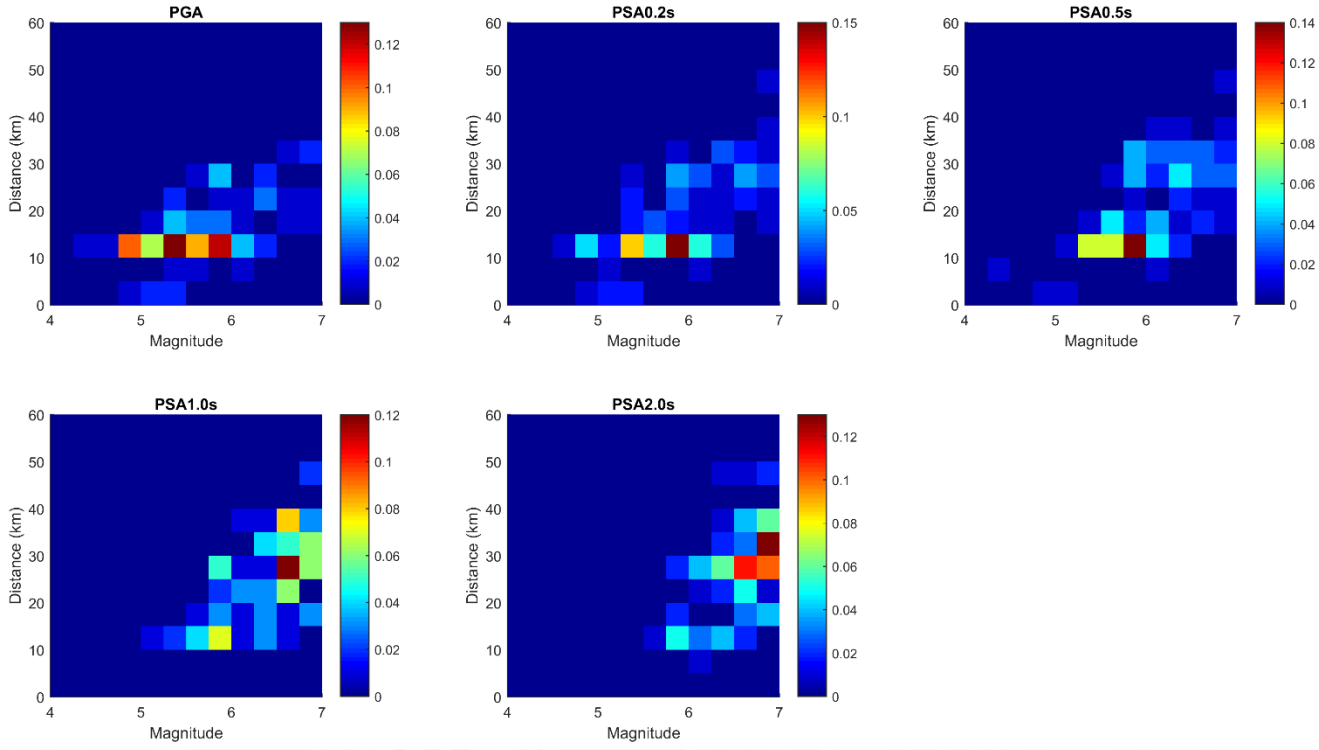

Appendix 2 – ShakeMaps

Nanometrics

Ground Motion and Intensity Maps for **M**≥3.5 Earthquakes in Fox Creek, Alberta

Revision 1.1
Prepared for: Alberta Energy Regulator
Submitted: August 4, 2016

Alberta Energy Regulator

STRATEGIC INTELLIGENCE
fueled by SCIENCE

ATTENTION: PLEASE READ CAREFULLY.

This document is prepared by Nanometrics Inc. ("**Nanometrics**") for the recipient organization. The information contained in this document is intended to report and provide insights for the use of the recipient organization, who accepts full responsibility for its use. Recipient organization acknowledges that the overall outputs contained in this document must be considered estimates by their nature, as they are dependent upon measurements and mathematical models with varying levels of inherent uncertainty and assumptions that are typical of empirical and statistical analysis. The findings in this document should be assessed as a whole and any attempt to rely on partial analysis or summary descriptions in this document could lead to undue emphasis on particular factors or inaccurate conclusions.

The information in this document is provided with the understanding that this document is intended for use as part of a wider scope of work provided by Nanometrics and Nanometrics is not providing any professional advice or recommending any one course of action based on the contents of this document.

Nanometrics endeavours to provide accurate and reliable information and insights. This document has been provided in good faith based on data collected by Nanometrics which were available at the time the document was generated and which is dependent on various factors including, but not limited to, the number, geographical distribution and performance of commissioned stations which may be affected by factors outside of the control of Nanometrics. All information in this document is provided "as is", without warranty of any kind, express or implied, including, but not limited to any warranties of merchantability, merchantable quality or fitness for a particular purpose. In no event will Nanometrics, or its partners, suppliers, employees or agents, be liable to the recipient organization or anyone else for any loss, damage, cost or expense of any kind, including any consequential, special or similar damages, arising in connection with results obtained from the use of this information, any decision made or action taken in reliance on this document or any information contained in this document.

TABLE OF CONTENTS

1.0 INTRODUCTION

An increase in the seismic activity rate has been observed in Fox Creek, Alberta, and a number of earthquakes of moment magnitude above **M**3.5 have been recorded in the region, since 2013. Recent studies (e.g., Eaton and Babaie Mahani, 2015; Schultz et al., 2015; Atkinson et al., 2016) suggest that the elevated seismicity is likely to be correlated with hydrocarbon production in the region. In order to gain an understanding on the overall hazard from such events, AER initiated a project to conduct a preliminary study on the probabilistic seismic hazard assessment of induced seismicity in Fox Creek. In a similar direction, AER has expressed interest in generation of peak ground motion and intensity maps (a.k.a. *shake maps*) for **M**≥3.5 events in the region. This report has been prepared by Nanometrics Inc. for AER, and describes the methodology utilized for the derivation of shake maps.

Shake maps show how the intensity of ground shaking created by a seismic event is distributed over a region around the epicenter. Such information is complementary to the magnitude and location of the event, demonstrating the effects of radiated seismic energy on the ground surface. Shake maps have become a valuable tool for real-time hazard and risk management worldwide. They are commonly used for rapid spatial evaluation of potential damage following a major earthquake for emergency response, loss estimation and public information (Wald et al., 2005).

Shake maps are typically generated for maximum horizontal component motions (Y_{max}). There are two key components to create a shake map:

1. a ground motion prediction equation (GMPE) applicable for the region of interest, and
2. a site amplification map consistent with the reference site condition for which the GMPE was developed

In this study, we generate shake maps for peak ground acceleration (PGA), peak ground velocity (PGV) and instrumental intensity, for four recent **M**≥3.5 earthquakes occurred in Fox Creek (Table 1).

Table 1 List of study events for which shake maps to be generated. Event sizes are given in terms of moment magnitude (**M**).

Event Date and Time (UTC)	Latitude	Longitude	Depth (km)	Magnitude
2015-01-14 16:06:25	54.35	-117.38	3.9	**M**3.5
2015-01-23 06:49:20	54.43	-117.30	5.4	**M**3.8
2015-06-13 23:57:55	54.10	-116.95	3.0	**M**4.0
2016-01-12 18:27:23	54.41	-117.31	4.2	**M**4.1

We use a regionally-adjusted predictive model adopted from the GMPE suite that was developed for assessment of induced seismicity hazard in the region (Yenier et al., 2016). The adopted model was derived for the geometrical mean of two horizontal-component peak motions (Y_{gm}). Therefore, we scale the model to convert estimated amplitudes into the maximum horizontal component motions (Y_{max}), for use in generation of shake maps. The Y_{gm}-to-Y_{max} scaling factor is computed by averaging the ratio of observed motions for recordings obtained within the distance range of interest (<50km).

We also develop site amplification maps for peak motions, by correlating site effects with the surficial geology of the recording stations. The adopted predictive model was derived for the average site condition, which was assumed to be NEHRP D (Yenier et al., 2016). We determine site effects relative to this reference site condition, based on the analysis of ground-motion residuals. The residuals are averaged for each unique geological unit to create surficial geology-dependent amplification maps.

We generate shake maps using the derived predictive model and site amplification maps.

2.0 GROUND MOTION PREDICTION EQUATION

Yenier et al. (2016) developed a suite of GMPEs for use in probabilistic seismic hazard assessment of induced events in Fox Creek region. It was derived from published predictive models, considering the empirically-determined regional adjustments for source and attenuation attributes in Fox Creek.

In this study, we adopted the regionally-adjusted Atkinson (2015) model, which is the center model of the GMPE suite used in hazard analysis. The adjusted A15 (Atkinson, 2015) model is written as,

$$\log Y_{A15} = (c_0 + \Delta c_0) + c_1\mathbf{M} + c_2\mathbf{M}^2 + c_3 log R + \begin{cases} 0 & R < 70\text{km} \\ \Delta c_3 \log(R/70) & 70 \le R < 140\text{km} \\ \Delta c_3 \log(140/70) & R \ge 140\text{km} \end{cases} \quad (1)$$

in which Y is the ground-motion parameter (specifically, the geometric mean of two horizontal-component PGA, PGV or 5% damped PSA), $\mathbf{M}$ is moment magnitude and R is an effective point-source distance that includes near-source distance-saturation effects:

$$R = \sqrt{D_{hyp}^2 + h_{eff}^2} \quad (2)$$

The close-distance saturation effects are modeled by the h_{eff} term that is given as a function of event magnitude:

$$h_{eff} = \max[1,\ 10^{-1.72+0.43\mathbf{M}}] \quad (3)$$

c_0, c_1, c_2 and c_3 terms are model coefficients adopted from the original A15 model, and Δc_0 and Δc_3 terms are coefficients of model adjustment for $\mathbf{M} \ge 2.8$ induced events in Fox Creek. Reader is referred to Yenier et al. (2016) for the methodology and assessment of the regional GMPE calibration. Table 2 shows model coefficients of adjusted A15 model for geometric mean horizontal PGA and PGV. The predictive model is compared to the observed motions in Figure 1.

Table 2 Coefficients of regionally-adjusted A15 model for peak ground motions

Coefficients	PGA	PGV
c_0	-2.376	-4.151
c_1	1.818	1.762
c_2	-0.115	-0.095
c_3	-1.752	-1.669
Δc_0	-0.212	0.000
Δc_3	1.992	1.582

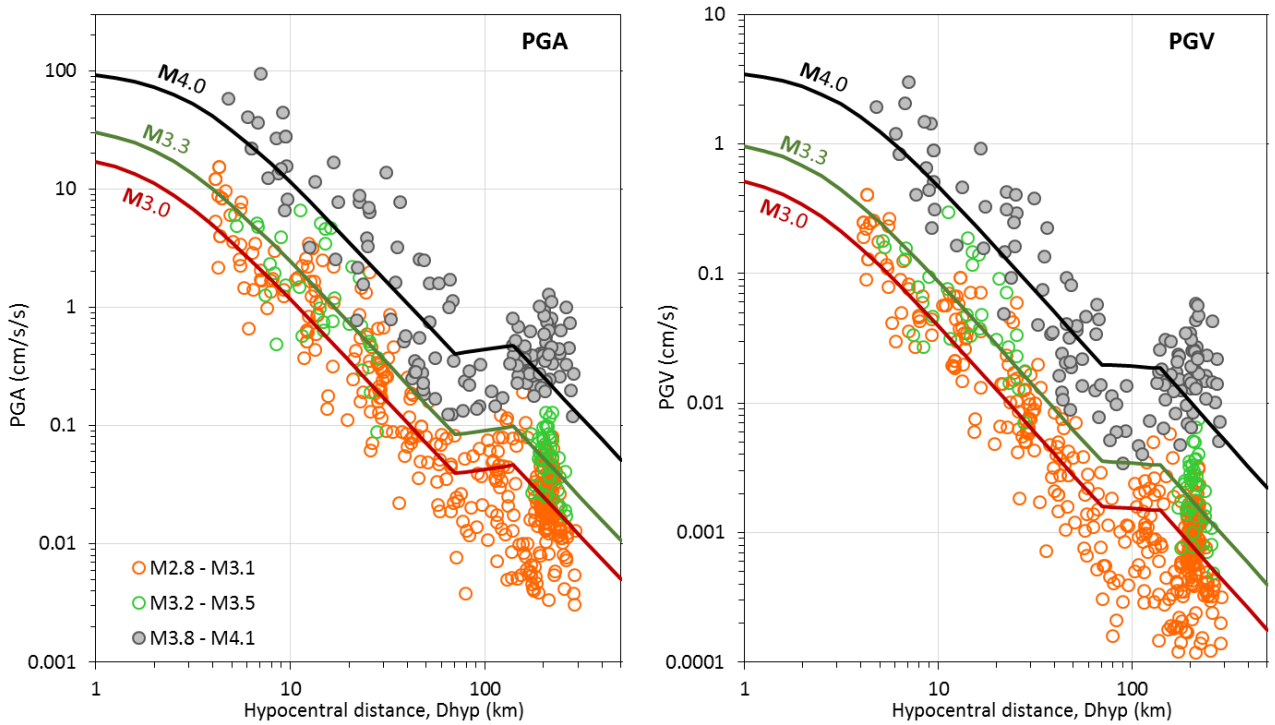

Figure 1 Regionally-adjusted A15 model (lines) in comparison to observed peak ground motions (circles), for earthquakes of **M**≥2.8 in Fox Creek region. Both predictive model and observed peak motions are plotted for the geometric mean of two horizontal components.

Prediction equations are typically derived for the geometric mean of two horizontal-component peak motions. This is also the case for the GMPE used in this study. Despite the common use of geometric mean values in prediction equations, shake maps are generated for maximum observed horizontal peak motions because depicting average motions effectively reduces information and discards the largest values of shaking that may occur in highly directional near-fault pulse-like ground motions (Worden and Wald, 2016).

We examine the ratio of maximum and geometric mean peak motions (Y_{max}/Y_{gm}) as a function of distance, for well-recorded Fox Creek events (**M**≥2.8), as shown in Figure 2. The Y_{max}/Y_{gm} ratio is mostly range between 0 and 0.3 log units (i.e., factor of 2), for distances less than 50 km. The dispersion in ground-motion ratios decreases by 0.1 log units at further distances. Y_{max}/Y_{gm} attains values up to a factor of 1.6, at distance larger than 100 km. These observations are valid for both PGA and PGV.

Figure 3 shows the distribution of source-to-station azimuths as a function of distance, for ground motion data obtained from **M**≥2.8 Fox Creek events. As illustrated, ground motions at distances less than 50km are well-sampled over the entire azimuthal range, whereas ground motions at further distances are mostly recorded at azimuths less than 180° or greater than 300°. There are only few ground motions recorded at azimuths between 180° and 300° and distances larger than 50 km. In order to investigate azimuthal effects on the ground-motion ratio, Y_{max}/Y_{gm} values are color-coded based on the two azimuth ranges, as labeled in Figure 2. However, no apparent discrepancy is observed in Y_{max}/Y_{gm} ratios between the two azimuth ranges, for distances < 50 km.

Due to the unresolved decay in variation of Y_{max}/Y_{gm} ratio for large distances, we determine its average value considering only recordings obtained within the distance range of interest of this study (< 50 km). The mean Y_{max}/Y_{gm} ratios for PGA and PGV are listed in Table 3. We scale the adopted predictive model (Equation 1) by these empirical factors to obtain predictions for the maximum horizontal peak ground motions (i.e., $Y_{A15,max} = Y_{A15} \times Y_{max}/Y_{gm}$).

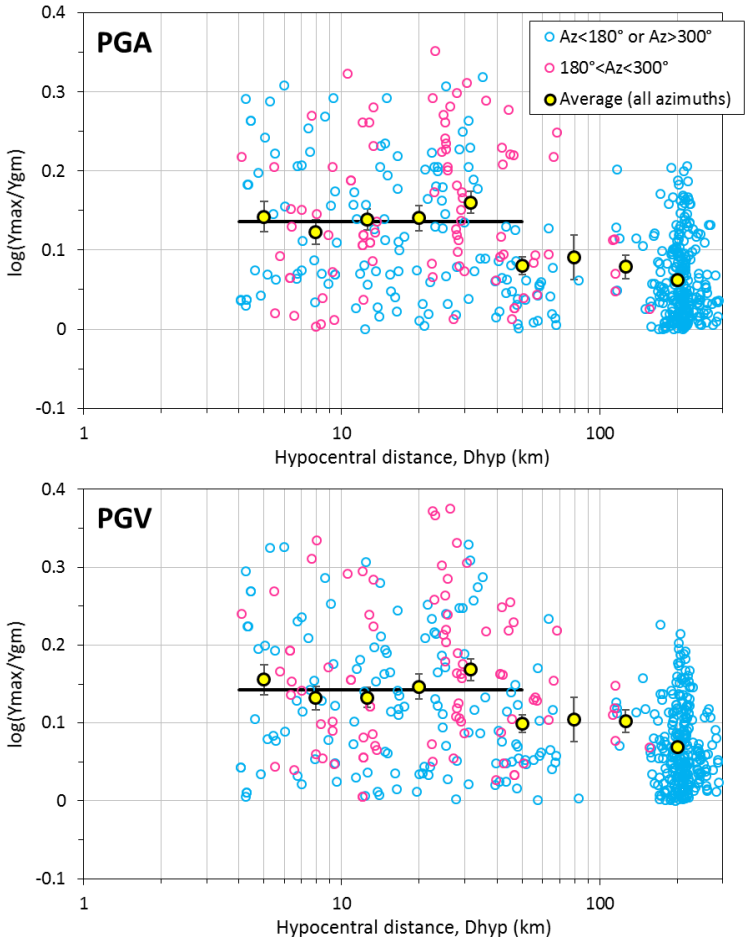

Figure 2 Ratio of the maximum horizontal peak ground motions to their geometric mean (Y_{max}/Y_{gm}) for Fox Creek earthquakes (**M**≥2.8). Symbols are color-coded based on source-to-station azimuth, as indicated in the label. Filled circles represent average ratios determined for equal spacing of logarithmic distance. Solid line indicate the average Y_{max}/Y_{gm} ratio for stations within 50 km of an event (Table 3).

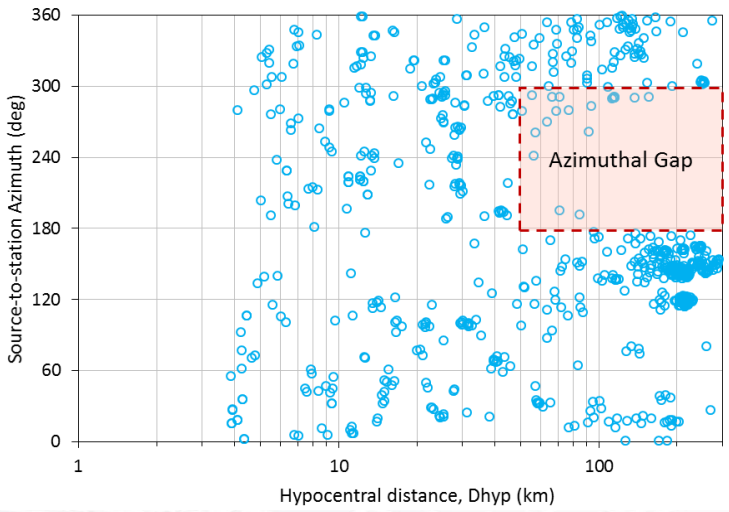

Figure 3 Azimuthal distribution of ground motion recordings as a function of distance, for Fox Creek events of **M**≥2.8

Table 3 Average Y_{max}/Y_{gm} ratio for distances D_{hyp} < 50 km of Fox Creek earthquakes (**M**≥2.8)

Ground motion parameter	Y_{max}/Y_{gm}
PGA	1.37
PGV	1.39

Figure 4 compares predictions of the scaled GMPE ($Y_{A15,max}$) and observed maximum horizontal motions, for study events (Table 1). The predictive model, is in good agreement with the observed amplitudes on average, and well captures the regional decay of ground motions with distance. However, there are some discrepancies between individual events and the corresponding predictions. This is primarily because the adopted GMPE was derived for the average of events of varying mechanisms and stress drop, observed in the region. It is noteworthy that the overall bias between observed and predicted amplitudes will be considered as a correction factor for the GMPE in order to obtain zero-biased predictions for individual events, when shake maps are generated.

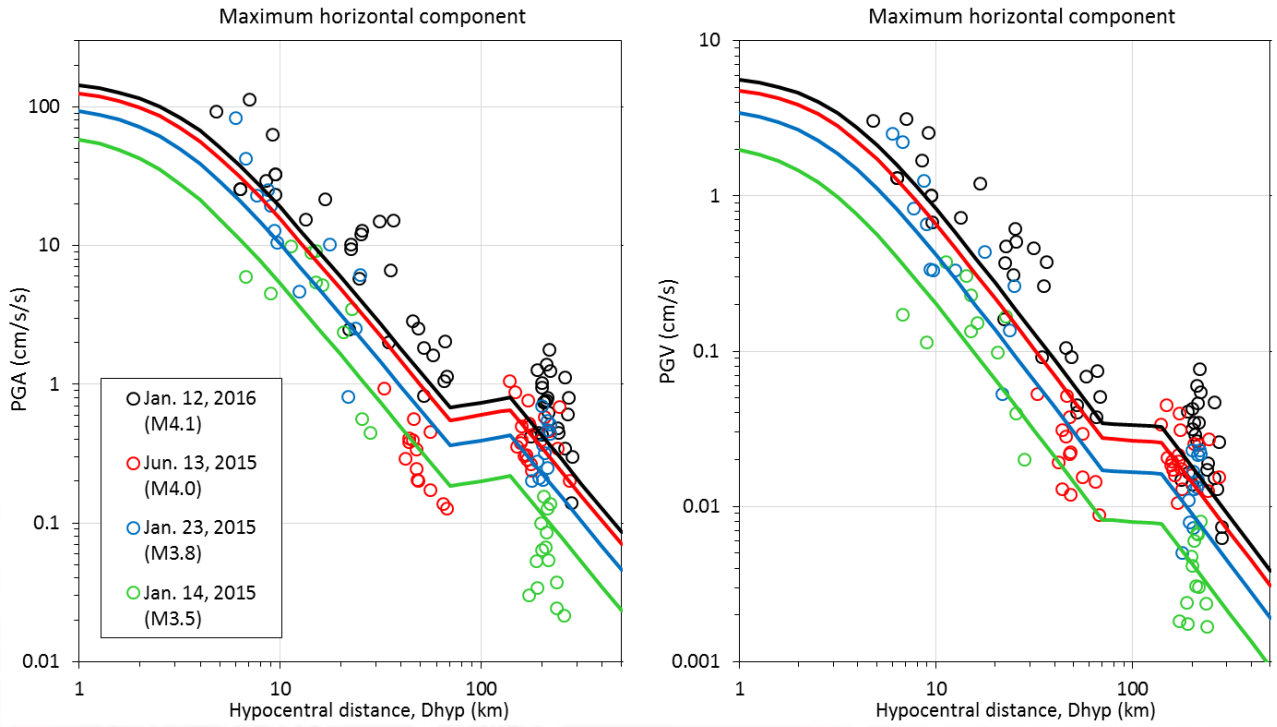

Figure 4 Comparison of observed maximum horizontal peak motions (circles) and the scaled predictive model, $Y_{A15,max}$, (lines) for study events (Table 1)

3.0 SITE AMPLIFICATION MAPS

Another key input required to create shake maps is a site amplification map that represents the effect of near-surface material on ground motion amplitudes, over the region of interest. It is typically defined relative to the reference site condition for which the input GMPE was derived.

In this study, we derive site amplification maps from the analysis of ground-motion residuals. To this end, we first categorize stations based on their site conditions, using the surficial geology map published by Alberta Geological Survey (Fenton et al., 2013). Figure 5 illustrates the surface geology in Fox Creek region. We identify a total of 12 site classes with unique surficial geology in the area (Table 4), and the majority of the region consists of Moraine-type sites. Consequently, the most of the recordings were obtained at such site conditions, as shown in Figure 6.

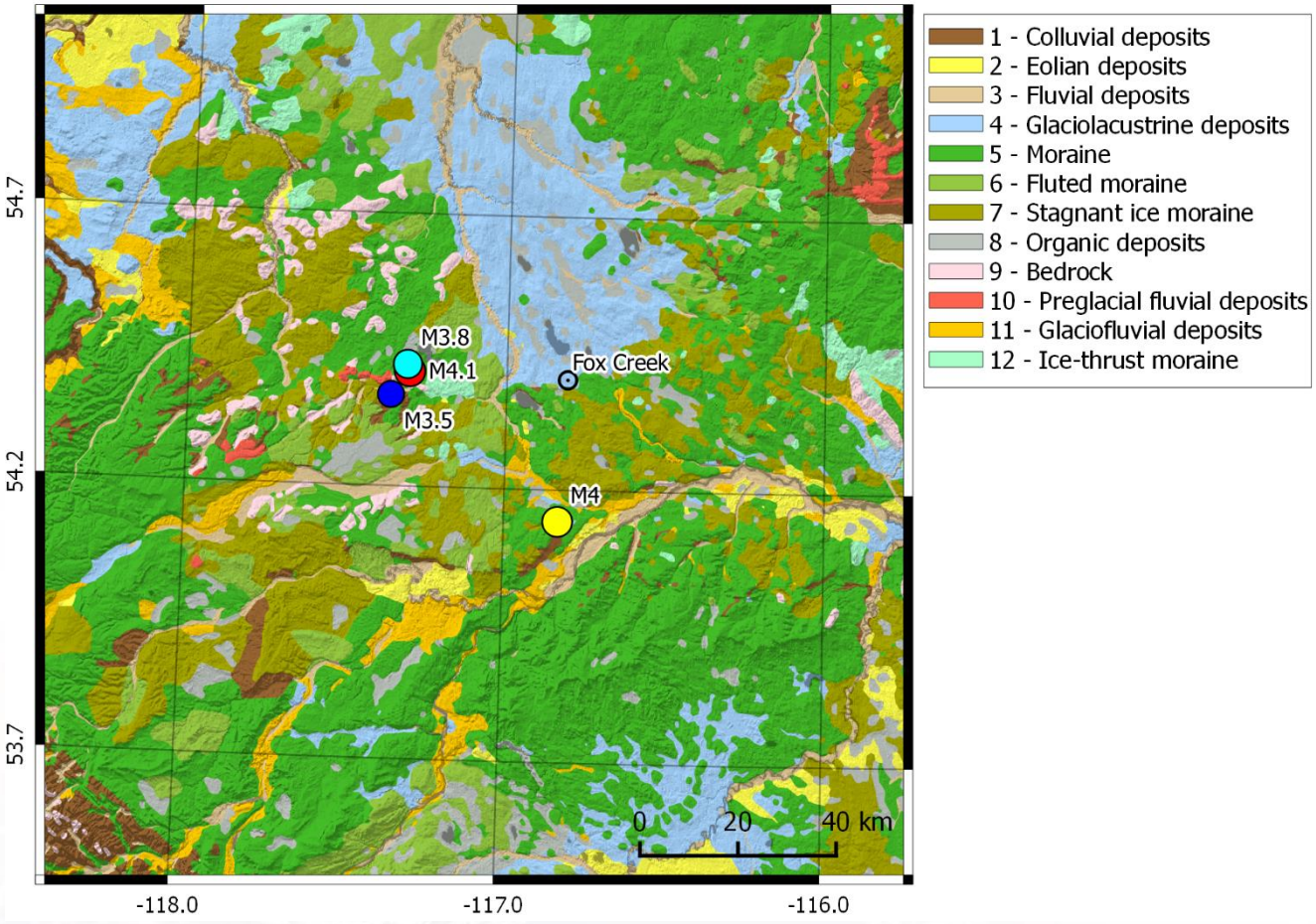

Figure 5 Surficial geology map for Fox Creek region. Open circle indicate the town of Fox Creek and filled circles show epicenters of the study events (**M**≥3.5)

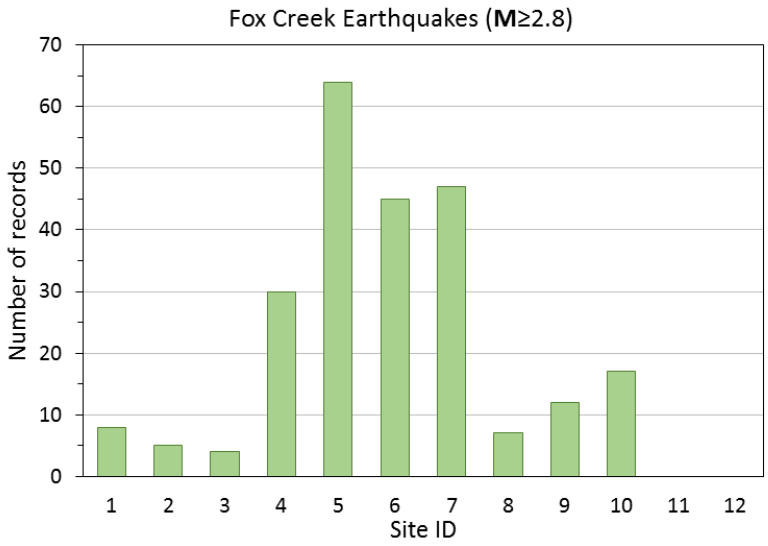

Figure 6 Number of records obtained from Fox Creek events (**M**≥2.8) at each geological unit. Sites ID are as listed in Table 4.

Next, we determine residuals between observed and predicted peak motions (i.e., $\log Y_{observed,max} - \log Y_{A15,max}$), considering only stations within the region of interest for **M**≥2.8 events. We average residuals for each geological unit to estimate their site effects. By doing this, we identify a systematic offset in ground-motion amplitudes for each site class relative to the predictive model, which was derived for average site condition in Fox Creek. Here, we assume that all other residual effects resulting from inter-event variation of source and attenuation attributes average out to zero (see Figure 8, discussed later). This is a reasonable assumption given the fact that the same ground-motion dataset was used for the derivation of GMPE. Table 4 lists computed site effects for the peak ground motions. It should be noted that site effects of glaciofluvial deposits (#11) and ice-thrust moraine (#12) sites could not be determined because no recordings were available for them (Figure 6). These sites assumed to attain similar site effects with the average site condition in Fox Creek region, and no relative site correction is considered for them. Figure 7 shows the variation of site amplification between sites classes. Organic sites (#8) show the highest amplification for both PGA and PGV. Sites identified as bedrock (#9) attain amplitudes lower than the average site in the region (i.e., negative site effect). However, they show relatively large uncertainty, particularly for PGA. Interestingly, Colluvial (#1), Eolian (#2) and Fluvial (#3) deposits attain opposite signed site correction for PGA and PGV, relative to the average site in the region. All three site classes attain positive correction factors for PGA, whereas they attain negative correction factors for PGV. It should be noted that these sites attain large standard error about their mean amplification due to the limited number of observations (Figure 6), and they constitute only a small portion of the mapped region in Figure 5.

Table 4 Site effects for each geological unit, for maximum horizontal-component PGA and PGV

Site ID	Surficial Geology	Site Amplification (log units)	
		PGA	PGV
1	Colluvial Deposits	0.060	-0.066
2	Eolian Deposits	0.053	-0.129
3	Fluvial Deposits	0.136	-0.020
4	Glaciolacustrine Deposits	0.084	0.072
5	Moraine	0.026	-0.018
6	Fluted Moraine	0.127	0.079
7	Stagnant Ice Moraine	0.049	0.068
8	Organic Deposits	0.150	0.112
9	Bedrock	-0.080	-0.021
10	Preglacial Fluvial Deposits	0.024	-0.036
11	Glaciofluvial Deposits	---	---
12	Ice-Thrust Moraine	---	---

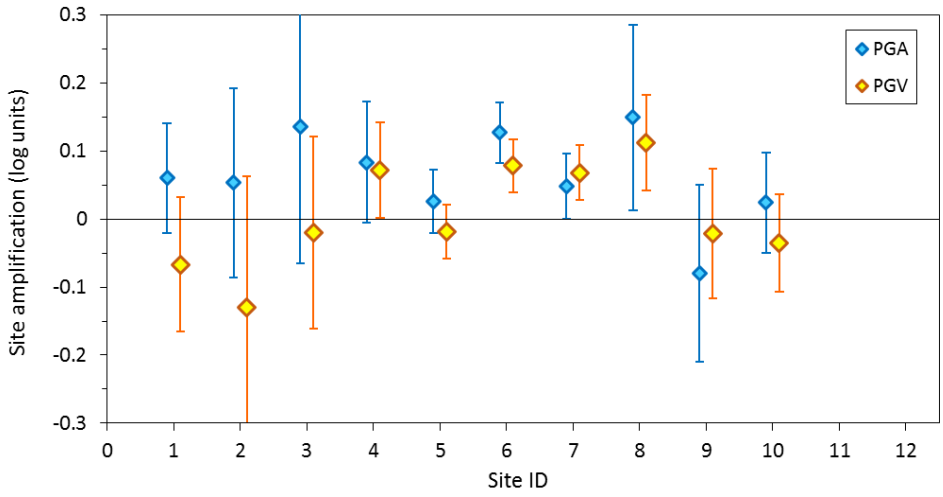

Figure 7 Site amplification for each site class. Vertical bars indicate standard error about the mean.

As a quality check, we determine ground-motion residuals after correcting predictions for the computed site effects. Figure 8 indicates that site-corrected residuals show no discernable trends, and their mean attain values around zero. This suggests that the predictive model and determined site effects are in good agreement with the observed motions in Fox Creek.

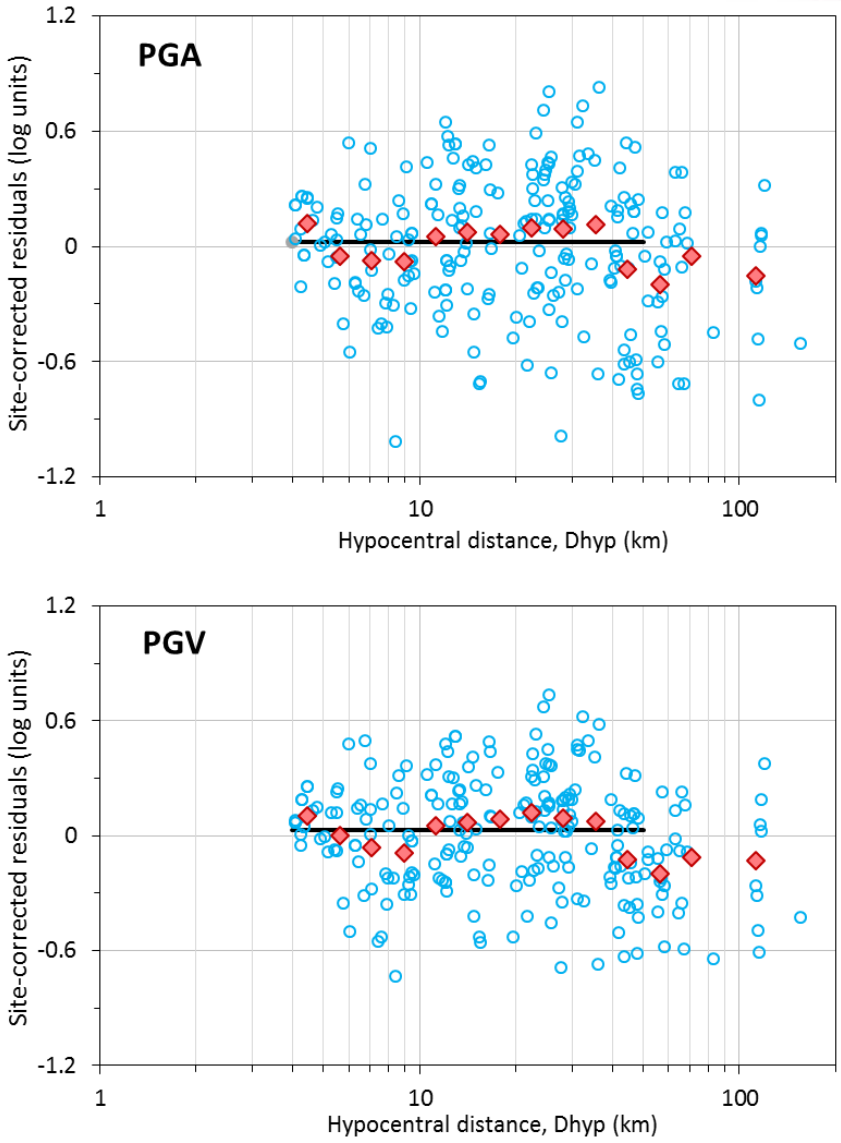

Figure 8 Residuals for the predicted maximum horizontal-component motions after accounting for site corrections, for Fox Creek events of **M**≥2.8. Red symbols represent average residuals determined for uniformly log-spaced distance bins. Solid line indicate the average residual over distance range of interest (D_{hyp} < 50 km)

We use the calculated site factors to generate site amplification maps for Fox Creek. This is achieved by creating a grid of points with 1 km spacing, and identifying site class of each point according to the surficial geology map. Then, we assign empirical site factors to the points with same site class. Figure 9 shows surficial geology-dependent site amplification maps for PGA and PGV.

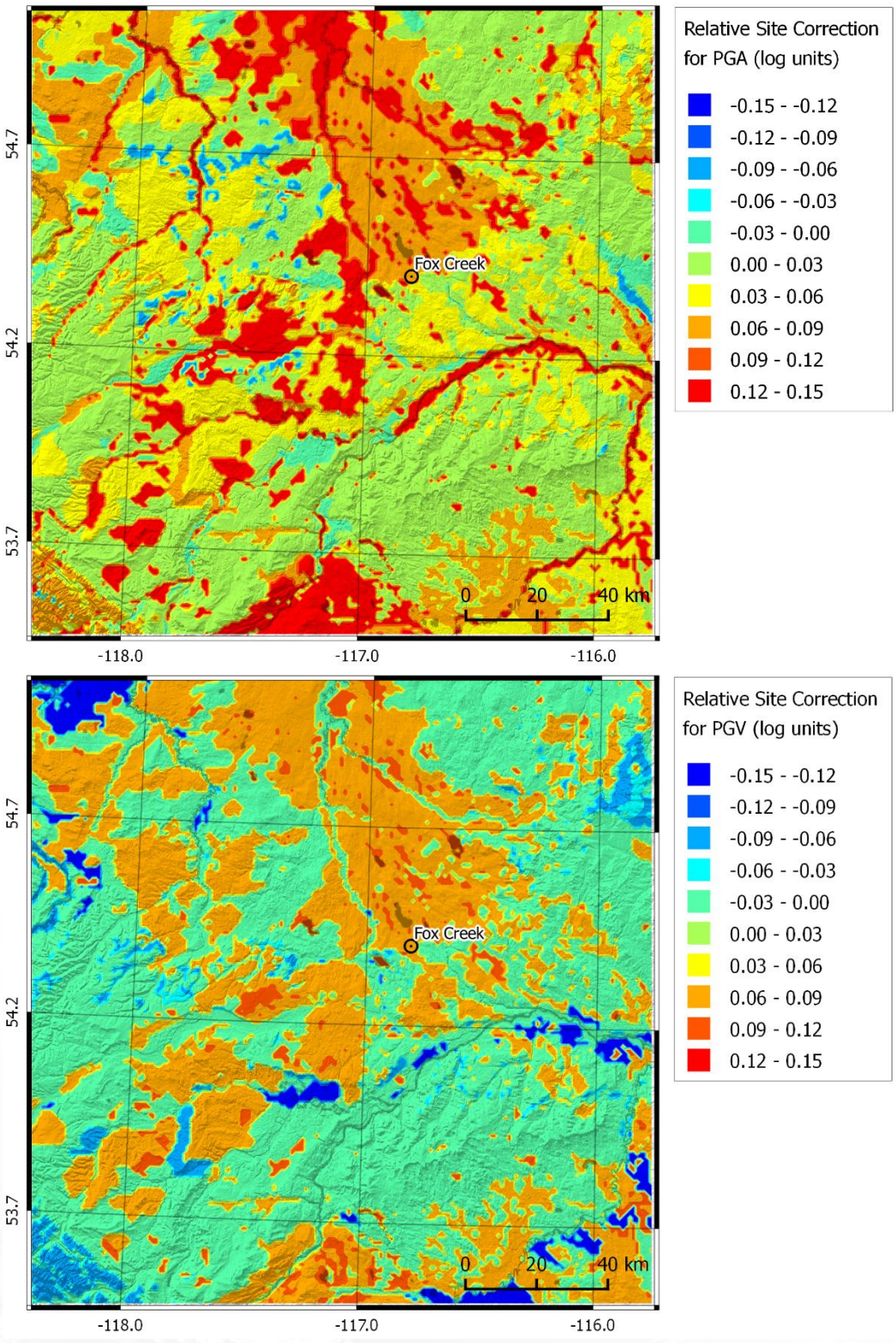

Figure 9 Site amplification maps relative to the adopted GMPE, for the maximum horizontal-component motions ($Y_{A15,max}$).

4.0 GROUND MOTION AND INTENSITY MAPS FOR **M**≥3.5 EARTHQUAKES

Peak ground motion and intensity shake maps are generated for the recent **M**≥3.5 Fox Creek events (Table 1). For a given event, the shake map algorithm starts with correcting observed motions to the reference site based on the derived amplification factors. Next, an overall bias between site-corrected motions and the GMPE ($Y_{A15,max}$) is determined. The GMPE is scaled by this factor to obtain zero-biased predictions in areas that are not instrumented. Ground motions are estimated over a grid of points, using the scaled GMPE and site amplification map. Shake maps are created by spatially interpolating through the grid of predicted motions, while preserving the recorded motions available for points near stations.

The generated ground motion and intensity maps for study events are provided in following sub-sections, in chronological order. Also, peak motions and intensities estimated for the epicenter and Fox Creek town are given in tables.

4.1 JAN. 14, 2015 M3.5 EVENT

N54.35 W117.38 Depth: 3.9km
36.2km from Fox Creek, Alberta

PGA (%g)

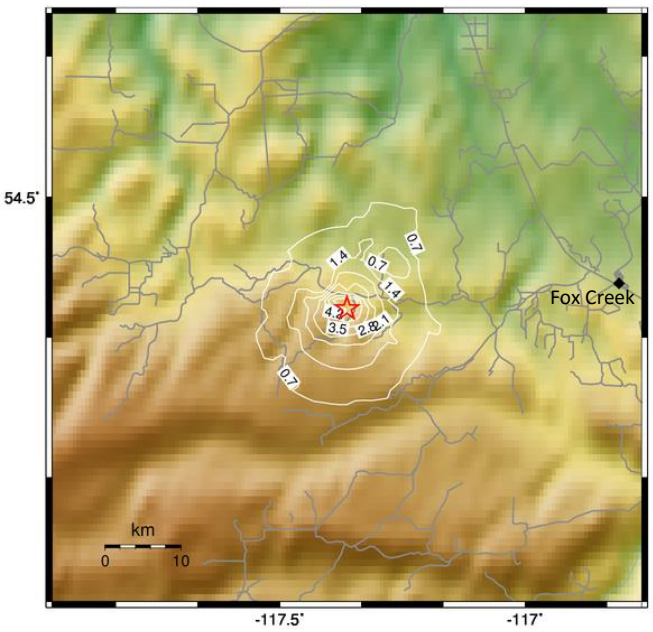

PGV (cm/s)

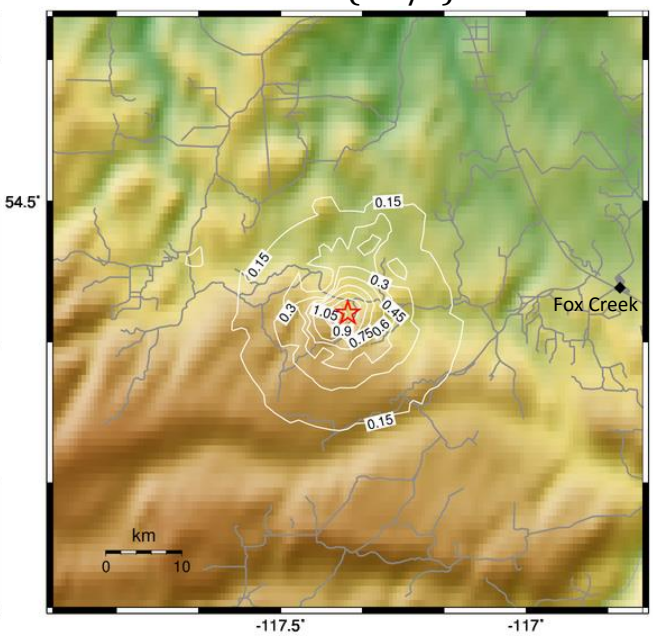

Intensity

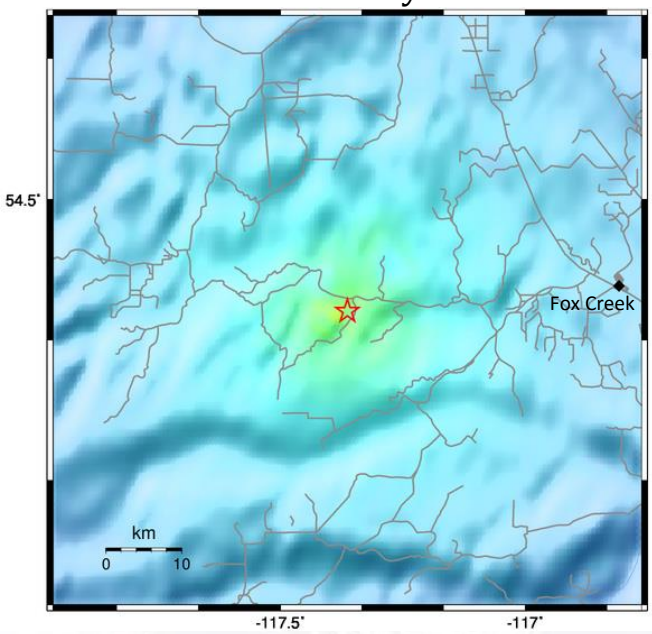

	PGA (%g)	PGV (cm/s)	Intensity
Epicenter	5.166	1.154	V
Fox Creek	0.108	0.037	III

PERCEIVED SHAKING	Not felt	Weak	Light	Moderate	Strong	Very strong	Severe	Violent	Extreme
POTENTIAL DAMAGE	none	none	none	Very light	Light	Moderate	Mod./Heavy	Heavy	Very Heavy
INSTRUMENTAL INTENSITY	I	II-III	IV	V	VI	VII	VIII	IX	X+

4.2 JAN. 23, 2015 M3.8 EVENT

N54.43 W117.30 Depth: 5.4km
32.9km from Fox Creek, Alberta

PGA (%g)

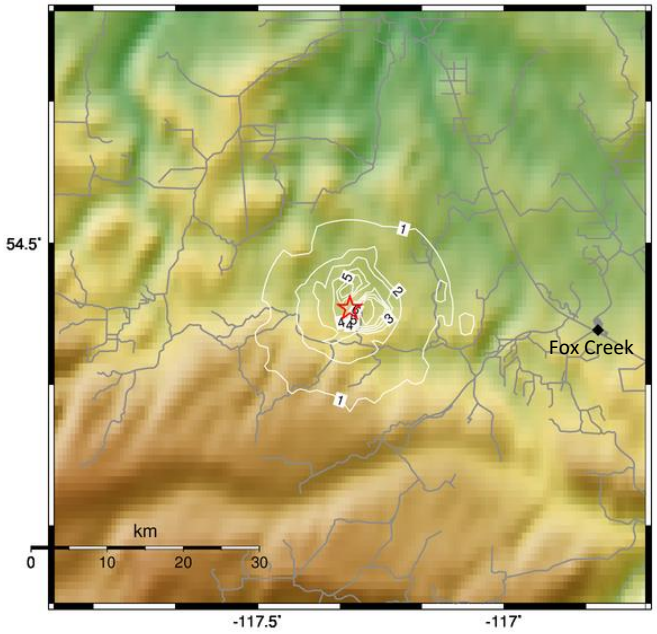

PGV (cm/s)

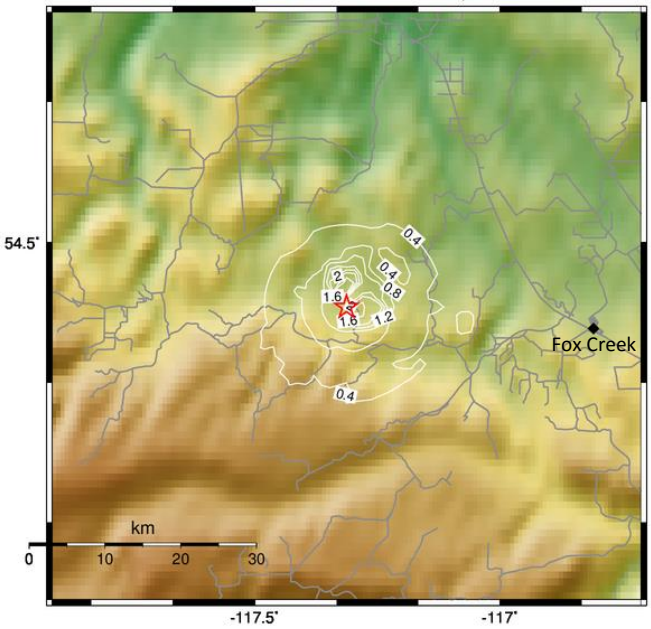

Intensity

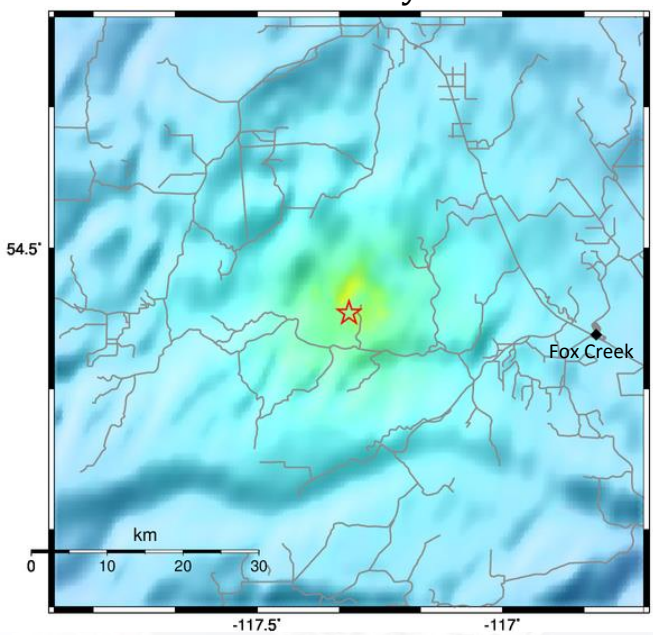

	PGA (%g)	PGV (cm/s)	Intensity
Epicenter	3.586	1.558	V
Fox Creek	0.216	0.093	III

PERCEIVED SHAKING	Not felt	Weak	Light	Moderate	Strong	Very strong	Severe	Violent	Extreme
POTENTIAL DAMAGE	none	none	none	Very light	Light	Moderate	Mod./Heavy	Heavy	Very Heavy
INSTRUMENTAL INTENSITY	I	II-III	IV	V	VI	VII	VIII	IX	X+

STRATEGIC INTELLIGENCE
fueled by SCIENCE

4.3 JUN. 13, 2015 **M**4.0 EVENT

N54.10 W116.95 Depth: 3.0km
28.6km from Fox Creek, Alberta

PGA (%g)

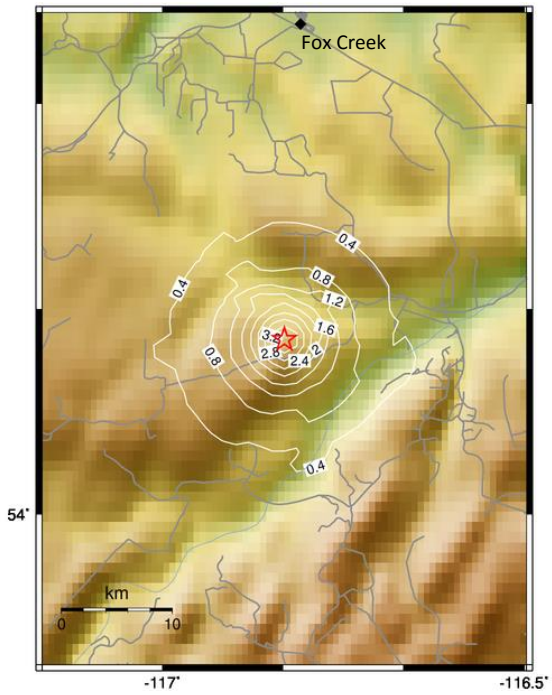

PGV (cm/s)

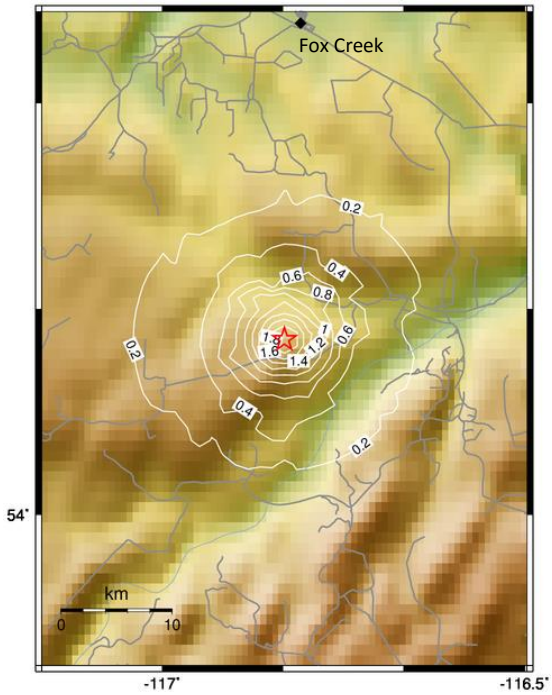

Intensity

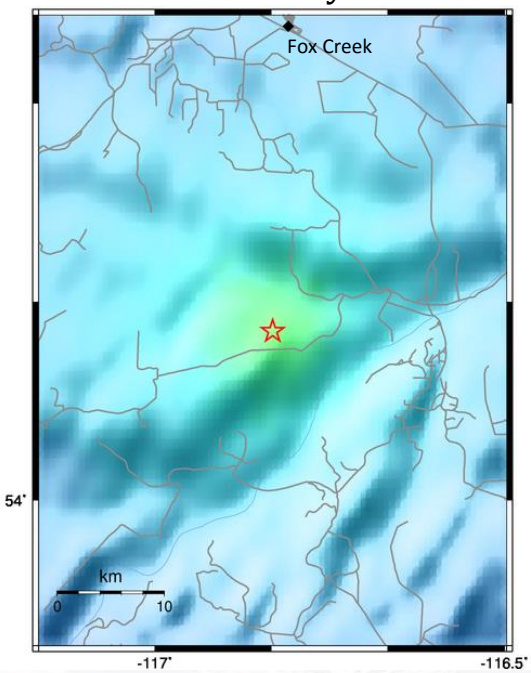

	PGA (%g)	PGV (cm/s)	Intensity
Epicenter	3.597	2.026	V
Fox Creek	0.081	0.059	III

PERCEIVED SHAKING	Not felt	Weak	Light	Moderate	Strong	Very strong	Severe	Violent	Extreme
POTENTIAL DAMAGE	none	none	none	Very light	Light	Moderate	Mod./Heavy	Heavy	Very Heavy
INSTRUMENTAL INTENSITY	I	II-III	IV	V	VI	VII	VIII	IX	X+

4.4 JAN. 12, 2016 M4.1 EVENT

N54.41 W117.31 Depth: 4.2km
32.3km from Fox Creek, Alberta

PGA (%g)

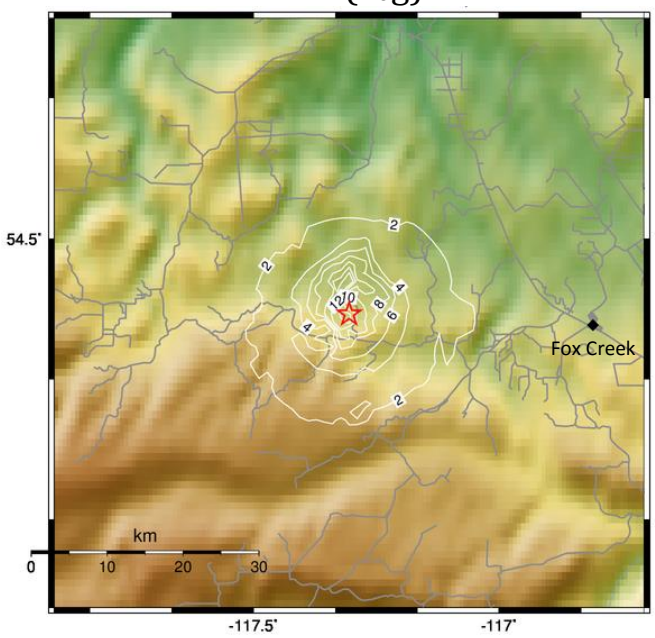

PGV (cm/s)

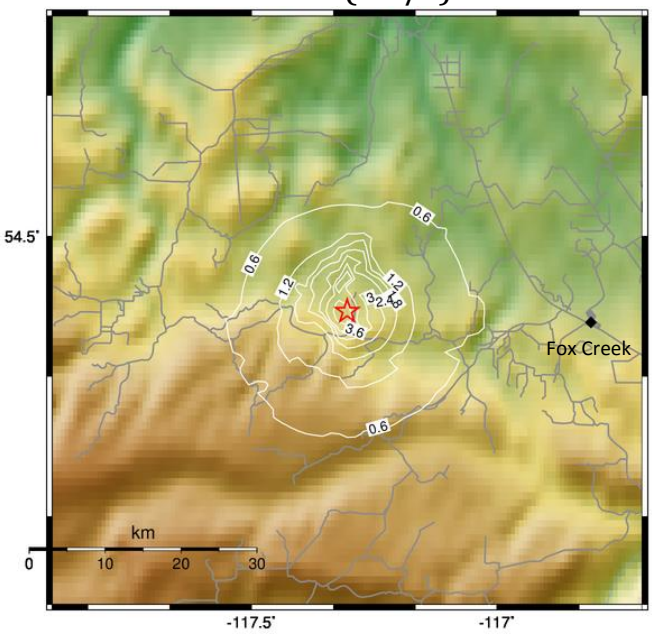

Intensity

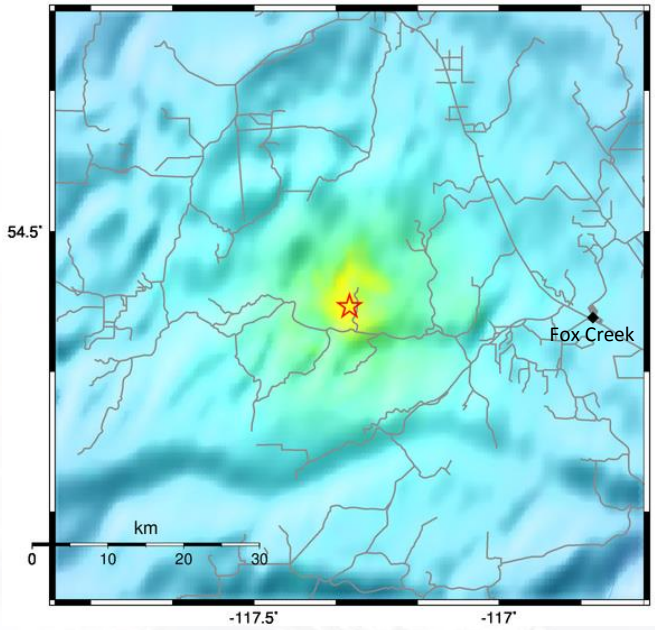

	PGA (%g)	PGV (cm/s)	Intensity
Epicenter	14.345	4.563	VI
Fox Creek	0.473	0.194	III-IV

PERCEIVED SHAKING	Not felt	Weak	Light	Moderate	Strong	Very strong	Severe	Violent	Extreme
POTENTIAL DAMAGE	none	none	none	Very light	Light	Moderate	Mod./Heavy	Heavy	Very Heavy
INSTRUMENTAL INTENSITY	I	II-III	IV	V	VI	VII	VIII	IX	X+

5.0 SUMMARY

Peak ground motion and intensity maps are generated for the recent **M**≥3.5 earthquakes in Fox Creek, Alberta. To this end, a regional GMPE that was derived for geometric mean of horizontal peak motions is adopted. The prediction equation is scaled to match the observed maximum horizontal amplitudes, based on the empirical ratio ground motions (i.e., Y_{max}/Y_{gm}).

The adopted predictive model was developed for the average site condition in the region. Site amplification maps are derived to account for the variations in local site effects, in shake map calculations. The region of interest is categorized based on the surface material using the surficial geology map of Fox Creek. Ground motion residuals are correlated with the geological classes to generate amplification maps relative to the average site condition.

Shake maps are created for study events, using the scaled GMPE ($Y_{A15,max}$), site amplification maps, and observed peak motions. Overall, ground motions at the epicenters range between 3.6 – 14.3 percent of g for PGA, and between 1.2 – 4.6 cm/s for PGV. The corresponding shaking intensity at the epicenters is V for all events, except the **M**4.1 Jan 12, 2016 event. The **M**4.1 event is estimated to cause a shaking intensity of VI at its epicenter. Both ground motions and intensities are much lower for the town of Fox Creek because events are located about 30 km from the town. The ground motions at Fox Creek town is estimated between 0.08 – 0.47 percent of g for PGA, and between 0.04 – 0.19 cm/s for PGV. The predicted shaking intensity at Fox Creek is III for all events, except the **M**4.1 event, for which it is between III and IV. These intensity estimates agree well with the weak-to-lightly felt reports at Fox Creek town, for the study events.

It is important to acknowledge that the presented methodology and results are largely based on the seismological and statistical analysis of the observations from Fox Creek events. Uncertainties in seismic source parameters (e.g., epicenter location, depth and magnitude), predicted motions and surficial geology transfers into the shake map results. Further research on ground-motion prediction and site characterization with a richer empirical dataset can help to reduce such uncertainties.

6.0 REFERENCES

Atkinson, G. M. (2015). Ground-motion prediction equation for small-to-moderate events at short hypocentral distances, with application to induced seismicity hazards, *Bull. Seismol. Soc. Am.* 105, 981–992.

Atkinson, G. M., D. W. Eaton, H. Ghofrani, D. Walker, B. Cheadle, R. Schultz, R. Shcherbakov, K. Tiampo, J. Gu, R. M. Harrington, Y. Liu, M. van der Baan, and H. Kao (2016). Hydraulic fracturing and seismicity in the Western Canada Sedimentary Basin, *Seismol. Res. Lett*., 87, 1–17.

Eaton, D., and A. Babaie Mahani (2015). Focal mechanisms of some inferred induced earthquakes in Alberta, Canada, *Seismol. Res. Lett.* 86, 1078–1085

Fenton, M. M., E. J. Waters, S. M. Pawley, N. Atkinson, D. J. Utting, and K. Mckay (2013). Surficial geology of Alberta, *Alberta Geological Suryey*.

Schultz, R., V. Stern, M. Novakovic, G. Atkinson, and Y. Gu (2015a). Hydraulic fracturing and the Crooked Lake Sequences: Insights gleaned from regional seismic networks, *Geophys. Res. Lett*. 42, 2750–2758.

Wald, D. J., C. B. Worden, K. W. Lin, and K. Pankow (2005). ShakeMap manual: technical manual, user's guide, and software guide, *U. S. Geological Survey*, Techniques and Methods 12-A1, 132 pp.

Worden, C. B., and D. Wald (2016) ShakeMap manual: Release 2.0, *U. S. Geological Survey*, 113p.

Yenier, E., G. M. Atkinson, S. Karimi and D. Baturan (2016). Prediction of earthquake ground motions in western Alberta, *Seismol. Soc. Am. 2016 Annual Meeting*, Reno, Nevada.